Engineering-Based FE Approach to Appraise Slender Structures Affected by Alkali-Aggregate Reaction (AAR)

By

RODRIGO VILELA GORGA

Under the supervision of

Dr. Leandro F. M. Sanchez

Co-supervisor

Dr. Beatriz Martín-Pérez

A thesis submitted to the Faculty of Graduate and Postdoctoral Studies in partial fulfilment of the requirements for the degree of

Masters of Applied Science in Civil Engineering

uOttawa

Department of Civil Engineering
University of Ottawa
Ottawa, Ontario, Canada

June 2018

Abstract

Alkali-aggregate reaction (AAR) is one of the most harmful distress mechanisms affecting the performance of aging reinforced concrete structures worldwide. Although several prediction models have been developed to assess the chemical reaction, a thorough and comprehensive approach with the capabilities to correlate important parameters that affect AAR and the mechanical properties of deteriorated materials, as well as the abilities to describe the current damaged state of AAR-affected structures (diagnosis) and predict the potential of further damage (prognosis) is still lacking. Such information is essential in selecting efficient remedial/rehabilitation actions for existing structures in the field. This project aims to develop a practical, yet accurate engineering-based finite element (FE) model for assessing AAR damage and predicting the future behaviour of affected infrastructure. The model is validated through three analyses. First, its capability to accurately simulate sound concrete under mechanical loading is verified by successfully simulating different beam failure mechanisms and cracking patterns, as well as predicting the members' full force-deflection curves. Next, AAR anisotropic expansion under different stress-state (confinement) conditions is accurately simulated and verified by correlation with laboratory tests. Lastly, an AAR-affected slender reinforced concrete structure (Robert-Bourassa/Charest overpass) is successfully simulated by performing a condition assessment based on several tests performed prior to its demolition.

Keywords: Alkali-aggregate reaction, concrete, finite element, prognosis, diagnosis

Table of Contents

List of Figures

List of Tables

Important Definitions and Acronyms

The following abbreviations and acronyms will be consistently used throughout this thesis to avoid confusion:

- AAR = alkali-aggregate reaction
- ACR = alkali-carbonate reaction
- ASR = alkali-silica reaction
- CDP = concrete damaged plasticity (material model)
- CPT = concrete prism test
- CSA = Canadian Standard Association
- DRI = damage rating index
- FE = finite element
- FT = freeze-thaw (cycles)
- E = exposed
- NE = non-exposed
- RBC = Robert-Bourassa/Charest Overpass
- RH = relative humidity
- SDT = stiffness damage test
- USDFLD = specific type of Abaqus user subroutine

Acknowledgements

First of all, I'd like to thank both my supervisor professor Leandro Sanchez and my co-supervisor professor Beatriz Martín-Pérez for all the support you provided me throughout the past two years. Your insightful recommendations, thoughtfulness and patience made this work not only possible, but also enjoyable.

I'd also like to express my gratitude to professor Martin Noël for sharing a bit of his extensive knowledge with me and for being always available to assist me whenever necessary.

Next, I thank all the people that made it possible for me to receive the NSERC Engage-OCE VIP grant, especially GHD and Pierre-Luc Fecteau. Thank you for believing in the potential of the work me and my supervisors developed.

I can't forget to acknowledge the assistance from another two people. Luc Cloutier, thank you for always helping us (students) as much as you possibly can. Professor Dan Palermo, thank you for recommending me to my current supervisors and for assisting me since my undergraduate studies.

Lastly, I would like to thank my friends from both Canada and Brazil and my family, especially my parents (Cristovão Nunes Gorga and Ara Célis Vilela Sousa) and my wife Colleen Sutton, for always being there for me. I have to say that I wouldn't be able to do it without the support of each one of you, regardless of how close or far you are.

1. INTRODUCTION

1.1 General

Alkali aggregate reaction (AAR) has been reported to lead to severe structural damage and to significantly reduce the service life of a number of reinforced concrete structures worldwide (Shayan, et al., 2009; Nomura, et al., 2013; Chulliat, et al., 2017). AAR is a very complex anisotropic reaction, which is influenced by several parameters, such as temperature, alkali loading, type and nature/minerology of aggregates, presence of moisture, stress-state, etc. (Gautam, et al., 2017; Goshayeshi, et al., 2018). In general, AAR is divided in two categories: alkali-silica reaction (ASR) and alkali-carbonate reaction (ACR). ASR is the most common type of AAR, and it is usually described as a chemical reaction between the alkalis from the concrete pore solution and the reactive silica from the aggregates, which forms an expansive gel (Fournier & Bérubé, 2000). In the presence of water, the ASR gel swells, eventually leading to concrete cracking and deterioration of the mechanical properties of the material. Alternatively, ACR is not fully understood, with some researchers suggesting that it is a specific type of ASR (Katayama, 2010; Katayama & Grattan-Bellew, 2012), while others defending that it is a totally different distress mechanism (Fecteau, et al., 2012; CSA-A864, 2000).

The implications on the serviceability and the risk of global and/or local failure of structures affected by AAR enhance the importance of properly assessing the current and future states of reinforced concrete structures. By analyzing the present state of deterioration (i.e., diagnosis), it is possible to both evaluate the structural safety and to understand the mechanisms leading to the damage observed in the different members or in the entire structure. Otherwise, it is known that the reaction varies over time as a function of the surrounding conditions, such as alkali and moisture availabilities (Larive, 1997). Therefore, the potential of further damage due to AAR (i.e.,

prognosis) must be thoroughly evaluated to fully and confidently appraise the safety and integrity of the structure as the reaction progresses.

Figure 1-1 illustrates the extent of AAR-induced damage in the reinforced concrete pier of the Robert-Bourassa Charest Overpass, located in Québec City, Canada.

a b

Figure 1-1. AAR damage extent on Robert-Bourassa Charest Overpass: a. Close up of the cracks on the side of the pier, b. Overview of the pier distress. Source: (Sanchez, et al., 2015).

Several finite element (FE) models have been developed over the years to describe the implications of the reaction at several scales, ranging from microscopic models describing the ion diffusion (Multon, et al., 2009; Poyet, et al., 2007) to macroscopic approaches assessing the overall structural implications (Charlwood, 1994; Ulm, et al., 2000; Saouma & Perotti, 2006; Grimal, et al., 2008). It is clear that considerable progress has been achieved recently in the area, especially

due to a better understanding of the reaction parameters and behaviour. However, there is still a need for an approach that intuitively describes the reaction without oversimplifying the physicochemical aspects involved nor overcomplicating them by requiring extensive fitting of parameters for each case based on the literature, laboratory test procedures or even non-technical guesses.

1.2 Objectives and scope of the work

The objective of this work is to develop a new intuitive engineering-based FE model to fully describe AAR and evaluate the future structural implications of the reaction (prognosis) based on the current state of the structure/structural member (diagnosis). The model can assess the most important parameters involved in the reaction in a simple and intuitive way by introducing new coefficients to the well-established equation proposed by Larive (1997) to describe the evolution of AAR-induced expansion over time according to Gautam et al. (2017). This approach is particularly realistic because it allows the coefficients to vary as a function of time, thus allowing for a full simulation of the environmental conditions affecting the chemical reaction.

The AAR FE modelling approach is first validated for sound concrete by simulating six reinforced concrete beams that had previously been tested and modeled at the University of Toronto (Vecchio & Shim, 2004). The beams presented different reinforcement configurations and three different geometries, which affected the observed behaviour and led to different failure modes. By conducting these analyses, the proposed AAR FE model proved its applicability to describe reinforced concrete structures and the mechanical implications of applied loads, especially by comparing it to another well-established FE approach to simulate damage in concrete structures.

Next, the AAR FE model is validated by simulating the expansion of three different ASR-affected push-off specimens, which were tested by Sanchez et al. (2016). Each one of the specimens had a different transverse reinforcement configuration, which led to different confinement magnitudes and, consequently, different expansion levels. To describe the anisotropic nature of the reaction, the stress-state dependence relationship proposed by Gautam et al. (2017) is implemented through the use of a subroutine. In summary, the latter allows to demonstrate the model's capacity to simulate the development of the reaction over time and the influence of restraining on the induced expansion.

Lastly, the approach is applied to a real case where severe ASR damage was observed. The Robert-Bourassa/Charest Overpass (RBC) was located in Quebec City, Canada, and it had to be demolished in 2010/2011 due to the structural implications of the reaction. Sanchez et al. (2016; 2018) performed several tests before and after the RBC was demolished, which were used to validate the computational model. Hence, by properly predicting the actual condition of the structure based only on simple measurable parameters, the model proves its applicability to simulate AAR in slender reinforced concrete structures over time.

1.3 Overview of the thesis

The thesis consists of 5 chapters. Chapters 3 and 4 are written in a journal paper format and are currently being considered for publication in two of the best journals in the area. These chapters consist of the reproduction of these papers; therefore, some repetition of concepts and discussions is unavoidable. The overall description of each chapter is presented below.

- Chapter 1 introduced the research needs, objectives and scope of the work.

- Chapter 2 provides both a literature review of the current AAR-modeling state-of-the-art and a brief discussion highlighting the existing knowledge gaps to justify the need for the development of the proposed approach. It first discusses the main topics related to modeling the reaction and then compares the existing AAR macro-models by highlighting its similarities, differences and basic concepts.

- Chapter 3 presents the first two validations of the new approach proposed: the sound concrete and the AAR-induced expansion validation in the format of a technical paper, which is cited below:

Gorga, Sanchez, Martín-Pérez and Noël, 2018. Engineering-based FE approach to appraise slender reinforced concrete structures affected by alkali-aggregate reaction (AAR).

- Chapter 4 presents the application of the proposed FE approach by analyzing the RBC overpass. This chapter is presented in the format of a technical paper, which is cited below:

Gorga, Sanchez and Martín-Pérez, 2018. FE approach to perform the condition assessment of a concrete overpass damaged by ASR after 50 years in service.

- Chapter 5 provides a summary of the research contributions presented, the conclusions and future research recommendations.

1.4 References

Charlwood, R., 1994. A review of alkali aggregate in hydro-electric plants and dams. *International Journal on Hydropower Dams,* p. 73–80.

Chulliat, O., Grimal, E. & Bourdarot, E., 2017. *Chambom dam - a struggle against AAR.* London, DSC 2017 - Swelling concrete in dams and hydraulic structures.

CSA-A864, 2000. Guide to the Evaluation and Management of Concrete Structures Affected by Alkali-Aggregate Reaction. *Canadian Standards Association.*

Fecteau, P., Fournier, B., Choquette, M. & Duchesne, J., 2012. *Contribution to the understanding of the so-called alkali–carbonate reaction (ACR).* Austin, Texas, U.S.A., s.n.

Fournier, B. & Bérubé, A., 2000. Alkali-aggregate reaction in concrete: a review of basic concepts and engineering implications. *Canadian journal of civil engineering,* 27(2), p. 167–91.

Gautam, B. P., Panesar, D. K., Sheikh, S. A. & Vecchio, F. J., 2017. Multiaxial expansion-stress relationship for alkali silica reaction-affected concrete. 114(1).

Goshayeshi, N., Gorga, R. V., Sanchez, L. F. M. & Alencar, V., 2018. Contribution to the development of an analytical model to describe AAR kinetics and induced expansion.

Grimal, E., Sellier, A., Le Pape, Y. & Bourdarot, E., 2008. Creep, shrinkage, and anisotropic damage in alkali-aggregate reaction swelling mechanism-Part I: A consti-tutive model. *ACI Materials Journal,* Volume 105, p. 227–235.

Katayama, T., 2010. The so-called alkali–carbonate reaction (ACR) — its mineralogical and geochemical details, with special reference to ASR. *Cement and Concrete Research,* Volume 40, p. 643–675.

Katayama, T. & Grattan-Bellew, P., 2012. *Petrography of Kingston experimental sidewalk at age 22 years - ASR as the cause of deleteriously expansive, so-called alkali-carbonate reaction.* Austin, Texas, U.S.A., s.n.

Larive, C., 1997. *Apports combinés de l'éxpérimentation et de la modélisation à la compréhension de l'alcali-réaction et de ses effets mécaniques,* France: Laboratoire Central des Ponts et Chaussées.

Multon, S., Sellier, A. & & Cyr, M., 2009. Chemo-mechanicalmodeling for prediction of alkali silica reaction (ASR) expansion. *Cement and Concrete Research,* Volume 39, p. 490–500.

Nomura, M., Komastubara, A., Fujimoto, K. & Torii, K., 2013. *Evaluation of maintenance methods for ASR-damaged structures in Hokuriku district, Japan.* Kyoto, Japan, Third International Conference on Sustainable Construction Materials and Technologies.

Poyet, S. et al., 2007. Chemical modelling of alkali silica reaction: Influence of the reactive aggregate size distribution. *Materials and Structures,* Volume 40, p. 229–239.

Sanchez, L. F. M. et al., 2016. *Overall assessment of an ASR affected overpass "Robert-Bourassa/Charest" after nearly 50 years in service.* Foz do Iguaçu, Brazil, 8th International Conference on Bridge Maintenance, Safety and Management.

Sanchez, L. F. M., Noel, M. & Santos, V. A. A., 2018. *Techniques to Rehabilitate Bridge Columns Affected by Alkali-Silica Reaction (ASR).* Melbourne, Australia, s.n.

Sanchez, M., Fournier, B., Jolin, M. & J., D., 2015. Reliable quantification of AAR damage through assessment of the Damage Rating Index (DRI). *Cement and Concrete Research,* Volume 67, p. 74–92.

Saouma, V. & Perotti, L., 2006. Constitutive model for alkali-aggregate reactions. *ACI Materials Journal,* Volume 103, p. 194–202.

Shayan, A., Xu, A. & Salamy, R., 2009. *Effectiveness of CFRP wrapping in confining the expansion of AAR- affected concrete.* Auckland, New Zealand, 7th Austroads Bridge Conference, pp. 24-26.

Ulm, F., Coussy, O., Li, K. & Larive, C., 2000. Thermo-chemo-mechanics of ASR expansion in concrete structures. *ASCE Journal of Engineering Mechanics,* Volume 126, p. 233–242.

Vecchio, F. J. & Shim, W., 2004. Experimental and analytical reexamination of classic concrete beam tests. 130(3), pp. 460-469.

2. LITERATURE REVIEW

2.1 Alkali-aggregate reaction (AAR)

Alkali aggregate reaction (AAR) is one of the most harmful distress mechanisms affecting concrete infrastructure worldwide (Fournier & Bérubé, 2000). Overall, AAR can be subdivided in two main categories: alkali-carbonate reaction (ACR) and alkali-silica reaction (ASR), with the latter being the most frequently observed reaction type. The distress mechanism of ASR is fairly well understood, at least in its major steps, and it can be summarized in the following stages. First, a chemical reaction between the "unstable" silica mineral forms, which are found within fine and/or coarse reactive aggregate materials, and the alkali hydroxides (Na, K – OH) dissolved in the concrete pore solution takes place and generates a secondary product, the so-called alkali-silica gel. This gel then uptakes water from its surrounding environment and swells, therefore inducing expansive pressures (and tensile stresses) within the reacting aggregate material(s) and the adjacent cement paste. Finally, when these stresses reach the tensile strength of the material, major microcracking is generated, which often leads to the loss of material's integrity (mechanical/durability) and, sometimes, functionality of the affected structure (Fournier & Bérubé, 2000; Giaccio, et al., 2008). Conversely, ACR is a much rarer chemical reaction and its distress mechanism is not fully comprehended. Some researchers believe that ACR is a specific form of ASR (Katayama, 2012; Katayama & Grattan-Bellew, 2012) while others attribute to ACR a distinct mechanism (Fecteau, et al., 2012; CSA-A864, 2000).

From a chemical point of view (micro-scale), ASR is described as follows (Kurtis, 2003; Bazant & Steffens, 2000; Glasser & Kataoka, 1981). First, the OH^- ions from the concrete pore solution react with the silanol groups ($Si-O$), which causes the breakage of the siloxane bonds and the creation of additional bonds. Then, on the surface of the aggregate, the silanol groups react with

the OH^- ions, resulting in the liberation of more water. Next, cations of the concrete pore solution (Na^+, K^+ and Ca^{2+}) are attracted to the alkali-silicate ($Si - O^-$) and diffuse into the gel, therefore balancing the negative charge. When saturation is reached, an expansive gel composed of silica, alkalis, water and other ions is generated. This alkali-silicate gel is hydrophilic (swells in the presence of water) and it has a specific volume greater than the reactant substances. Additionally, the gel's chemical composition is variable, which means that its physicochemical properties can be quite diverse, therefore making the prediction of its behaviour difficult.

From a deterioration perspective, Sanchez et al. (2015) proposed a qualitative damage model (Figure 2-1) that describes ASR distress generation and development at the meso-scale (based on petrographic analysis performed at 16x magnification):

At low expansion levels (around 0.05%): cracks type A and B can be observed inside the aggregate particles, cracks in the cement paste are rare and the presence of gel is unlikely. Type A are sharp cracks that correspond to opened cracks cutting the aggregates particles and they are normally produced in previously fractured or more porous zones within the particles. In general, these zones facilitate the alkali ions penetration, therefore leading to a faster reaction process when compared to other areas of the bulk aggregate particle. Complimentarily, type B cracks are referred to as "onion skin" or "en echelon" cracks and they are usually formed in aggregate particles that do not present a preexisting fractured/porous zone. They lead to an almost homogeneous penetration of the alkali ions and the cracks' features are almost parallel (peripheral) to the aggregate's boundaries.

At moderate expansion levels (from 0.10% to 0.12%): the cracks previously described start growing and gel can be observed, especially in the opened cracks in the aggregate particles. Some

cracks type A reach and extend into the cement paste, up to a limited extent. However, cracks type B continue their development inside the aggregate boundary.

At high expansion levels (approximately 0.20%): ASR gel is observed in both the aggregate particles and the cement paste. Cracks type A have completely extended to the cement paste at both sides of the aggregate particles. At the same time, type B cracks usually have already enveloped more than half of the aggregate particles.

At very high expansion levels (0.30% and beyond): an even higher amount of gel is observed when compared to the previous expansion level. Type A cracks link with other cracks (types A and or B) generated at different reactive aggregate particles within the bulk concrete, forming an extensive cracking network. Moreover, type B cracks sometimes extend into the cement paste, either into the interfacial transition zone (ITZ), thus causing aggregate particle debonding, or into the bulk cement paste, therefore connecting to the cracking network.

Note that both cracks described will not mandatorily be present in all reactive aggregates, and that particular crack types may be forming preferentially in certain types of aggregates, depending on their nature.

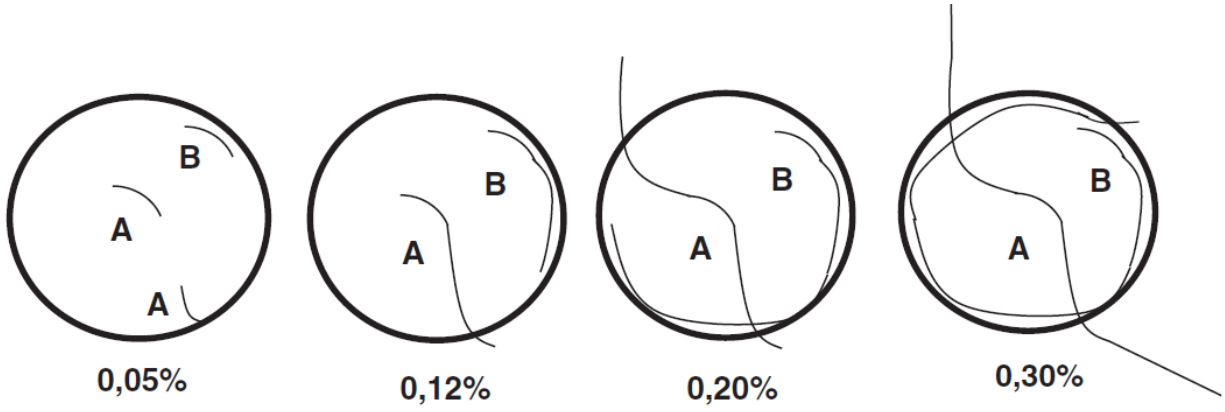

Figure 2-1. Qualitative ASR damage model for expansions varying from 0.05% to 0.30%. Source: Sanchez et al. (2015)

Alternatively, according to Fournier & Bérubé (2000), ACR is a completely different mechanism than ASR. It develops when the dolomite crystals from the aggregates are exposed to the alkali hydroxides from the concrete pore fluid and undergo a dedolomitization process, which forms brucite, calcite and alkali carbonates. This opens up channels (micro-cracks) through which the ions from the pore fluid can penetrate even deeper in the reaction particles. Additionally, the alkali carbonates generated can eventually react with the portlandite in the concrete matrix and regenerate alkali hydroxides in the pore solution, which suggests that the reaction could proceed almost indefinitely. According to Rogers et al. (2000), ACR induces very fast and extensive expansion in concrete prism specimens, as well as severe damage within three years in the field when the conditions are propitious.

Lastly, it is important to emphasize that the approach proposed in Chapters 3 and 4 has been developed for AAR, even though all the validations presented were based on ASR-affected specimens/structural members. Similarly, several of the authors cited in the following sections worked with AAR while others worked only with ASR. Therefore, whenever "ASR" is used it means that the research covered only that reaction, whereas "AAR" refers to broader statements/conclusion, that are applicable to both ASR and ACR.

2.2 Factors affecting AAR expansion

2.2.1 Temperature

It has been found that temperature plays a major role on both AAR kinetics and the final expansion. The effect of temperature on AAR's expansion rate has been reported in the literature several times (Hobbs, 1988; Larive, 1997; Fournier & Bérubé, 2000). According to Ulm et al. (2000), the reaction is thermo-activated, with higher temperatures resulting in faster reaction rates. This phenomenon can be explained by the thermal activation of two processes involved: the dissolution

of the reactive silica at the interfacial transition zone (ITZ) and the reaction product formation. Figure 2-2 shows the results obtained by Larive (1997), which not only shows a faster reaction at a higher temperature, but also a slightly greater final expansion value. The latter is believed to happen due to the higher amount of leaching and lower gel viscosity triggered under higher temperatures.

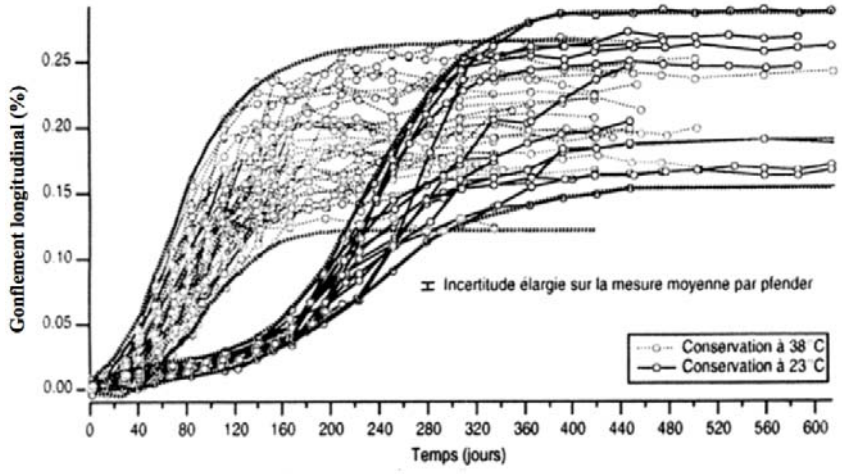

Figure 2-2. Expansion over time for specimens at different temperatures (38ºC and 23ºC). Source: Larive (1997).

Some studies have shown that there is a "pessimum" temperature (38-40ºC) that can be related to the largest ASR expansion when the amount of alkalis is fixed (Locher, 1973; Olafsson, 1986). According to the theory proposed by Urhan (1987) and corroborated by several other authors (Nishibayashi, et al., 1992; Sideris, 1979; Chatterji & Christensen, 1990), an increase in temperature increases both the kinetics of silica dissolution and C-S-H formation. However, beyond a certain threshold, the rate of C-S-H formation exceeds the silica dissolution and the expansion due to ASR deaccelerates. Additionally, Comi & Pignatelli (2012) state that high temperatures not only lead to a faster reaction, but also to a lower viscosity gel, which can enter the concrete voids more easily and reduce the reaction's overall expansive potential.

However, recent correlations between the results from the Accelerated Brazilian Concrete Prism Test (ABCPT), the Accelerated Mortar Bar Test (AMBT) and the Accelerated Concrete Prism Tests (ACPT) have shown that temperature has an effect on both the kinetics and the maximum expansion of AAR (Goshayeshi, et al., 2018). Moreover, higher temperatures (up to 80ºC) display an increase in both the reaction rate and final expansion, without a "pessimum" temperature being observed.

According to Larive (1997), Arrhenius law can be used to take the effect of temperature on the rate of the expansion into consideration. Pesavento et al. (2012) states that Arrhenius law is a concept from the Classic Irreversible Thermodynamics, which defines that the value of a parameter (e.g., the characteristic time τ_c from Larive (1997)) for a given temperature (θ) follows an exponential equation. This new parameter value is based on the original parameter value for a known temperature ($\tau_c(\theta_0)$) and the activation energy of that parameter (U_c), which represents the minimum energy required for the reaction to take place. The equation proposed by Ulm et al. (2000) is presented in Equation 2-1:

$$\tau_c(\theta) = \tau_c(\theta_0) e^{U_c\left(\frac{1}{\theta}-\frac{1}{\theta_0}\right)} \quad (2\text{-}1)$$

Additionally, the original Arrhenius equation is presented in Equation 2-2, where k is the reaction rate, A and R are constants, U_c is the activation energy and θ is the temperature.

$$k = Ae^{\frac{U_c}{R\theta}} \quad (2\text{-}2)$$

2.2.2 Humidity

Water plays an essential role in the development of the reaction for three main reasons (Bazant & Steffens, 2000). First, it constitutes the transport medium for diffusion of the hydroxyl and alkali

ions through the pore solution. Next, water is chemically necessary for the formation of the expansive gel through the dissolution of the siloxane bond. Lastly, the expansion of the gel is directly related to the absorption of water from the surrounding porous medium.

The first to observe the effect of water on ASR development was Vivian (1981), who stated that low enough levels of water (relative humidity) could stop the ASR-induced mechanism. This was later confirmed by other researchers (Olafsson, 1986; Kurihara & Katawaki, 1989).

Larive (1997) highlighted the role of water as both a reagent and a reaction medium. As a reagent, water influences the amplitude of swelling, which is directly related to the amount of water available at the time the reaction takes place. However, only water not consumed by cement hydration may react and lead to AAR development. As a reaction medium, the author states that water must be present in a large enough amount to transport the reactants, therefore corroborating the existence of a humidity threshold capable of ceasing both the swelling and the chemical reaction. Additionally, Larive (1997) also explains that the migration of water within the concrete (i.e., shrinkage) is not affected by AAR, which means both phenomena can be assumed to happen independently of each other.

Poyet et al. (2006) conducted a comprehensive series of tests to evaluate the effect of water on ASR. The lowest relative humidity value they evaluated was 59%, which was found to still be providing enough water for ASR to develop, even though at a slower rate and resulting in a lower maximum expansion (Figure 2-3a). Moreover, the authors evaluated the effect of long (28 days) and short (14 days) wetting and drying cycles on the ASR-induced expansion (Figure 2-3b) and found that the expansion of both short and long cycle cases was always bound by those corresponding to 59% RH and 96% RH.

a b

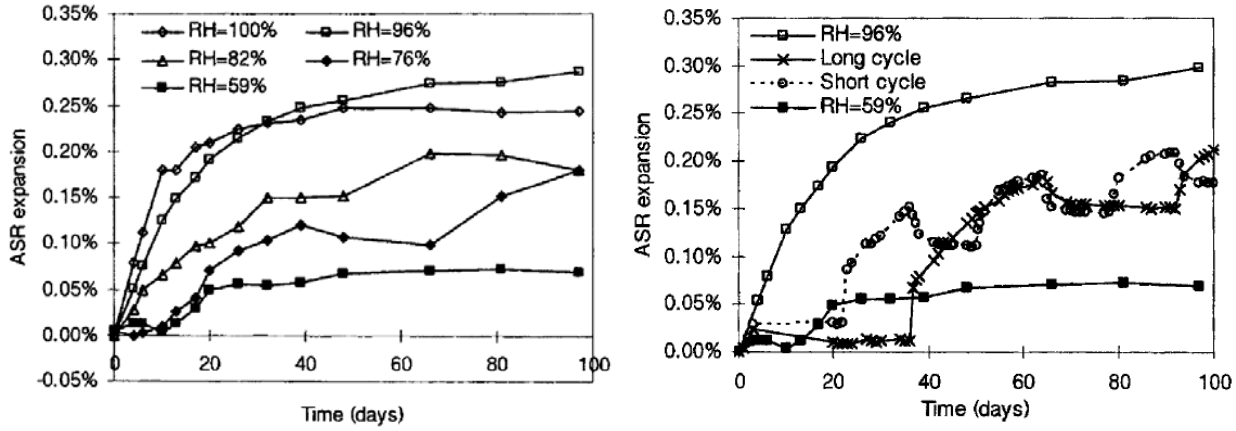

Figure 2-3. Effect of constant and varying relative humidity conditions on ASR expansion. Source: Poyet et al. (2006).

Several models adopt the relationship proposed by Capra and Bournazel (1998) to take relative humidity (h) into consideration. The general approach proposed is presented in Equations 2-3 and 2-4, where ε_{ASR} is the ASR expansion as a function of time (t), relative humidity (h), temperature (T) and stress-state (σ), $\varepsilon^{100\%}$ is the swelling observed at 100% relative humidity, $g(T,\sigma)$ is a function to take temperature and stress-state into consideration, f(h) is a function to take relative humidity into consideration and m is an empirical constant (usually taken equal to 8).

$$\varepsilon_{ASR}(t,h,T,\sigma) = \varepsilon^{100\%}(t)f(h)g(T,\sigma) \tag{2-3}$$

$$f(h) = \left(\frac{h}{100}\right)^{m} \tag{2-4}$$

Alternatively, two other models, one proposed by Bazant & Steffens (2000) and the other by both Li et al. (2000) and Li & Coussy (2002), assume that the initial dry ASR expansive gel needs to absorb/imbibe water in order to create a fluid and expand. The model developed by Bazant & Steffens (2000) assumes that this water absorption/imbibition only happens above a threshold of

85% relative humidity. The second model does not specify a threshold, but instead it assumes that the gel incorporates water continuously based on water availability.

Another more complex model that assesses the effects of water on the reaction was proposed by Poyet et al. (2006). The authors assumed that the rate of the ASR expansion ($\dot{\varepsilon}^{ASR}$) can be described by Equations 2-5 to 2-9. A dimensionless parameter (A) is introduced to describe the ASR progress based on time (t) and the saturation ratio (Sr), which is a function of the mass of water per unit volume of concrete (C) and the saturated mass of water per unit volume of concrete (C_{sat}). The parameter A is described based on the value of a constant characterizing the kinetics of ASR (α_0), on the minimal ASR advancement needed to initiate swelling (A_0, i.e., amount of gel to fill the porous volume around the aggregate), on a function that accounts for the fact that the involved chemical phenomena are limited around residual saturated zones of concrete (β) and on a function that alters ASR kinetics based on Sr (α). Additionally, K is a parameter that relates the expansion to the advancement, $\langle X \rangle^+$ represents the positive part of X, Sr_0^α and Sr_0^β define the thresholds below which α and β are zero, respectively, and m_α and m_β stand for possible non-linearity.

$$\dot{A}(Sr,t) = \frac{\partial A}{\partial t}(Sr,t) = \alpha_0 \alpha(Sr)[\beta(Sr) - A(Sr,t)] \tag{2-5}$$

$$if \begin{cases} A(Sr,t) < A_0 \rightarrow \dot{\varepsilon}^{ASR}(Sr,t) = \dfrac{\partial \varepsilon^{ASR}}{\partial t}(Sr,t) = 0 \\ A(Sr,t) \geq A_0 \rightarrow \dot{\varepsilon}^{ASR}(Sr,t) = \dfrac{\partial \varepsilon}{\partial t}(Sr,t) = K\dot{A}(Sr,t) \end{cases} \tag{2-6}$$

$$\alpha(Sr) = \left(\frac{\langle Sr - Sr_0^\alpha \rangle^+}{1 - Sr_0^\alpha} \right)^{m_\alpha} \rightarrow 0 \leq \alpha(Sr) \leq 1 \tag{2-7}$$

$$\beta(Sr) = \left(\frac{\langle Sr - Sr_0^{\beta}\rangle^{+}}{1 - Sr_0^{\beta}}\right)^{m_\beta} \rightarrow 0 \leq \beta(Sr) \leq 1 \quad (2\text{-}8)$$

$$Sr = \frac{C}{C_{sat}} \quad (2\text{-}9)$$

Note that α_0, A_0, K have to be defined for each case, Sr can be estimated from experimental mass variation recorded data and, according to the parametric study performed by Poyet et al. (2006), the best fit found for the following parameters was $Sr_0^{\alpha} = 0$, $Sr_0^{\beta} = 0$, $m_\alpha = 1$ and $m_\beta = 1$. Additionally, Equations 2-5 to 2-9 cannot be solved analytically when Sr changes over time, which means that Equations 2-5 to 2-9 should be based on the mean value of Sr (represented by $\overline{Sr}$) between two times t and $t + \partial t$, with t_1 being a time included in that interval, as presented in Equation 2-10.

$$A(\overline{Sr}, t) = \beta(\overline{Sr}) - [\beta(\overline{Sr}) - A(\overline{Sr})]e^{-\alpha_0 \alpha(\overline{Sr})(t_1 - t)} \quad (2\text{-}10)$$

Recent studies by Goshayeshi et al. (2018), based on Poyet et al. (2006), indicate that humidity has an effect on both AAR kinetics and the final expansion, which can be correlated to the original AAR kinetics equation proposed by Larive (1997). Moreover, the authors corroborate the theory that there is a minimum humidity threshold that would completely stop the development of AAR, which was assumed to be equal to 50% RH.

2.2.3 Alkali Content

As previously discussed, alkali hydroxides (i.e., Na^+, K^+ and OH^-) from the concrete pore solution are one of the essential components to develop AAR (Fournier & Bérubé, 2000). In general, increasing the alkali content of the mix leads to an increase of the final AAR expansion, as shown in Figure 2-4.

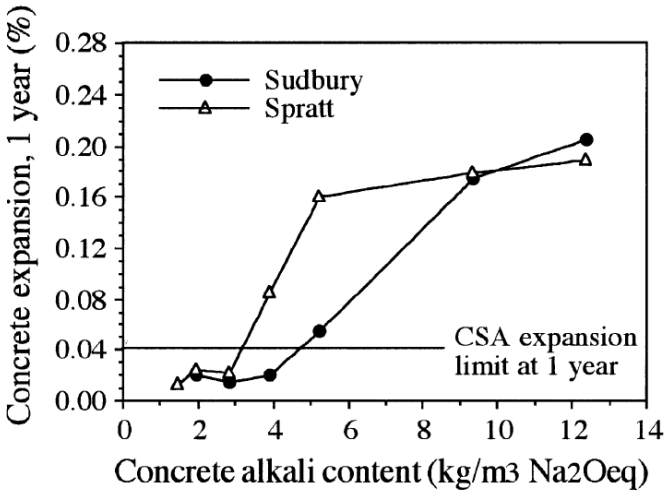

Figure 2-4. One-year expansions of concrete prisms made with highly-reactive Spratt limestone and moderately-reactive Sudbury gravel and different concrete alkali contents. Source: Fournier & Bérubé (2000).

Additionally, it is worth noting that even though Portland cement is the main source of alkalis in concrete, other materials such as aggregates, water, supplementary cement materials (SCM's), special admixtures, seawater and even deicing salts can also contribute in raising the alkali content in the pore solution, thus increasing the risk of distress due to AAR (Diamond, 1989; Fournier & Bérubé, 2000).

Lastly, it has been observed that migration of alkalis thought various processes such as local surface evaporation, electric/magnetic fields or currents and cathodic protection can locally contribute to the alkali content of the concrete pore solution, which contribute to the anisotropic expansion of AAR and the overall distress of the structure (Moore, 1978; Ozol, 1990; Shayan & Song, 2000; Fournier & Bérubé, 2000).

2.3 AAR-induced expansion development

A number of mathematical approaches were developed in the past to represent AAR-induced expansion mechanism. Amongst those, the most widely adopted model was presented by Larive

(1997). The exponential equation presented in Figure 2-5 and Equation 2-11 is capable of simulating the major meso-macro scale steps of AAR expansion (ε_{AAR}) based only on time (t) and three mathematical variables (characteristic time τ_c, latency time τ_l and AAR expansion at infinity $\varepsilon_{AAR}^{\infty}$).

$$\varepsilon_{AAR}(t) = \frac{1 - e^{-\frac{t}{\tau_c}}}{1 + e^{-\frac{(t-\tau_l)}{\tau_c}}} \times \varepsilon_{AAR}^{\infty} \tag{2-11}$$

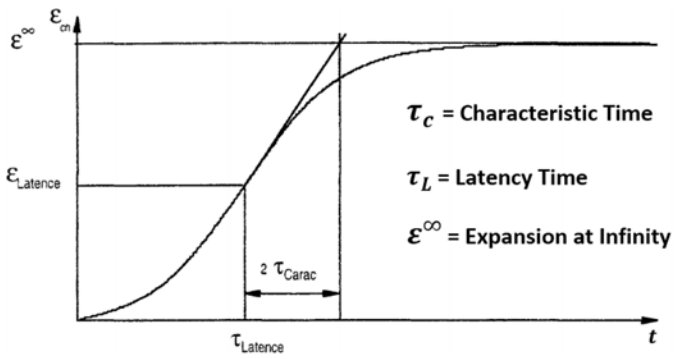

Figure 2-5. Larive's Equation. Source: Adapted from Larive (1997)

Even though most recently developed models describe the kinetics of the reaction by implementing the equation proposed by Larive (1997) or variations of the equation with great success (Comi & Pignatelli, 2012; Pan, et al., 2013b; Saouma & Perotti, 2006), it has one major drawback: the mathematical parameters in Equation 2-11 do not have a clear physical meaning, making it hard to develop an intuitive understanding regarding their range of values.

Alternatively, some researchers have selected a different approach to describe the reaction (Capra & Sellier, 2003; Bangert, et al., 2004; Grimal, et al., 2008a; Grimal, et al., 2008b). Instead of basing their assumptions on mathematical equations to simulate AAR, they have developed chemical equations based on the consumption of AAR's compounds (i.e., alkalis, silica, water, ions, etc.) to try to simulate the reaction's mechanism.

A third and less common option to simulate the reaction is to assume it increases linearly over time. Gocevski & Yildiz (2017) assumed in their AAR-affected dam model that the expansion can be simplified to a linear equation (constant rate), because the expansion rate variation over time during the service life of a massive structure would be negligible.

As previously explained, the most important macroscopic consequence of ASR in concrete is the induced expansion and consequent development of tensile stresses due to gel swelling. Early models treated this expansion as equivalent to a thermal isotropic expansion (Charlwood, 1994); however, several recent studies have shown that the reaction behaves anisotropically and that it is directly related to the stress-state of each region where the reaction develops. Note that the approaches presented below only took into consideration the expansion due to ASR, which was determined by deducting the strain generated by the applied mechanical loads (Poisson effect), creep and shrinkage.

Even though stress-state dependency and expansion redistribution had been observed by Larive (1997) on specimens unrestrained in one direction, Saouma & Perotti (2006) proposed one of the first simple macroscopic approaches to describe the effect of local stress-state on the ASR expansion based on the work of Multon (2003). The authors assumed that when the expansion is restrained by compressive stresses, it is redistributed to the other less-restrained directions as a function of predefined weights along each principal direction. Figure 2-6 shows the weights for uniaxial, biaxial or triaxial stress-state conditions (Saouma & Perotti, 2006), where σ_u represents the ultimate stress and $f`_c$ is the concrete's compressive strength. Additionally, it is worth noting that the approach assumes that a triaxial compressive stress-state will reduce, but not fully neutralize, the expansion.

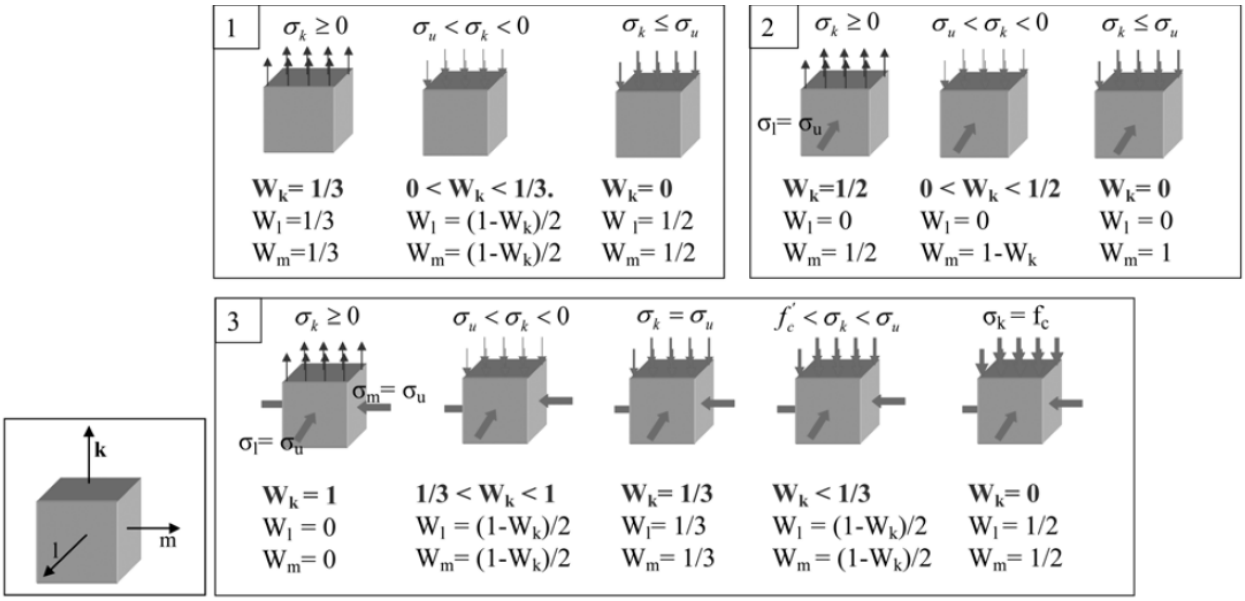

Figure 2-6. Redistribution weights for uniaxial (1), biaxial (2) and triaxial (3) stress-states. Source: (Saouma & Perotti, 2006).

Multon & Toutlemonde (2006) deepened the understanding of the anisotropy of the ASR expansion by evaluating the expansion of several ASR-affected concrete cores subjected to three different confinement conditions. The specimens were either unconfined or passively confined by steel rings of two different thicknesses (3 mm or 5 mm) placed radially along the length of the specimen. The applied stresses for each of the 3 confinement cases were either 0 MPa, 10 MPa or 20 MPa. Therefore, the authors proposed the relationship shown in Figure 2-7 based on the gathered data, where α_{ASR} represents the ASR anisotropy (ratio between the longitudinal expansion/strain ε_{zz}^{imp} and the radial expansion/strain ε_{rr}^{imp}), $\sigma_{zz} - \sigma_{mean}$ is the axial stress deviator, which is defined by the axial stress σ_{zz} and the mean stress σ_{mean}, σ_{res} is the restraining stress generated by the steel rings, R_i is the internal radius (core radius) and R_e is the external radius (core plus steel ring radius). In general, whenever the axial stress deviator is negative (axial direction is more compressed than the radial direction), expansion is reduced axially and increased radially. This effect stabilizes at an ASR anisotropy equal to 0.3, which means that, independently

of the confining pressure on a giving direction, the remaining expansion will still be applied along that axis. Likewise, the authors found that when the axial stress deviator is positive (radial stress is larger than the axial stress), the axial expansion is increased while the radial is reduced. Multon & Toutlemonde (2006) suggest a maximum value of 5 for the ASR anisotropy based on the inverse of the asymptotical coefficient for negative axial stress deviator, but it is important to emphasize that no tensile stresses were applied during the experiments to fully validate this hypothesis.

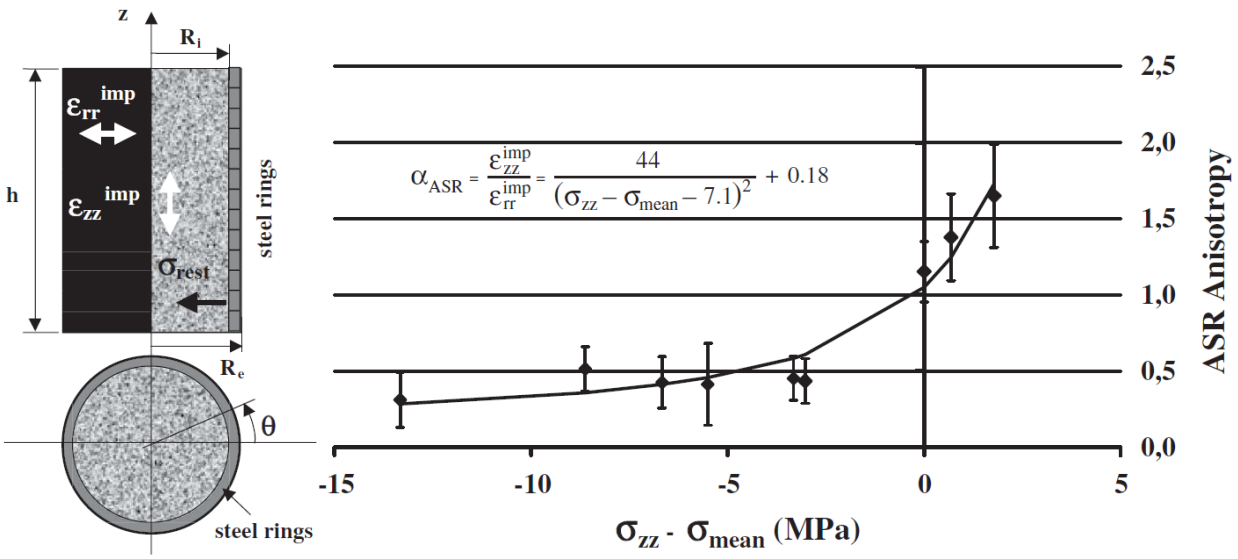

Figure 2-7. Specimen's set up on the left and proposed ASR anisotropy vs axial stress deviator relationship. Source: Multon & Toutlemonde (2006).

Additionally, it is worth noting that the authors were able to assess uniaxial, biaxial and triaxial stress-state conditions based on the restraint imposed by the steel rings. However, biaxial and triaxial stress states with different stresses along the x and y directions were not evaluated.

Another step forward was taken by Gautam et al. (2017). The authors from the University of Toronto tested several reactive and non-reactive 254-mm square cubes (Figure 2-8a) under uniaxial, biaxial and triaxial stress-state conditions to determine a global stress-state dependency

relationship of the ASR expansion. It is clear by analyzing Figure 2-8b that different stress states (given in MPa) have a great influence on the ASR expansion.

a b

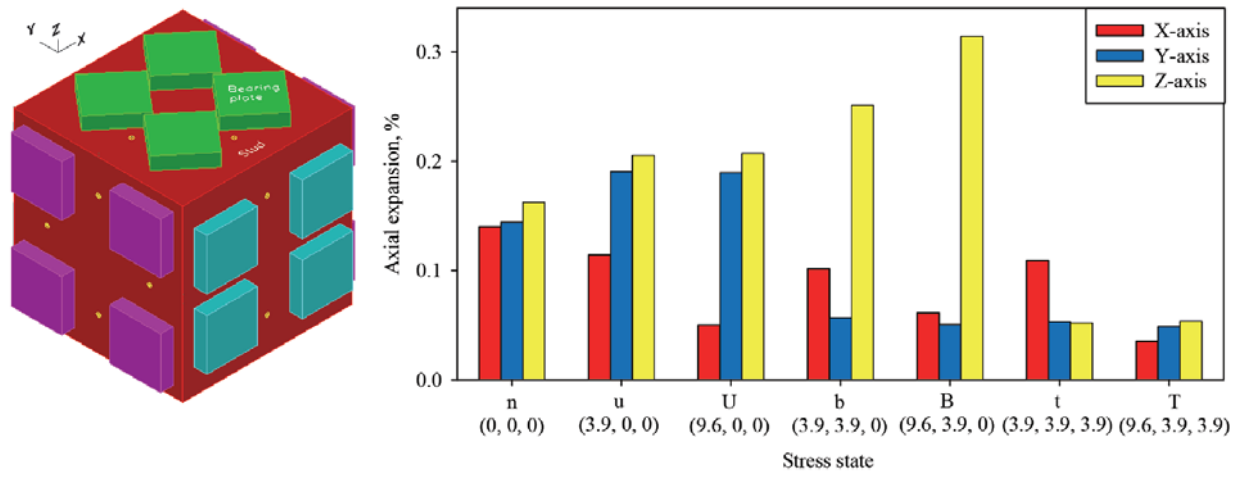

Figure 2-8. Concrete cube specimen on the left and ASR axial expansion (%) vs stress-state (MPa). Source Gautam et al. (2017).

The authors proposed an S-shaped exponential equation to describe the independent behaviour of the reaction in each direction (i) based on the stress (f) and on the initial free volumetric expansion ($pe_{free\ vol}$) - equal to 100%, with 33.3% free expansion ($pe_{free\ i}$) in each direction, as shown in Figure 2-9. According to Equations 2-12 to 2-14, their approach suggests that there is an uncoupled strain (independent of the strain in the other directions) and a maximum possible axial strain in each direction, pe_{un} and pe_{max}, respectively. If the sum of the pe_{max} in the three principal directions is smaller than 100%, then the expansion in each direction (pe_i) is equal to its respective pe_{max}. Otherwise, the difference between the free expansion (100%) and the sum of the pe_{un} has to be distributed among the principal directions according to certain weights. Each weight is calculated as the ratio between the difference between $pe_{max} - pe_{un}$ in each direction and the sum of $pe_{max} - pe_{un}$. Then, the pe_i equals the sum of $pe_{un\ i}$ and the weighed value of $w_i pe_{max\ i}$.

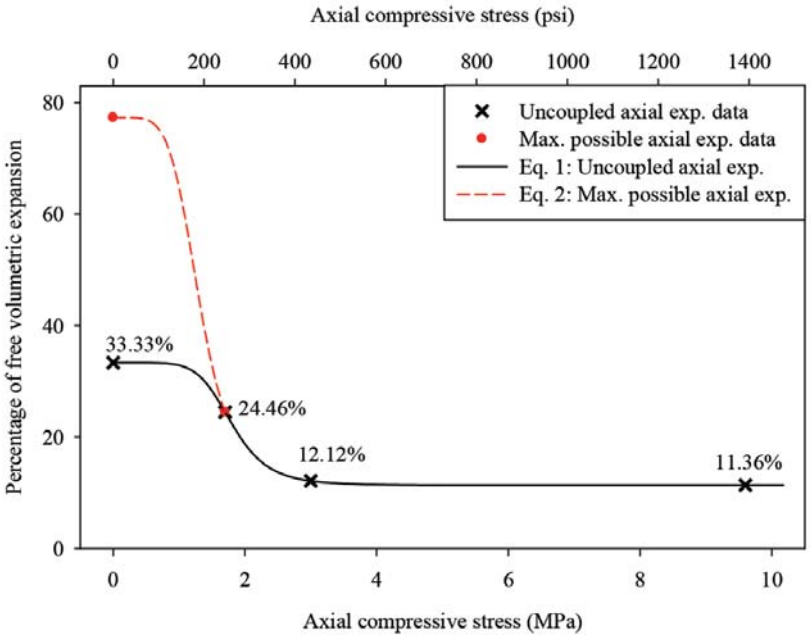

Figure 2-9. Percentage of free ASR volumetric expansion vs axial compressive stress. Source: Gautam et al. (2017)

$$pe_{un} = 11.4 + \frac{33.3 - 11.4}{1 + \left(\frac{f}{1.8}\right)^{6.5}} \; for \; f \leq 0 \tag{2-12}$$

$$pe_{max} = 11.4 + \frac{77.2 - 11.4}{1 + \left(\frac{f}{1.3}\right)^{5.4}} \; for \; f \leq 0 \tag{2-13}$$

$$if \begin{cases} \sum_{i=1}^{3} pe_{max\,i} \leq 100\% \rightarrow pe_i = pe_{max\,i} \\ \sum_{i=1}^{3} pe_{max\,i} > 100\% \rightarrow w_i = \frac{pe_{max\,i} - pe_{un\,i}}{\sum_{i=1}^{3}(pe_{max\,i} - pe_{un\,i})} \rightarrow pe_i = pe_{un\,i} + w_i pe_{ma} \end{cases} \tag{2-14}$$

Other researchers have proposed other approaches, which are sometimes simpler and sometimes more complex. For example, Gocevski & Yildiz (2017) assume that the redistribution is a function

of the stress at which the confinement starts affecting the expansion and the stress at which it totally prevents the reaction from happening, with a linear variation between the two values. Alternatively, Grimal et al. (2008a) and Grimal et al. (2008b) assume that the reaction's swelling stress-state dependency is a consequence of the swelling anisotropy induced by oriented cracking and the interaction between gel pressure and long-term strain (creep). Nevertheless, all approaches presented clearly show that the reaction is highly anisotropic, which means that the it cannot be accurately represented by an isotropic expansion.

2.4 Influence of AAR on the affected material's mechanical properties

According to Crouch & Wood (1990), sound concrete presents high compressive strength and modulus of elasticity, relatively low tensile strength and brittle failure under both compressive and tensile uniaxial loads. However, both its ductility and strength in compression and tension are increased when concrete is confined (triaxially loaded). Additionally, note that the material's sensitivity to confinement can be linked to the presence of small defects or microcracks in the composite material. The complexity of the confinement effect is magnified when dealing with damaged materials (Crouch & Wood, 1990), therefore properly understanding and describing the deterioration in mechanical properties due to AAR expansion is essential in the assessment of structures affected by the reaction (Kubo & Nakata, 2012).

Several researchers found that AAR leads to a substantial and rapid drop in the tensile strength and modulus of elasticity of affected concrete, but the compressive strength seems to be less affected since it only decreases significantly at high expansion levels (Smaoui, et al., 2004; Sanchez, 2014). Furthermore, the Institute of Structural Engineers (ISE, 1992) states that the in-service compressive strength of concrete of structures is generally higher than the 28-day design

value, which means that the deterioration generated by AAR is usually not enough to reduce the actual compressive strength below the original design specifications. However, studies performed by Wood & Johnson (1993) and Wood et al. (1989) suggest that this is true only for low to moderate expansion values (up to 0.10%). Therefore, concrete mixtures subjected to higher expansions have to be carefully assessed because their mechanical properties might actually be a cause of concern.

Giaccio et al. (2008) verified two interesting aspects about the mechanical properties deterioration caused by AAR. First, the compressive strength is affected at all the steps of the reaction (i.e., crack initiation, stable and unstable crack's propagation), which can be linked to the microscopic distress features of AAR damage. Second, the authors found that the reaction rate, the cracking pattern and the mechanical properties deterioration as a result of AAR would vary depending on the type/nature of aggregate used in the mix.

Sanchez et al. (2017) went one step further and measured the influence of the type/nature of aggregates, along with the compressive strength of the specimen, on the mechanical properties of AAR-affected concrete. The authors found that the modulus of elasticity (Figure 2-10) and tensile strength (Figure 2-11) are indeed more heavily affected than the compressive strength, but at higher expansion values the compressive strength can be significantly reduced (up to 30%, as shown in Figure 2-12). The latter was found to be linked to ASR microscopic distress features, which tend to start within the aggregates particles and extend to the cement paste only in moderate to high expansion levels.

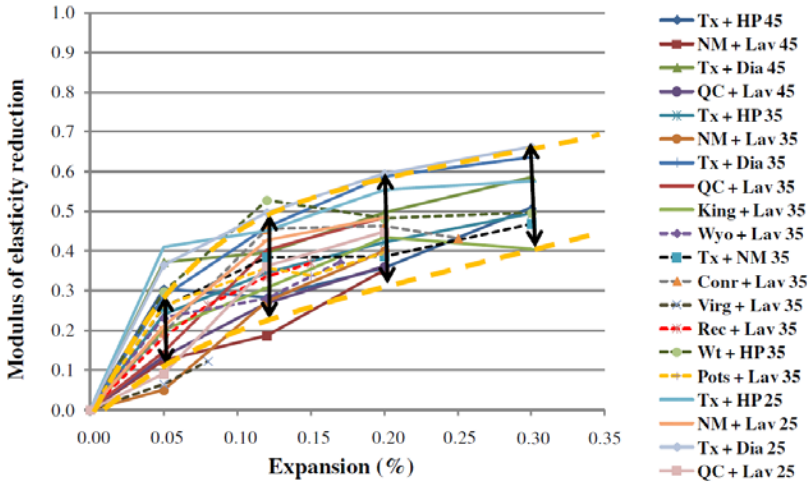

Figure 2-10. Decrease in modulus of elasticity as a function of AAR expansion. Source: Sanchez et al. (2017).

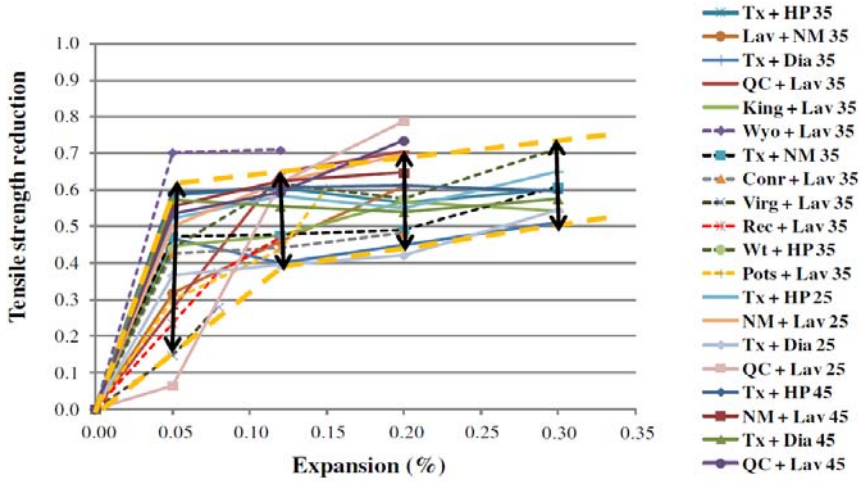

Figure 2-11. Decrease in modulus of elasticity as a function of AAR expansion. Source: Sanchez et al. (2017).

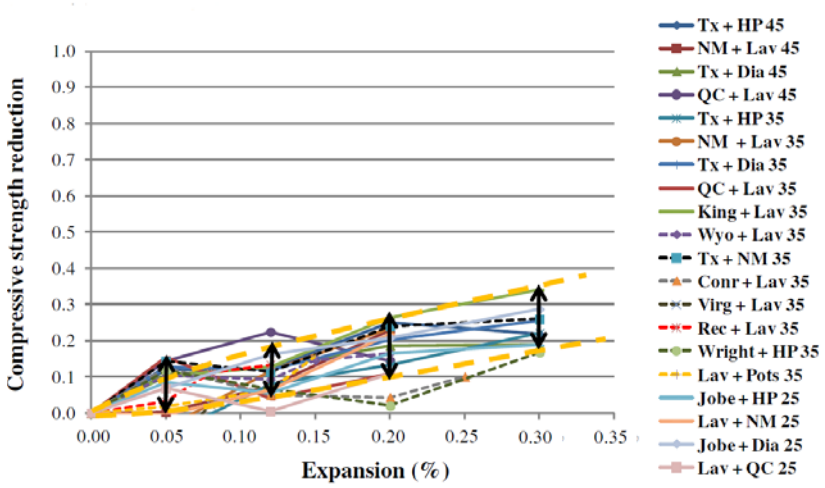

Figure 2-12. Decrease in modulus of elasticity as a function of AAR expansion. Source: Sanchez et al. (2017).

Therefore, it is clear that the deterioration of the mechanical properties of concrete is a very important phenomenon that is directly related to the expansion level, the type/nature of the aggregate and the compressive strength of the material. Most AAR expansion models take this effect into consideration to some extent, but a few models assume either the undamaged (design) or the deteriorated (tested in the field) mechanical properties for the entire service-life of the structure. Based on what was presented, it is possible to state that both these simpler assumptions are not accurate procedures for the prediction of the structural performance of AAR-affected systems over time, because they respectively overestimate the performance at later ages or underestimate the performance at early stages.

2.5 FE modeling of AAR-affected structures

2.5.1 Damage propagation (cracking)

To simulate structural damage (material nonlinearity) in the finite element analysis of reinforced concrete structures, a damage propagation approach has to be specified for the concrete. The approach can be either discrete or continuum (Figure 2-13), with three of the most widely used

continuum approaches being the smeared cracking (either fixed or rotated), the brittle cracking and the damaged plasticity (Malm, 2016). The mathematical implementation of each approach varies from author to author, but the basic concepts of each of the procedures is described next.

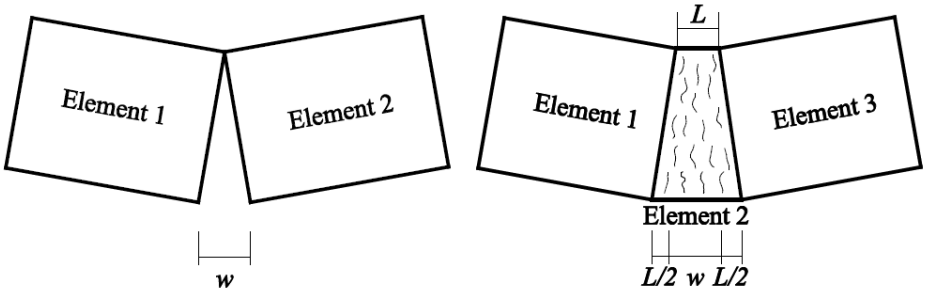

Figure 2-13. Discrete crack on the left and continuum crack on the right. Source: Malm (2016)

The discrete crack approach is usually initiated at the intersection between two adjacent finite elements, where a physical distance representing the real crack is generated (Malm, 2016). However, based on the nature of AAR cracking in macro-structures, this approach is not often used.

Smeared cracking is the most common approach, wherein the cracks are not tracked independently, but rather assumed to be a component of the total strain of the element (Malm, 2016). The total strain is the result of the elastic strain in uncracked concrete and the plastic strain representing the nonlinear behaviour of the crack(s), which is defined by the crack opening displacement divided by the crack band length. Note that if the size of the finite element is larger than the characteristic crack spacing, the cracking strain in that element will represent two or more cracks. However, if the elements are small enough, there will be uncracked elements between cracks and the crack spacing will be captured. This means that the model is highly dependent on the mesh size specified.

Cracks are assumed to occur when the principal tensile stress reaches a stress value defined by the "crack detection surface", which can be either in the biaxial tension region or in a combined tension-compression region (Chaudhari & Chakrabarti, 2012). A representative failure surface in the two-dimensional principal stress planes is presented in Figure 2-14. According to Johnson (2006), the formulation usually forces the constitutive calculations (stress and strain) to be performed independently at each integration point, which allows for a local reduction of the values of stress and stiffness when cracks are present. Additionally, Chaudhari & Chakrabarti (2012) and Johnson (2006) state that the model is usually capable of accounting for tension stiffening, concrete crushing, tension softening, compression hardening and (in the fixed approach) shear retention. The latter is usually defined based on reduction coefficients or predefined curves describing the non-linear behaviour of the material (stress-strain, stress-displacement, fracture energy-crack opening displacement, etc.).

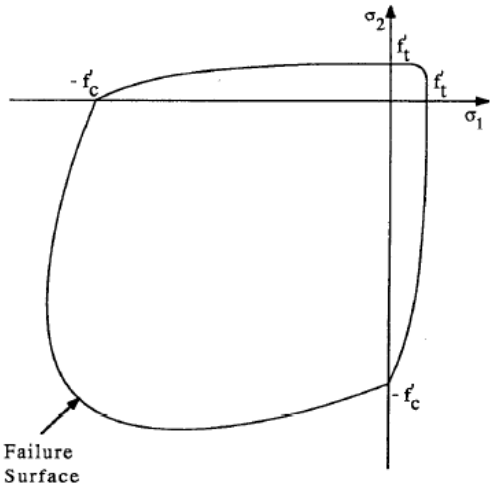

Figure 2-14. Two-dimensional idealized failure surface. Source: Chaudhari & Chakrabarti (2012)

According to Johnson (2006), brittle cracking usually assumes that the concrete behaviour is dominated by tensile cracking. Analogously to the smeared crack model, this model also takes

cracks into consideration in a smeared manner, and the tension stiffening post-cracking behaviour is assumed to be a function of a stress-strain relation or a fracture energy criterion. However, it also includes a brittle failure criterion, which leads to the failure of a certain point when it displays a predefined certain number of cracks, with the associated concrete element losing its tensile stiffness. Additionally, cracks are detected by a specific crack criterion (e.g., Rankine), which means that cracks occur when the maximum principal tensile stress exceeds the specified tensile strength of concrete.

The damaged plasticity approach, sometimes referred to as the equivalent plastic strain, describes a model where cracks are represented by the plastic component of the element total strain in each independent element, which has its mechanical properties reduced based on a specific failure criterion. As shown in Figure 2-15 and according to Wahalathantri et al. (2011), concrete behaves linear-elastically until the elastic limit (yield) surface is reached. From that point on, the tensile or compressive non-linear inelastic behaviour governs, which allows the model to fully describe the damage characteristics of the material by developing plastic strain locally until global equilibrium is reached. Malm (2016) states that the mechanical properties are reduced based on tensile and compressive damage parameters, which can be roughly understood as the damage evolution being accounted for by the ratio of the remaining concrete area in tension, as presented in Figure 2-16. Note that, as the load increases, the plastic zone also increases, therefore simulating damage accumulation. Also, it is possible to qualitatively estimate the size and orientation of cracks by evaluating the plastic strain of each element (Malm, 2016), as well as to simulate tension stiffening, concrete crushing, tension softening and compression hardening by specifying a stress-strain relationship, stress-displacement relationship or by applying a fracture energy criterion (Johnson, 2006).

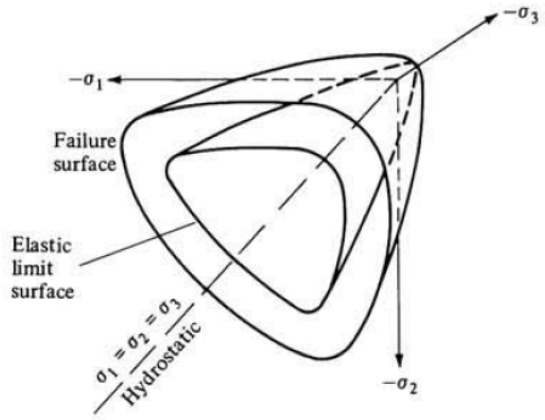

Figure 2-15. Schematic Failure Surface of Concrete in Three-Dimensional Stress Space. Source: Chen (2007)

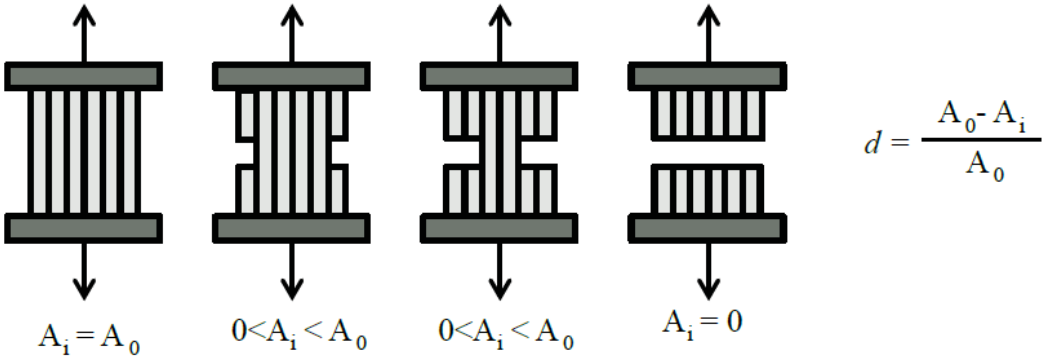

Figure 2-16. Damage parameter simplified concept. Source: Jirasek (2014).

Another important aspect of the damaged plasticity approach is the viscosity coefficient (rate effect), which is especially important in finite element analysis, because it tends to reduce pathological mesh size dependencies. The concrete damaged plasticity model is a local continuum damage model (i.e., strain softening model), which means that the constitutive behaviour at a point is independent of the actions/variables at a distance (neighboring points). Therefore, as soon as an element softens, it takes up all the deformation, leading the damage to grow only in that point and resulting in further softening. To avoid this, viscosity tends to stiffen the element as the deformation rate increases in the softer (damaged) element, which prohibits the deformation to

accumulate in only one element and, consequentially, allows the damage to be propagated to neighboring elements (Niazi, et al., 2012).

According to Malm (2016), one of the main advantages of material models based on fracture mechanics, like the smeared cracking and the damaged plasticity approach, is that they are a function of a small number of parameters, most of which can be correlated to actual physical mechanical properties.

2.5.2 Concrete Material Model

In general, macro-models discretize concrete as either a porous medium (Grimal, et al., 2008a) or as a continuous medium (Saouma & Perotti, 2006), with each approach having its advantages and drawbacks based on their specific computational implementations.

According to Bear & Bachmat (1991), models for a porous medium consist of a solid matrix (also referred to as the solid phase or the skeleton) and void space, which might be occupied by a single-phase fluid or a number of fluid phases (i.e., water, air, etc.). If a number of fluid phases are present, each one occupies a separate portion of the void space, which means that a porous material can be understood as a material consisting of a continuously distributed solid portion through the volume to form a loosely connected matrix and voids (pores). The material can be either a connected porous medium, where all pore spaces are connected (Bear & Bachmat, 1991), or a disconnected porous material, where some pore spaces are separated from the remainder regions (Luikov, 1980). However, the microscopic nature of the void's configuration, which influences the fluid flow, heat transfer, chemical reactions, etc., is extremely complex and random according to Bear & Bachmat (1991). Therefore, a continuous porous medium material model is usually implemented in order to allow for an analytical solution (based on differentiable quantities) for the transport phenomena.

This means that the material is basically a quasi-homogeneous medium that behaves as a continuum that fills up the entire domain, with each phase occupying its own continuum. Note that this procedure intrinsically comes at the expense of the detailed information about the microscopic configuration of the interface boundary conditions and the actual variation of quantities within each phase, but the macroscopic effect of these factors is still maintained through coefficients, whose structure and relationship to the statistical properties of the different phases configuration can still be evaluated (Amhalhel & Furmanski, 1997).

On the other side of the spectrum, continuous medium material models assume that the material completely fills the space that it occupies, leaving no pores or empty spaces, according to Malvern (1969). Moreover, it is also assumed to be described by continuous functions, which implies that all the derivatives will also be continuous and, therefore, the classic theories of elasticity, plasticity, fluid mechanics and thermodynamics lead to predictions that closely match the behaviour observed in the real world for a wide range of conditions. Of course, this approach is a simplification of the real microscopic structure of the material, which means that it might not be applicable for every type of analysis.

Even though the concrete medium of AAR models can be discretized by either one of the two material models presented, selecting which option is the best fit to represent the macro-scale effects of AAR is still one of the biggest arguments within the AAR engineering community. If concrete is assumed to be a continuous medium, the computational implementation is simplified, and the number of parameters required for the analysis is reduced, but the chemical aspects of the reaction (i.e., gel formation, water absorption, consumption of alkalis, consumption of silica, etc.) are assessed only indirectly. However, if it is defined as a continuous porous medium, those aspects

can be taken into consideration directly, but several additional parameters will have to be defined based on complex experiments, literature, fitting or non-technical guesses.

2.5.3 Creep

According to Collins & Mitchell (1997), the stress-strain response of concrete depends on the rate of loading and on the time history of loading. Therefore, creep can be understood as a phenomenon related to the increase in strain when concrete subjected to a constant stress rate, which may be generated from mechanical loading, thermal loading, chemical expansion, etc. Classically, creep is represented as a reduction in the modulus of elasticity, which is defined as the instantaneous ratio of the stress by the strain. However, other more complex modeling approaches also exist, such as that implemented by Pesavento et al. (2012), where the creep strain is decomposed in a viscoelastic and a flow component.

Collins & Mitchell (1997) state that there is great variability in the results when estimating the actual amount of creep induced in the structure. They estimate that an error of $\pm 30\%$ can be expected when tests are not performed. Additionally, note that the value of the modulus of elasticity can easily be reduced by more than 50% over time based on approximate code procedures (which are often used by standards around the world).

In AAR-affected structures, creep is a phenomenon that happens in parallel with AAR-induced expansion. It affects the overall behaviour of the structure – mostly displacement and strain, even though the stresses and the consequential anisotropic (stress-state dependent) AAR expansion is not directly affected. Therefore, from a macroscopic point of view, accounting for creep is important to fully describe the structural response of the system over time.

2.5.4 Shrinkage

According to Collins & Mitchell (1997), concrete naturally loses moisture to the surrounding environment over time and, consequently, decreases in volume unless it is kept at 100% relative humidity or under water. This process is referred to as drying shrinkage, and it is directly proportional to the environmental conditions (relative humidity), time, area exposed to drying, volume of concrete and composition of the concrete, especially the amount of water and the type of aggregate (low or high absorptivity). In general, shrinkage is represented in most standards by a negative strain (decrease in volume) imposed to the structure.

Shrinkage can influence AAR development as follows. First, if enough differential expansion due to shrinkage is generated and the concrete's surface cracks, the ingress and accumulation of water due to rain, snow or splashing might be sufficient to slightly affect the reaction rate locally. Also, even if concrete does not crack, shrinkage is going to change the moisture content in the surface of the concrete, which might also change the reaction kinetics in that region. However, since shrinkage is usually more prominent at the early ages of concrete, and AAR may take a number of years to develop significant internal stresses, the overall combined effect of the two phenomena at the macro scale does not seem to be as crucial as the other mechanisms described in this section, such as creep and mechanical properties deterioration. This has been confirmed by the experiments performed by Larive (1997).

2.6 Types of AAR models

According to Esposito (2016), there are four main categories of AAR models according to the scale being assessed: micro, micro-meso, meso and macro scale. Note that several researchers

assume different criteria for categorizing the models, but the division proposed by Esposito (2016) is very intuitive and simple to follow, and it is adopted here in the following review.

Macro-scale models are based on the simulation of concrete expansion at the structural level, generally by imposing strains that represent the effect the expansive gel has over time. Initially this strain was assumed to be equivalent to a thermal isotropic strain, but recent studies (Section 2.3) have shown that AAR behaves anisotropically and that the kinetics play a very important role in the development of the reaction. Macro-models usually focus more on the macroscopic effect of AAR on structural members or structural systems, i.e., failure load, reinforcement yielding, cracking, deformation, effects on serviceability, etc., without going too much in depth into modeling the chemistry involved in the reaction.

Meso-scale models can be defined as approaches based on the internal pressure at the concrete material level, which is usually modeled as a heterogeneous material composed primarily of aggregates (coarse and fine) and a matrix phase. The matrix is usually assumed to consist of cement paste and, sometimes, an interfacial transition zone (ITZ) that bonds the aggregates and the cement paste. In general, the expansion is obtained as a direct result of the swelling gel, which means that a clear definition of the microstructure of the concrete (volume fraction and shape of aggregates) in a representative elementary volume (REV), as well as the mechanical properties of each phase, are essential for the accuracy of the simulation. Note that, due to the higher complexity of the microstructure and description of the physicochemical aspects involved, meso-scale models naturally have more variability than macro-scale models.

Micro-meso-scale models describe the reaction at the aggregate level as a function of the gel production. They usually couple the physicochemical aspects of AAR based on mass or volume

change of the gel with the mechanical behaviour of concrete, which is imposed to the model as strain or pressure at the aggregate level.

Lastly, micro-scale models focus on the ion diffusion-reaction mechanisms at the chemical reaction products level, therefore being the most accurate type of approach to describe the chemistry of AAR in detail (silica consumption, alkali consumption, alkali leaching, etc.). Even though their main goal can be understood as describing why and how the chemical reaction leads to the formation of reaction products, they have also been used to describe the mechanical consequences of AAR at the concrete material level.

2.7 AAR macro-models

2.7.1 Introduction

This section reviews proposed macro-scale models that describe AAR-induced expansion and damage. The review only focuses on macro models, since the goal of the present work is to develop a simple yet reliable model to assess the macroscopic structural implications of AAR in concrete structures, where the chemistry involved is only accounted for indirectly. A summary of all the models is provided in Table 2-1. Note that only papers published after 2000 were considered. Previous AAR models were assumed to be outdated, because recent researches have dramatically changed the way the reaction is understood. Therefore, models like those developed by Charlwood (1994), Léger et al. (1996), Huang & Pietruszczak (1996), Capra & Bournazel (1998) and Malla & Wieland (1999) are not discussed in depth. The model developed by Grimal et al. (2008a) and Grimal et al. (2008b), which is presented in the next section, requires special attention. It is categorized by Esposito (2016) as a micro-meso model (based on gel production at the aggregate level), but it was included here as a potential "macro-model," because it has already been successfully used to model both concrete members and massive concrete structures.

		Ulm et al. (2000)	Li & Coussy (2002, 2004)	Capra & Sellier (2003)	Bangert et al. (2004)	Fairbairn et al. (2004) & Farage et al. (2004)	Saouma & Perotti (2006)	Grimal et al. (2008 a, b)	Esposito & Hendrix (2012)	Comi et al. (2012)	Pesavento et al. (2012)	Pan et al. (2013a, b)	Winnicki et al. (2014)	Ben Ftima et al. (2017)	Gocevski & Yildiz (2017)	Gorga et al. (2018)
Kinetics	based on Larive	X	X			X	X		X	X	X	X	X	X		X
	based on chemical equations			X	X			X								
	linear														X	
ASR expansion	Ortho or Anisotropic (stress-state dependent)			X			X	X	X			X		X	X	X
	Isotropic (stress-state independent)	X	X		X	X				X	X		X			
ASR temperature dependency	varying temp over time	X	X			X	X		X	X	X	X	X	X	X	X
	constant temp			X	X			X								
ASR humidity dependency	varying humidity over time				X	X				X	X		X	X	X	X
	constant humidity	X	X	X			X	X	X			X				
mechanical properties	yes - function of ASR expansion or other			X	X		X	X	X	X	X	X	X			X
	no - undamaged values or field measurements only	X	X			X								X	X	
damage propagation (cracking)	smeared cracking approach	X	X	X		X	X	X	X	X	?		X	X		
	damaged plasticity cracking approach										?	X			X	X
	brittle model				X						?			X		
Concrete material type	Porous media			X	X	X		X	X	X	X					
	Continuous (isotropic or anisotropic)	X	X				X					X	X	X	X	X
Creep	yes							X			X	X		X		X
	no	X	X	X	X	X	X		X	X			X		X	
Shrinkage	yes							X			X			X		
	no	X	X	X	X	X	X		X	X		X	X		X	X
Application	Massive structures											X		?	?	
	Slender structures							X		X				?	?	X
	Cores or Specimens			X		X	X	X	X	X	X	X	X	?	?	
Validation	Massive structures	X	X			X	X	X		X		X	X	X	X	X[1]
	Slender structures	X	X	X	X											X
	Cores or Specimens				X											X
Number of dimensions of the	3D		X			X		X		X		X		X	X	X
	2D	X	X	X	X		X		X	X	X		X			

[1] ongoing work

Table 2-1 – Comparison of existing AAR models

Ulm et al. (2000) were the first to implement Larive's (1997) findings on their model, which allowed them to start describing ASR more accurately than ever before. Their approach presents a few downsides (isotropic expansion, no creep, constant humidity, based on outdated sources, etc.), but it was undoubtedly a big step towards accurately simulating the reaction.

The original model developed by Li & Coussy (2002) and Li & Coussy (2004) was quite interesting, but it had similar issues to that proposed by Ulm et al. (2000). Regardless of the proven applicability of the model, not accounting for the anisotropy of the reaction, creep and varying humidity unfortunately makes the model too outdated to be largely implemented as an analysis tool today, especially based on the current knowledge about the physicochemical mechanisms of the reaction.

Several poromechanical models were developed by Capra & Sellier (2003), Bangert et al. (2004) and both Fairbain et al. (2004) and Farage et al. (2004). These models started going on a slightly different direction by describing the physicochemical aspects of the reaction in greater detail and as a function of several additional variables. The mathematics implemented are quite elegant but complex, and the need to fit several parameters is unavoidable, since complex micro-scale phenomena are being represented macroscopically. This, unfortunately, tends to make those models less user-friendly and less attractive for large-scale implementation by the engineering community.

Saouma & Perotti (2006) developed what is probably the most important AAR model up to date. The approach is simple but accurate, intuitive but not trivial, which is probably why so many models after 2006 refer to theirs when looking for a solid strong starting point. Unfortunately, the model presents three main limitations: it was only used in 2D simulations, it was only applied to

simulate concrete cores and it does not account for creep. However, its relevance in the state-of-the-art is unquestionable.

Grimal et al. (2008a) and Grimal et al. (2008b) took the poromechanical approach previously described to the next level by modeling both the chemistry and physics involved in the AAR reaction in detail. It accounts for almost every single parameter possible (from the amount of gel required to fill the porosity connected to the reactive aggregates to capillarity effects), but it comes at the cost of defining 32 variables. The approach has proved its applicability in modeling macro-structures, but the large number of variables involved makes it a complex model for widespread validation.

On a similar fashion to the model developed by Grimal et al. (2008a) and Grimal et al. (2008b), even though not to the same extent, were the poromechanical models developed by Esposito and Hendrix (2012) and Pesavento et al. (2012). Both are interesting approaches, but their main drawback is that they lack validations and, especially, applications. The models present only concrete core applications, which is not enough to fully prove its capacity to describe the structural implications of ASR.

Comi et al. (2012) proposed a poromechanical model that was slightly simpler and more intuitive than the other previously presented. It accounts for several of the most important parameters, but unfortunately the researchers still assumed the reaction to behave isotropically and they disregarded the effect of creep. This, unfortunately, limits the full description of the distress mechanism by the model as previously stated, even though the model is undoubtedly very promising.

One of the most auspicious models developed recently was proposed by Pan et al. (2013a) and Pan et al. (2013b). They take into consideration almost all relevant aspects of the reaction, with the exception of the effect of the varying humidity over time on the kinetics and the compressive strength deterioration. The authors also proved the applicability of the model (especially that by Pan et al. (2013b)). Even so, the model could still be made more intuitive by attributing a physical meaning to some of the coefficients and by updating it based on the current literature (mechanical properties deterioration, for example).

Winnicki et al. (2014) continuous model is quite attractive as well; however, similarly to Comi et al. (2012), the authors assume the reaction to be isotropic and do not take creep into consideration. Moreover, the controversial conclusion they reached regarding ASR improving the structural response of a dam structure goes against what has been observed by most analyses in the literature. Therefore, it can be assumed that the model is not capable of describing the structural implications of ASR in its full extent.

The model developed by Ben Ftima et al. (2017) accounts for every single one of the parameters defined as the most important for AAR, with the exception of the mechanical properties deterioration as a function of the expansion level. However, the approach seems to be very specific for dams, instead of being a general AAR model, and the authors do not provide a lot of details regarding how they take those parameters into consideration. Therefore, it is hard to really evaluate what the model proposes and how the simulation is actually accounting for in the variables.

Lastly, the approach proposed by Govevski & Yildiz (2017) is another recent model that is noteworthy to mention. However, the assumption that the expansion can be assumed to be linear is only acceptable for massive structures, therefore limiting the applicability of the approach to other types of structures. Moreover, it does not account for creep, and it has its own approach to

simulate the anisotropic behaviour of the expansion, which does not exactly follow what has been proposed by other authors when stating, for example, that there is a stress capable of completely stopping AAR. Therefore, this model is not assumed to be the ideal AAR model.

A description of each individual model follows. They are described according to whether or not they account for the following: (i) kinetics, (ii) stress-state dependency, (iii) temperature, (iv) humidity, (v) mechanical properties deterioration, (vi) cracking, (vii) concrete material medium (i.e., porous or continuum medium), (viii) creep, (ix) shrinkage, (x) application, and (xi) validation. Application refers to analyses that were used to compare the results of the model to measured data (displacements, stresses, strains, etc.) or observed patterns (cracking, failure mechanism, etc.) without the need of fitting parameters to each specific situation. Conversely, validation refers to analyses where results were fitted to match the desired data (for example, several displacements points measured were used to define the kinetics of the reaction and estimate the future behaviour), where results were evaluated though parametric studies of specific coefficients or where results were not compared to any recorded or observed data.

2.7.2 Ulm et al. (2000)

Kinetics: Based on Larive (1997)

AAR expansion: Isotropic (stress-state independent)

Temperature: Assumed to influence the kinetics and to vary over time (based on transient thermal analyses and Arrhenius law)

Humidity: Is not accounted for

Mechanical properties deterioration due to AAR: Values are assumed to be constant (the author implies that either the initial or damaged values are used)

Damage propagation (cracking): Smeared cracking approach (based on William & Warnke (1975))

Concrete material type: Continuous medium

Creep: Is not accounted for

Shrinkage: Is not accounted for

Application: None

Validation: Idealized 2D gravity dam and 2D bridge box-girder

Comment: The role of water (humidity) is referred to as critical, but it is not accounted for due to a lack of available data at the time. Also, the concept of thermal and humidity characteristic lengths is introduced. In summary, the length predicts that the region between the surface and the characteristic length is subjected to temperature and relative humidity gradients, respectively, based on the ambient conditions, while the remaining central region remains unaffected by the surroundings. The main conclusion drawn from this approach is that the humidity characteristic length has values much lower than those of the heat characteristic length (usually centimeters instead of meters), which implies that the role of nonuniform moisture distribution in slender structures (bridges, for example) may be similar to that of nonuniform temperature on the structural degradation of massive structures. Additionally, it is important to emphasize that the authors observed the formation of an ASR front propagation in the dam in the zone described by the heat characteristic length (due to differential expansions), which chronologically lead to irreversible localized cracking, crack propagation to the surface and delamination.

2.7.3 Li & Coussy (2002) and Li & Coussy (2004)

Kinetics: Based on Larive (1997)

AAR expansion: Isotropic (stress-state independent)

Temperature: Assumed to influence the kinetics and to vary over time (based on transient thermal analyses)

Humidity: Is not accounted for

Mechanical properties deterioration due to AAR: Values are assumed to be constant (the author implies that either the initial or damaged values are used)

Damage propagation (cracking): smeared cracking approach

Concrete material type: Continuous medium

Creep: Is not accounted for

Shrinkage: Is not accounted for

Application: None

Validation: 2D bridge pier - (Li & Coussy, 2002), 3D suspension bridge pylon - (Li & Coussy, 2004) and 3D hydraulic powerplant (Veytaux facility, Switzerland) - (Seignol, et al., 2016).

Comment: Humidity is assumed to always be fully available for the reaction to fully develop, even though the authors emphasize the role of water on the kinetics and gel swelling mechanism. Moreover, the model can be implemented as an imposed chemo-plastic model, suitable for structural analyses, or a coupled chemo-plastic model, which is capable of assessing both structural and material levels (even though it has more parameters that require fitting). Finally, it is important

to emphasize that Seignol et al. (2016) enhanced the model when analyzing a powerplant, by implementing the stress-state dependent anisotropic expansion relationship proposed by Multon & Toutlemonde (2006), by modifying the mechanical properties according to Seignol et al. (2012) and by incorporating the influence of temperature and humidity on the reaction kinetics proposed by Seignol et al. (2009).

2.7.4 Capra & Sellier (2003)

Kinetics: Based on mathematical equations to simulate the gel formation chemistry as a function of the percentage of reacted alkalis

AAR expansion: Orthotropic (stress-state dependent)

Temperature: Assumed to influence the kinetics, but it is assumed to be constant over time (based on Arrhenius law)

Humidity: Assumed to influence the kinetics, but it is assumed constant over time

Mechanical properties deterioration due to AAR: Are not accounted for as a function of the expansion (only tensile strength and modulus of elasticity)

Damage propagation (cracking): smeared cracking approach (based on a probabilistic orthotropic model)

Concrete material type: Saturated continuous porous medium

Creep: Is not accounted for

Shrinkage: Is not accounted for

Application: 2D concrete cores

Validation: Idealized 2D reinforced concrete beams

Comment: The only application presented was for the 2D AAR-affected concrete cores, with more accurate results being found for lower uniaxially-applied loads. However, the authors demonstrated the applicability of the approach by analyzing idealized AAR-affected reinforced concrete beams (without transverse reinforcement) under self-weight only and applied loads plus self-weight. Note that this approach can be seen as the predecessor of the model developed by Grimal et al. (2008a) and Grimal et al. (2008b).

2.7.5 **Bangert et al.** (2004)

Kinetics: Based on chemical equations proposed by the authors

AAR expansion: Isotropic (stress-state independent)

Temperature: Assumed to influence the kinetics (indirectly), but it is assumed to be constant over time

Humidity: Assumed to influence the kinetics and to vary over time (based on mathematical approach)

Mechanical properties deterioration due to AAR: Are accounted for as a function of the expansion

Damage propagation (cracking): Brittle isotropic cracking approach

Concrete material type: Partially saturated continuous porous medium

Creep: Is not accounted for

Shrinkage: Is not accounted for

Application: None

Validation: Idealized 2D unreinforced concrete beams and idealized 2D concrete specimens

Comment: The kinetics of the reaction are assumed to be directly dependent on non-constant humidity conditions (input in the formulation) and indirectly dependent on constant temperature conditions, concrete mix and type of aggregate, which are used to calibrate the unknown parameters of the model. Also, mechanical properties deterioration (modulus of elasticity and concrete strength) are only assumed to take place when restraining or differential expansion is present (i.e., the free expansion case maintains the original properties), and this deterioration is a function of the expansion level.

2.7.6 Fairbain et al. (2004) and Farage et al. (2004)

Kinetics: Based on Larive (1997)

AAR expansion: Isotropic (stress-state independent)

Temperature: Assumed to influence the kinetics and to vary over time (based on Arrhenius law)

Humidity: Assumed to influence the kinetics and to vary over time

Mechanical properties deterioration due to AAR: Are not accounted for – values are assumed to be constant and equal to the undamaged concrete properties

Damage propagation (cracking): Smeared cracking approach

Concrete material type: Saturated continuous porous medium

Creep: Is not accounted for

Shrinkage: Is not accounted for

Application: 3D concrete cores tested by Larive (1997)

Validation: 3D concrete gravity dam (Furnas dam, Brazil)

Comment: The reaction kinetics, even though based on Larive (1997), are determined through a reverse analysis, i.e., FE results are adjusted to match measured values and determine the expansion vs time behaviour. Also, the model assumes that regions with values lower than the minimum humidity to activate the reaction display only 5% of the final expansion. Finally, the FE application results for displacement at the top of the dam matched measured data from the real dam; however, this was the only result that was evaluated.

2.7.7 Saouma & Perotti (2006)

Kinetics: Based on Larive (1997) and on Ulm et al. (2000)

AAR expansion: Anisotropic (stress-state dependent) based on Multon (2003)

Temperature: Assumed to influence the kinetics and to vary over time (based on transient thermal analyses)

Humidity: Assumed to influence the kinetics, but it is assumed to be constant over time

Mechanical properties deterioration due to AAR: Are accounted for as a function of the expansion

Damage propagation (cracking): Smeared cracking approach

Concrete material type: Continuous medium

Creep: Is not accounted for

Shrinkage: Is not accounted for

Application: Concrete cores tested by Multon (2003)

Validation: 2D arch-gravity dam (name and location not specified)

Comment: The suggested approach to analyze dams is to assume humidity equal to 100% at all times for the entire structure and to perform a transient thermal analysis based on the initial temperature of the dam, surrounding air and water, to define the variation of the thermal fields over time. Then, those thermal field values are imported to the mechanical model, which defines the strains (and consequential stresses) due to differential temperature-dependent AAR expansions, thermal loads and mechanical loads.

2.7.8 Grimal et al. (2008a) and Grimal et al. (2008b)

Kinetics: Based on the chemical advancement law proposed by the authors.

AAR expansion: Anisotropic (stress-state dependent)

Temperature: Assumed to influence the kinetics, but it is assumed to be constant over time (based on Arrhenius law)

Humidity: Assumed to influence the kinetics, but it is assumed to be constant over time (based on Poyet et al. (2006))

Mechanical properties deterioration due to AAR: Are accounted for as a function of the expansion

Damage propagation (cracking): smeared cracking approach (based on a probabilistic orthotropic model)

Concrete material type: Partially saturated continuous porous medium

Creep: Is accounted for

Shrinkage: Is accounted for

Application: 3D concrete cores tested by Multon & Toutlemonde (2006) and 3D AAR-affected reinforced concrete beams tested in the lab by Grimal et al. (2008b)

Validation: 3D gate-structure dam (Temple-de-Sur dam, France) by Sellier et al. (2009) and 3D gravity dam (Chambon dam, France) by Chulliat et al. (2017)

Comment: Even though it is considered a micro-meso model, this approach has been successfully used to model macroscopic structures such as beams and dams. The model has a total of 32 variables, most of which require fitting based on the literature and extensive laboratory tests for specimens with different confinement ratios. Specific instructions on how to calibrate all variables for specific cases are described by Grimal et al. (2008b).

2.7.9 Esposito and Hendrix (2012)

Kinetics: Based on Larive (1997) and Ulm et al. (2000)

AAR expansion: Anisotropic (stress-state dependent) based on Saouma & Perotti (2006) and Multon (2003)

Temperature: Assumed to influence the kinetics and to vary over time (based on Arrhenius law)

Humidity: Assumed to influence the kinetics, but it is assumed to be constant over time

Mechanical properties deterioration due to AAR: Are accounted for as a function of the expansion

Damage propagation (cracking): smeared cracking approach

Concrete material type: Saturated continuous porous medium

Creep: Is not accounted for

Shrinkage: Is not accounted for

Application: 2D concrete cores tested by Ahmed et al. (2003)

Validation: None

Comment: Conversely to what most other researchers have done, the model is only capable of modeling two cases: sound concrete subjected to mechanical loads and free ASR-expansion. Also, the only application performed is a comparison of the mechanical properties deterioration as a function of the expansion of concrete cores. Note that the model predicted the stiffness loss more accurately than Saouma & Perotti (2006), but not the strength degradation.

2.7.10 Comi et al. (2012)

Kinetics: Based on Larive (1997)

AAR expansion: Isotropic (stress-state dependent)

Temperature: Assumed to influence the kinetics and to vary over time (based on thermal transport analyses)

Humidity: Assumed to influence the kinetics and to vary over time (based on moisture transport analyses)

Mechanical properties deterioration due to AAR: Are accounted for as a function of the expansion - only the modulus of elasticity, and it is based on a bilinear curve obtained from Larive (1997) and Multon (2003) experiments.

Damage propagation (cracking): smeared cracking approach

Concrete material type: Partially saturated continuous porous medium

Creep: Is not accounted for

Shrinkage: Is not accounted for

Application: 2D concrete cores tested by Larive (1997) and Multon & Toutlemonde (2010), as well as 3D reinforced concrete beams tested by Multon & Toutlemonde (2010)

Validation: 2D gravity dam (Beauharnois dam, Canada) with the findings being compared to Bérubé et al; (2000) and Kladec et al. (1995).

Comment: In order to take the effect of temperature and humidity on the ASR expansion into consideration, the authors suggest that the fields defined by the transport analyses should be imported to the mechanical analysis. Also, based on Ulm et al. (2000), they expanded the previously mentioned concepts of humidity and temperature characteristic lengths, and corroborated the findings of Ulm et al. (2000) regarding the effect of those parameters on slender and massive structures. Lastly, the authors mentioned that the effect of humidity on the dam analyzed was so small that it could have been disregarded, even though the same is not true for slender structures.

2.7.11 Pesavento et al. (2012)

Kinetics: Based on Larive (1997)

AAR expansion: Isotropic (stress-state independent)

Temperature: Assumed to influence the kinetics and to vary over time (based on Arrhenius law)

Humidity: Assumed to influence the kinetics and to vary over time (based on Ulm et al. (2000) and Steffens et al. (2003)).

Mechanical properties deterioration due to AAR: Are accounted for as a function of the reaction development – linear reduction

Damage propagation (cracking): is accounted for, but the type of approach is not mentioned (it is only referred to as based on non-local isotropic damage theory)

Concrete material type: Partially saturated continuous porous medium

Creep: Is accounted for (composed of a flow and a viscoelastic component)

Shrinkage: Is accounted for

Application: 2D concrete cores tested by Larive (1997) – constant temperature and humidity – and Poyet (2003) – constant temperature and varying humidity.

Validation: None

Comment: This model is a macro-model, but it presents aspects of meso-models because its focus seems to be the details of the chemistry involved, while still being potentially applicable to structures. Also, two different ASR phases are modeled in order to describe the reaction kinetics: first, the gel formation through a first-order kinetic law based on Larive (1997), Ulm et al. (2000) and Dron & Brivot (1993), and second, the water absorption and gel expansion through the rate of induced ASR isotropic strain based on Larive (1997) and Steffens et al. (2003). Finally, the model accounts for the evolution of both permeability and porosity due to ASR-induced cracking and microcracking, as well as shrinkage, in order to describe the effect of drying and rewetting observed by Poyet (2003), where the total strain measured would decrease during drying and increase again during rewetting.

2.7.12 Pan et al. (2013a) and Pan et al. (2013b)

Kinetics: Based on Larive (1997)

AAR expansion: Anisotropic (stress-state dependent) based on Saouma & Perotti (2006) and Multon (2003)

Temperature: Assumed to influence the kinetics and to vary over time (based on Ulm et al., 2000, Arrhenius law and thermal transport analyses)

Humidity: Assumed to influence the kinetics, but it is assumed to be constant over time (based on Capra & Bournazel (1998))

Mechanical properties deterioration due to AAR: Are accounted for as a function of the expansion (only tensile strength and modulus of elasticity, based on Capra & Sellier (2003))

Damage propagation (cracking): damaged plasticity cracking approach

Concrete material type: Continuous medium

Creep: Is accounted for

Shrinkage: Is not accounted for

Application: 3D concrete cores tested by Multon & Toutlemonde (2006) and 3D arch dam (Kariba dam, located between Zambia and Zimbabwe) – Pan et al. (2013b)

Validation: 3D gravity dam (Fontana dam, USA) – Pan et al. (2013a)

Comment: Note that Pan et al. (2013a) and Pan et al. (2013b) models are slightly different, with only the latter accounting for creep, introducing a parameter to take humidity into consideration based on Capra & Bournazel (1998) and treating the expansion as anisotropic (stress-state dependent). Also, humidity was assumed to be 100% in the entire structure in the analysis of the Fontana dam; therefore, only heat transport and mechanical analyses were performed. For that case, the authors disregarded the heat of hydration of concrete by assuming that it was not

important for the long-term behaviour, and the only parameter that was compared was the cracking pattern of the dam. For the Kariba dam, humidity was again taken as 100%, and the authors neglected the effect of temperature, because they assumed that the seasonal temperature variations were low enough. The calculated radial displacements and most of the vertical displacements matched well the measured data, which was gathered for over 30 years. Cracking pattern predictions were also good based on the limited information available.

2.7.13 Winnicki et al. (2014)

Kinetics: Based on Larive (1997)

AAR expansion: Isotropic (stress-state independent)

Temperature: Assumed to influence the kinetics and to vary over time (based on Arrhenius law and thermal transport analyses)

Humidity: Assumed to influence the kinetics and to vary over time (based on Capra & Bournazel (1998), and humidity transport analyses)

Mechanical properties deterioration due to AAR: Are accounted for as a function of the expansion

Damage propagation (cracking): smeared cracking approach

Concrete material type: Continuous medium

Creep: Is not accounted for

Shrinkage: Is not accounted for

Application: 2D concrete cores tested by Larive (1997) and Poyet (2003)

Validation: 2D gravity dam (Fontana dam, USA)

Comment: The approach used for the dam was to first perform a thermal analysis and a humidity transfer analysis to determine the temperature and relative humidity fields, and then those values were used as input parameters for the mechanical model, which accounts for the ASR dependency on those variables. It is also important to emphasize that the resulting cracking pattern obtained from the 2D analysis of the gravity dam matched relatively well the actual cracking patterns observed in the dam, even though no further comparison with measured data is presented. However, the authors reached a "controversial" conclusion by stating that the ASR-affected model has a global safety factor greater than that of the undamaged structure, which means that the structural implications of ASR improved the structural response of the dam. They explain that this probably happened because the ASR expansion led to higher compressive stresses in the critical zone, therefore having this beneficial effect.

2.7.14 Ben Ftima et al. (2017)

Kinetics: Based on Larive (1997)

AAR expansion: Anisotropic (stress-state dependent) based on Saouma & Perotti (2006) and Multon (2003)

Temperature: Assumed to influence the kinetics and to vary over time (based on Saouma & Perotti (2006), and transient thermal analyses)

Humidity: Assumed to influence the kinetics and to vary over time (based on Saouma & Perotti (2006), and humidity transport analyses)

Mechanical properties deterioration due to AAR: Values are assumed to be constant (the author implies that either the initial or damaged values are used)

Damage propagation (cracking): Smeared cracking approach and brittle cracking approach

Concrete material type: Continuous medium

Creep: Is accounted for

Shrinkage: Is accounted for

Application: Not presented

Validation: 3D gravity dam and 3D dam spillway (name and location not specified)

Comment: The author developed two complementary models to assess the sliding safety factor (SSF) and structural safety margin of dams: a quasi-static explicit continuum nonlinear finite element smeared cracking model (QSE-FEM-S) and a quasi-static explicit continuum nonlinear finite element discrete model using the strength reduction approach (QSE-FEM-D). According to Malm (2016), quasi-static analyses are suggested for cases where the material non-linearity is causing convergence problems. For example, brittle failure material models usually require this method because the brittle failure generally increases the kinetic energy content of the response as a result of the sudden drop in the load carrying capacity. Basically, the solution technique consists of using a dynamic solver (either implicit or explicit) to solve a static numerical analysis where the load is applied slowly enough to minimize the kinetic energy, which significantly reduces the inertia effects. Furthermore, Ben Ftima et al. (2017) state that this technique is advantageous in the specific case of highly nonlinear problems involving large concrete structural models with concrete softening and complex contact interactions.

The approach proposed by Ben Ftima et al. (2017) consists of the temperature and humidity fields being calculated first through thermal analyses and humidity transport analyses, and then those

values are used as input parameter in the QSE-FEM-S. The latter is then calibrated based on field measurements and used to identify the dominant crack patterns forming potential failure planes. After, the QSE-FEM-D is used to compute the initial condition to perform a "stability analysis" based on the results from the other steps. Additionally, note that the discrete model is adopted for two reasons. First, it yields classical engineering scalar stability indicators for the SSF, which are easier to interpret than the results from the smeared cracking model. Second, QSE-FEM-S displays intrinsic uncertainty when estimating the fracture parameters and, consequently, the safety margin of the dam.

2.7.15 Govevski & Yildiz (2017)

Kinetics: Linear

AAR expansion: Anisotropic (stress-state dependent)

Temperature: Assumed to influence the kinetics and to vary over time (based on thermal transport analyses)

Humidity: Assumed to influence the kinetics and to vary over time (based on humidity transport analyses)

Mechanical properties deterioration due to AAR: Values are assumed to be constant (the author implies that either the initial or damaged values are used)

Damage propagation (cracking): damaged plasticity approach

Concrete material type: Continuous medium

Creep: Is not accounted for

Shrinkage: Is not accounted for

Application: Not presented

Validation: 3D hydroelectric power plant (name and location not specified)

Comment: The model is used by Hydro-Quebec. It was developed for modeling dam structures, which is the reason why it assumes AAR kinetics are linear over time and the maximum expansion is equal to that of the optimum temperature and humidity AAR conditions. Also, the anisotropic volumetric expansion is assumed to be a function of a volumetric confinement parameter and a uniaxial confinement parameter, which are directly related to the stress at which the confinement starts affecting the expansion and the stress at which it totally prevents the reaction from happening, respectively. Finally, it is important to emphasize that the authors do not provide many details about how they address several components of AAR such as temperature dependency and the damage propagation approach, therefore making it hard to fully comprehend the proposed approach.

2.8 Gap in the state-of-the-art

Based on the review of existing models, there is still need for a model capable of accurately describing the physicochemical nature of AAR, without overcomplicating or oversimplifying the reaction or the parameters involved. In order to do so, a model must accomplish the following:

1- It should account for the most important parameters influencing the reaction: anisotropic expansion, kinetics dependency on varying temperature and varying humidity, mechanical properties deterioration as a function of the expansion, and creep.

2- It needs to be validated through comparisons with both experiments and real case scenarios, ideally in three dimensions.

3- It should be capable to intuitively attribute physical meaning to the parameters involved, without the need of fitting or non-technical guesses, to provide easy interpretation of the results.

The model proposed in this thesis and described in Chapters 3 and 4 attempts to meet the above criteria. The kinetics of the reaction are based on the model proposed by Larive (1997) and modified by Goshayeshi et al. (2018). The stress-dependency of the AAR expansion is anisotropic based on the approach proposed by Gautam et al. (2017). The model accounts for the influence of both temperature and humidity on the reaction kinetics and for their variation over time (based on Goshayeshi et al. (2018). The deterioration of the mechanical properties is accounted for as a function of the expansion based on Sanchez et al. (2017). To model damage propagation, a damaged plasticity cracking approach is adopted, based on the concrete damaged plasticity (CDP) material model available in Abaqus (Simulia, 2014), and concrete is treated as a continuous medium. Creep is accounted for, whereas shrinkage is neglected. All these phenomena are incorporated into a finite element structural model, which is validated by 3D simulations of sound reinforced concrete beams - tested by Vecchio and Shim (2004), AAR-affected push-off specimens - tested by Sanchez et al. (2016) and a reinforced concrete slender (bridge) pier, the Robert-Bourassa Charest Overpass, Canada, which was experimentally assessed by Sanchez et al. (2016).

2.9 References

Ahmed, T., Burley, E., Rigden, S. & Abu-Tarir, A., 2003. The effect of alkali reactivity on the mechanical properties of concrete. Construction and Building Materials, Volume 17, pp. 123-144.

Amhalhel, G. & Furmanski, P., 1997. Problems of modeling flow and heat transfer in porous media.

Bangert, F., Kuhl, D. & Meschken, G., 2004. Chemo-hygro-mechanical modelling and numerical simulation of concrete deterioration caused by alkali-silica reaction. Volume 28, p. 689–714.

Bazant, Z. & Steffens, A., 2000. Mathematical model for kinetics of alkali–silica reaction in concrete. Cement and Concrete Research, Volume 30, p. 419–428.

Bear, J. & Bachmat, Y., 1991. Introduction to modeling of transport phenomena in porous media. Netherlands: Kluwer Academic Publishers.

Ben Ftima, M., Léger, P. & Boussaha, F., 2017. Nonlinear finite elements for the assessment of hydraulic concrete structures affected by alkali-aggregate reaction: a case study. Chambéry, France, Wiley, pp. 176-187.

Bérubé, M. A., Durant, B., Vézina, D. & Fournier, B., 2000. Alkali–aggregate reactivity in Québec (Canada). Canadian Journal of Civil Engineering, Volume 27, p. 226–245.

Capra, B. & Bournazel, J. P., 1998. Modeling of induced mechanical effects of alkali-aggregate reactions. Cement and Concrete Research, Volume 28, p. 251–260.

Capra, B. & Sellier, A., 2003. Orthotropic modelling of alkali-aggregate reaction in concrete structures: Numerical Simulations. Mechanics of Materials, 35(8), p. 817–830.

Charlwood, R., 1994. A review of alkali aggregate in hydro-electric plants and dams. International Journal on Hydropower Dams, p. 73–80.

Chatterji, S. & Christensen, P., 1990. Studies of alkali-silica reaction. Part 7. modeling of expansion. Volume 20, p. 285–290.

Chaudhari, S. V. & Chakrabarti, M. A., 2012. Modeling of concrete for nonlinear analysis using finite element code ABAQUS. 44(7), pp. 14-18.

Chen, W., 2007. Plasticity in Reinforced Concrete. New York: J Ross.

Chulliat, O., Grimal, E. & Bourdarot, E., 2017. Chambon Dam - A struggle against AAR. Chambéry, France, Wiley.

Collins, M. & Mitchell, D., 1997. Prestressed concrete structures. Toronto, Canada: Response Publications.

Comi, C., Kirchmayr, B. & Pignatelli, R., 2012. Two-phase damage modeling of concrete affected by alkali–silica reaction under variable temperature and humidity conditions. Volume 49, p. 3367–3380.

Comi, C. & Pignatelli, R., 2012. Modeling of degradation induced by alkali-silica reaction in concrete structures, Milano, Italy: Politecnico de Milano - Department of Structural Engineering.

Crouch, R. & Wood, J., 1990. Damage evolution in ASR affected concretes. Engineering Fracture Mechanics, Volume 35, p. 211–218.

CSA-A864, 2000. Guide to the Evaluation and Management of Concrete Structures Affected by Alkali-Aggregate Reaction. Canadian Standards Association.

Diamond, S., 1989. ASR – Another look at mechanisms. Kyoto, Japan, Proceedings of the 8th International Conference on Alkali-Aggregate Reaction in Concrete - ICAAR, pp. 83-94.

Dron, R. & Brivot, F., 1993. Thermodynamic and kinetic approach to the alkali–silica reaction. Part 2: Experiment. Cement and Concrete Research, Volume 23, p. 93–103.

Esposito, R., 2016. The deterioration impact of alkali-silica reaction on concrete. Parma, Italy: Ipskamp Drukkers.

Esposito, R. & Hendrix, M. A. N., 2012. Degradation of the mechanical properties in ASR-affected concrete: overview and modeling. Aix-en-Provence, France, Strategies for Sustainable Concrete Structures - Numerical Modeling.

Fairbairn, E. et al., 2004. Smeared cracking FEM simulation of alkali silica expansion using a new macroscopic coupled model. Beijing, China, s.n.

Farage, M., Alves, J. & Fairbairn, E., 2004. Macroscopic model of concrete subjected to alkali-aggregate reaction. Cement and Concrete Research, Volume 34, p. 495–505.

Fecteau, P., Fournier, B., Choquette, M. & Duchesne, J., 2012. Contribution to the understanding of the so-called alkali–carbonate reaction (ACR). Austin, Texas, U.S.A., s.n.

Fournier, B. & Bérubé, A., 2000. Alkali-aggregate reaction in concrete: a review of basic concepts and engineering implications. 27(2), p. 167–91.

Gautam, B. P., Panesar, D. K., Sheikh, S. A. & Vecchio, F. J., 2017. Multiaxial expansion-stress relationship for alkali silica reaction-affected concrete. 114(1).

Giaccio, G., Zerbino, R., Ponce, J. & Batic, R., 2008. Mechanical behavior of concretes damage due to ASR. Cement and Concrete Research, Volume 38, p. 993–1004.

Glasser, D. & Kataoka, N., 1981. The chemistry of 'alkali-aggregate' reaction. Cement and Concrete Research, Volume 11, p. 1–9.

Gocevski, V. & Yildiz, E., 2017. Macro-modelling of AAR-affected hydraulic structures. Chambéry, France, Wiley.

Goshayeshi, N., Gorga, R. V., Sanchez, L. F. M. & Alencar, V., 2018. Contribution to the development of an analytical model to describe AAR kinetics and induced expansion.

Grimal, E., Sellier, A., Le Pape, Y. & Bourdarot, E., 2008a. Creep, shrinkage, and anisotropic damage in alkali-aggregate reaction swelling mechanism-Part I: A consti-tutive model. ACI Materials Journal, Volume 105, p. 227–235.

Grimal, E., Sellier, A., Le Pape, Y. & Bourdarot, E., 2008b. Creep, shrinkage, and anisotropic damage in alkali-aggregate reaction swelling-Part II: Identifications of model parameters and applications. ACI Materials Journal, Volume 105, p. 236–242.

Hobbs, D., 1988. Alkali–silica reaction in concrete, London, U.K.: Thomas Telford.

Huang, M. & Pietruszczak, S., 1996. Numerical analysis of concrete structures subjected to alkali-aggregate reaction. 1(4), p. 305–319.

ISE, I. o. S. E., 1992. Structural Effects of Alkali-Aggregate Reaction: Technical Guidance on the Appraisal of Existing Structures, London, UK: s.n.

Jirasek, M., 2014. Modeling of localized inelastic deformation, Prague: Course material from Advanced course on modelling of localized inelastic deformation, Czech Technical University.

Johnson, S., 2006. Comparison of Nonlinear Finite Element Modeling Tools for Structural Concrete, Champaign, Illinois, U.S.A.: University of Illinois at Urbana-Champaign - Department of Civil and Environmental Engineering.

Katayama, T., 2012. Late-expansive ASR in a 30-year old PC structure in eastern Japan. Austin, Texas, USA, s.n., p. 10.

Katayama, T. & Grattan-Bellew, P., 2012. Petrography of Kingston experimental sidewalk at age 22 years - ASR as the cause of deleteriously expansive, so-called alkali-carbonate reaction. Austin, Texas, U.S.A., s.n.

Kladek, I., Pietruszczak, S. & Gocevski, V., 1995. Modelling of mechanical effects of alkali–silica reaction in Beauharnois powerhouse. Proceedings 5th International Symposium on Numerical Models in Geomechanics, p. 639–645.

Kubo, Y. & Nakata, M., 2012. Effect of reactive aggregate on mechanical properties of concrete affected by alkali-silica reaction. Austin, Texas, s.n.

Kurihara, T. & Katawaki, K., 1989. Effects of moisture control and inhibition on alkali silica reaction. Kyoto, Japan, s.n., p. 629–634.

Kurtis, K., 2003. Chemical additives to control expansion of alkali–silica reaction gel: proposed mechanisms of control. Journal of Materials Science, p. 2027–2036.

Larive, C., 1997. Apports combinés de l'éxpérimentation et de la modélisation à la compréhension de l'alcali-réaction et de ses effets mécaniques, France: Laboratoire Central des Ponts et Chaussées.

Léger, P., Côté, P. & Tinawi, R., 1996. Finite element analysis of concrete swelling due to alkali-aggregate reactions in dams. Volume 60, p. 601–611.

Li, K. & Coussy, O., 2002. Concrete ASR degradation: From material modelling to structure assessment. Concrete Science Engineering, Volume 4, p. 35–46.

Li, K. & Coussy, O., 2002. Evaluation de l'état mécanique des ouvrages dégradés par la réaction alcali-granulat. Volume 6, p. 835–852.

Li, K. & Coussy, O., 2004. Numerical assessment and predic-tion method for chemo-mechanical deterioration of ASR-affected structures. Canadian Journal of Civil Engineering, Volume 31, p. 432–439.

Li, K. et al., 2000. Chemoelastic modelling of alkali-silica reaction in concrete. Québec City, Canada, 11th International Conference on Alkali-Aggregate Reaction in Concrete, p. 989–998.

Locher, F. W., 1973. Ursache und wirkungsweise der alkalireaktion. Volume 40.

Luikov, A., 1980. Heat and mass transfer. Moscow: Mir Publishers.

Malla, S. & Wieland, M., 1999. Analysis of an arch-gravity dam with a horizontal crack. Volume 72, p. 267–278.

Malm, R., 2016. Guideline for FE analyses of concrete dams, s.l.: Energiforsk.

Malvern, L., 1969. Introduction to the mechanics of a continuous medium. New Jersey: Prentice-Hall Inc..

Moore, A., 1978. Effect of electric current on alkali–silica reaction. Indiana, U.S.A., In Proceedings of the Fourth International Conference on Alkali–Aggregate Reaction - ICAAR, p. 69–71.

Multon, S., 2003. Evaluation Expérimentale et Théorique des Effets Mécaniques de l'Alcali Réaction sur des Structures Modéles, PhD. Thesis, Paris, France: Université de Marne la Vallée.

Multon, S. & Toutlemonde, F., 2006. Effect of applied stress on alkali-silica reaction-induced expansion. Cement and Concrete Research, Volume 36, pp. 912-920.

Multon, S. & Toutlemonde, F., 2010. Effect of moisture conditions and transfer on alkali silica reaction damaged structures. Cement and Concrete Research, Volume 40, p. 924–934.

Niazi, M., Wisselink, H. & Meinders, V., 2012. Viscoplastic Regularization of Local Damage Models: A Latent Solution. Volume 504-506, pp. 845-850.

Nishibayashi, S. et al., 1992. Alkali-silica reaction-Japanese experience - Alkali- silica reaction in concrete..

Olafsson, H., 1986. The effect of relative humidity and temperature on alkali expansion of mortar bars. Ottawa, Canada, 7th International Conference on Concrete Alkali-aggregate Reactions.

Ozol, M., 1990. Alkali–silica reaction of concrete electrical substation piers accelerated by electrical currents - Petrography applied to concrete and concrete aggregates, s.l.: ASTM STP 1061.

Pan, J., Feng, Y., Jin, F. & Zhang, C., 2013b. Numerical prediction of swelling in concrete arch dams affected by alkali-aggregate reaction. European Journal of Environmental and Civil Engineering, 17(4), pp. 231-247.

Pan, J., Feng, Y., Xu, Y. & Jin, F., 2013a. Chemo-damage modeling and cracking analysis of AAR-affected concrete dams. Science China – Technological Sciences, 56(6), pp. 1449-1457.

Pesavento, F. et al., 2012. Modeling alkali–silica reaction in non-isothermal, partially saturated cement based materials. Volume 225, p. 95–115.

Poyet, S., 2003. Etude de la degradation des ouvrages en beton atteints de la reaction alcali-silice: approche experimentale et modelisation numerique multiechelle des degradations dans un environnement hydro-chemo-mecanique variable, Ph.D. Thesis, Paris, France: University of Marne la Vallee.

Poyet, S. et al., 2006. Influence of Water on Alkali-Silica Reaction: Experimental Study and Numerical Simulations. ASCE Journal of Materials in Civil Engineering, 18(4), pp. 899-1561.

Rogers, C., Grattan-Bellew, P., Hooton, R. & Ryell, J., 2000. Alkali–aggregate reactions in Ontario. Canadian Journal of Civil Engineering, 27(2), p. 246–260.

Sanchez, L., 2014. Contribution to the Assessment of Damage in Aging Concrete Infrastructures Affected by Alkali-Aggregate Reaction, PhD. Thesis, Quebec City, Quebec: Department of Geology and Geological Engineering, Université Laval.

Sanchez, L. F. M. et al., 2017. Overall assessment of Alkali-Aggregate Reaction (AAR) in concretes presenting different strengths and incorporating a wide range of reactive aggregate types and natures. Volume 93, pp. 17-31.

Sanchez, L. F. M., Fournier, B., Bastien, J. & Mitchell, D., 2016. Assessment of structures subjected to concrete degradation, Quebec, Canada: ASCET.

Sanchez, L. F. M. et al., 2016. Overall assessment of an ASR affected overpass “Robert-Bourassa/Charest” after nearly 50 years in service. Foz do Iguaçu, Brazil, 8th International Conference on Bridge Maintenance, Safety and Management.

Sanchez, M., Fournier, B., Jolin, M. & J., D., 2015. Reliable quantification of AAR damage through assessment of the Damage Rating Index (DRI). Cement and Concrete Research, Volume 67, p. 74–92.

Saouma, V. & Perotti, L., 2006. Constitutive model for alkali-aggregate reactions. ACI Materials Journal, Volume 103, p. 194–202.

Seignol, J. F. et al., 2009. Hydro-power structure affected by alkali-aggregate reaction: a case study involving numerical re-assessment. Jeju, Korea, s.n.

Seignol, J. F., Boldea, L., Leroy, R. & Godart, B., 2016. Numerical model applied to the reassessment of the serviceability and safety of AAR-affected power-plant. Sao Paulo, Brazil, s.n., p. 10.

Seignol, J. F., Omikrine-Metalssi, O., Baghdadi, N. & Toutlemonde, F., 2012. From AAR to DEF: numerical modeling of structures affected by expansive reactions in concrete. Austin, Texas, s.n.

Sellier, A. et al., 2009. Combination of Structural Monitoring and Laboratory Tests for Assessment of Alkali-Aggregate Reaction Swelling: Application to Gate Structure Dam. 106(3).

Shayan, A. & Song, G., 2000. Electrochemical effects of combined AAR and cathodic protection in concrete, Quebec City, Canada: Proceedings of the Eleventh International Conference on Alkali–Aggregate Reaction - ICAAR.

Sideris, K., 1979. Uber das temperatur-expansionsmaximum bei der alkalikieselsaeurereaktion. 32(10), p. 508–509.

Simulia, D. S. C., 2014. Abaqus/CAE - Complete Abaqus Environment - version 6.14, Providence, RI, USA: Simulia Dassault Systèmes Corporation.

Smaoui, N., Bérubé, M., Fournier, B. & Bissonnette, B., 2004. Influence of specimen geometry, orientation of casting plane, and mode of concrete consolidation on expansion due to ASR. Cement, Concrete and Aggregates, 26(2), p. 58–70.

Steffens, A., Li, K. & Coussy, O., 2003. Ageing approach to water effect on alkali-silica reaction. Degradation of structures. Journal of Engineering Mechanics, Volume 129, p. 50–59.

Ulm, F., Coussy, O., Li, K. & Larive, C., 2000. Thermo-chemo-mechanics of ASR expansion in concrete structures. ASCE Journal of Engineering Mechanics, Volume 126, p. 233–242.

Urhan, S., 1987. Alkali silica and pozzolanic reactions in concrete. Part 1: Interpretation of published results and an hypothesis concerning the mechanism. Volume 17, p. 141–152.

Vecchio, F. J. & Shim, W., 2004. Experimental and analytical reexamination of classic concrete beam tests. 130(3), pp. 460-469.

Vivian, H. E., 1981. The effect of drying on reactive aggregate and mortar expansions. Cape Town, South Africa, s.n., p. 252–28.

Wahalathantri, B., Thambiratnam, D., Chan, T. & Fawzia, S., 2011. A material model for flexural cracks simulation in reinforced concrete elements using ABAQUS. Brisbane, Australia, eddBE2011, pp. 260-264.

Willam, K. J. & Warnke, E. P., 1975. Constitutive model for the triaxial behavior of concrete. Seminar on Concrete Structures Subjected to Triaxial Stresses. International Association for Bridge and Structural Engineering, Volume 19.

Winnicki, A., Serega, S. & Norys, F., 2014. Chemo-plastic-modelling of alkali-silica reaction (ASR). Computational Modelling of Concrete Structures (EURO-C), Volume 2, p. 765–774.

Wood, G. & Johnson, R., 1993. The Appraisal and Maintenance of Structures with Alkali-Silica Reaction, s.l.: Institution of Structural Engineers.

Wood, G., Norris, P. & Leek, D., 1989. Physical behavior of AAR damaged concrete in structures and in test conditions. Kyoto, Japan, 8th ICAAR - International Conference on Alkali-Aggregate Reaction in Concrete.

3. PAPER 1 - ENGINEERING-BASED FE APPROACH TO APPRAISE SLENDER REINFORCED CONCRETE STRUCTURES AFFECTED BY ALKALI-AGGREGATE REACTION (AAR)

Gorga, R.V.[a]; Sanchez, L. F. M.[b]; Martín-Pérez, B.[c]; Noël, M.[d]

(a) MASc. candidate – University of Ottawa, ON, Canada
(b) Assistant professor – University of Ottawa, ON, Canada
(c) Associate professor – University of Ottawa, ON, Canada
(d) Assistant professor – University of Ottawa, ON, Canada

Abstract

Modeling the expansion and damage generated by alkali-aggregate reaction (AAR) in reinforced concrete structures is quite complex, yet necessary to obtain accurate predictions of the structural response of distressed concrete members. Several AAR models have been developed over the past decades to predict expansion and damage at the material (microscopic) or the structural (macroscopic) scales. However, those models tend to either neglect or overemphasize the critical physicochemical parameters of the reaction, which limits their applicability. Therefore, a new simple yet reliable finite element approach is proposed to fill this gap. It accounts for the most important parameters affecting AAR through an engineering approach, without the need for non-technical guesses or to "fit" model parameters. The proposed finite element model is validated through the computational simulation of reinforced concrete specimens cast and monitored in the laboratory.

***Keywords**: alkali-aggregate reaction, macro-model, expansion, finite element*

3.1 Introduction

Alkali aggregate reaction (AAR) is one of the most harmful distress mechanisms affecting concrete infrastructure worldwide [1]. Overall, AAR can be subdivided in two main categories: alkali-carbonate reaction (ACR) and alkali-silica reaction (ASR), with the latter being the most frequently observed reaction type. The distress mechanism of ASR is fairly well understood, at least in its major steps, and it can be summarized in the following stages. First, a chemical reaction between the "unstable" silica mineral forms, which are found within fine and/or coarse reactive

aggregate materials, and the alkali hydroxides (Na, K – OH) dissolved in the concrete pore solution takes place and generates a secondary product, the so-called alkali-silica gel. This gel then uptakes water from its surrounding environment and swells, therefore inducing expansive pressures (and tensile stresses) within the reacting aggregate material(s) and the adjacent cement paste. Finally, when these stresses reach the tensile strength of the material, major microcracking is generated, which often leads to the loss of material's integrity (mechanical/durability) and, sometimes, functionality of the affected structure [1, 2]. Conversely, ACR is a much rarer chemical reaction and its distress mechanism is not fully comprehended. Some researchers believe that ACR is a specific form of ASR [3, 4], while others consider that ACR is a result of a "different" damage mechanism [5, 6]. Several parameters influence the damage generated by AAR, such as temperature, alkali loading of the concrete mixture, type (fine vs coarse) and nature (minerology) of aggregates and presence of moisture; therefore, significant distress may be observed after periods as short as 2 years or as long as 25 years depending on those conditions.

AAR is a complex non-linear mechanism, especially in the case of reinforced concrete structures, where the influence of anisotropic confinement and in-situ stress states must be considered. Therefore, to accurately predict AAR-induced expansion and damage in reinforced concrete structures/structural members over time, mathematical models able to account for both physical and chemical parameters should be considered.

3.2 Models to forecast AAR-induced expansion and damage

Several AAR models have been developed over the years to predict the induced expansion and consequential damage either at the materials (microscopic) [7, 8] or structural (macroscopic) scale [9, 10]. At the micro-scale, models usually try to address both the chemical reactions and

mechanical distresses caused by AAR, whereas the macro-scale models aim to realistically describe the overall macro behaviour of AAR-affected structures/structural members [11]. According to [12], AAR models may be classified into 4 different categories, as presented below:

1- Models based on ion diffusion/reaction products, which describe the chemistry involved in detail (micro-models). They take into consideration the dissolution and diffusion of alkali and silica ions as well as water availability. Examples of micro-models include those by [7, 8].

2- Models based on gel production, which describe the deterioration process at the aggregate level (micro-meso-models). They generally express the reaction kinetics as a function of the change in mass or volume of the gel and associate these variations to imposed strains or pressure. Examples of micro-meso-models include those developed by [13, 14].

3- Models based on internal pressure, which are capable of characterizing damage within the different constituents of the concrete (coarse aggregate, fine aggregate, cement paste, interfacial transition zone, etc.) by analyzing a representative elementary volume (meso-models). Examples of meso-models include those by [12, 15].

4- Models based on concrete expansion, in which the effects and structural implications of AAR are modeled by imposing an expansive time-dependent strain to the concrete elements (macro-models). The strain is based on either phenomenological laws or reaction kinetics laws of thermodynamics. Examples of macro-models include those developed by [9, 10, 16].

Even though important progress has been accomplished in the field recently, most existing approaches either neglect or overemphasize the critical physicochemical parameters of the chemical reaction. This leads the models to become either incapable of assessing the distress mechanism properly (i.e., oversimplified and inaccurate), or too complex, requiring heavy computer programing/processing and, more importantly, the need to “fit” some of the variables

with literature data or non-technical guesses (i.e., overcomplicated and impractical). This fact, unfortunately, tends to make these models less useful and attractive in practice.

This work aims to present the validation of a new simple yet reliable engineering-based finite element (FE) approach to assess damage in slender AAR-affected reinforced concrete structures. The macro-model (based on concrete expansion) intends to be a middle ground between the existing overcomplicated and oversimplified approaches. It is capable of technically accounting for the most important parameters influencing the physicochemical aspects of the reaction, thus removing the need to "fit" certain (sometimes unmeasurable) parameters. Moreover, the proposed model uses a commercially-available FE software (Abaqus/CAE v.6.14 by [17]), making it easily accessible to the engineering community.

3.3 Research significance

According to [18, 19], some of the biggest challenges in civil engineering nowadays regarding the condition assessment of AAR-affected infrastructure are the answers to the following questions:

1- How to properly perform the conditional assessment (i.e., diagnosis and damage degree) and evaluate the structural implications caused by AAR-induced expansion?

2- How to establish an accurate correlation between AAR-induced expansion and the reductions in mechanical properties, durability and long-term behaviour of the affected structure/structural members?

3- How to assess the influence of confinement (e.g., internal reinforcement), boundary conditions and loading in the overall damage initiation and propagation?

4- What is the potential of further induced expansion and damage of AAR-affected structures/structural members (i.e., prognosis)?

Recent developments in the area have demonstrated that a number of microscopic and mechanical laboratory techniques, such as the *Stiffness Damage Test (SDT)* and *Damage Rating Index (DRI)*, could be effectively used to appraise AAR damage degree (i.e., diagnosis) and to correlate its advancement with the mechanical properties reductions of affected concrete [20, 21, 22, 23]; thus, addressing questions 1 and 2. Otherwise, there is still a lack of understanding on the potential of AAR further development in the field (i.e., prognosis) along with its differential behaviour in reinforced structures due to the anisotropic conditions found in situ (questions 3 and 4). Hence, this research project aims to develop and validate a practical and accurate FE model capable of predicting AAR-expansive behaviour as well as its structural implications in affected concrete infrastructure.

The overall validation of the proposed model will be based on two steps. First, the material model selected to simulate the behaviour of reinforced concrete is validated through the analysis of six reinforced beams, whose tests have been reported previously in the literature [24]. These beams are not affected by AAR, which means that the failure mechanism is purely due to mechanical loads. Second, the proposed AAR model is discussed and validated by comparing the induced expansion over time of reinforced concrete specimens subjected to different confinement stresses as per [25].

3.4 Implementation

3.4.1 Modeling Reinforced Concrete

The commercial FE software package Abaqus [17] offers several material models to represent non-linearity and damage in concrete. Three of the most well-known are smeared cracking, brittle damage, and concrete damaged plasticity (CDP). Based on the mathematical implementation and customization options, it was determined that CDP was the model that better fits the needs of the current work.

CDP is based on the principle that the damage in quasi-brittle materials (i.e., concrete) can be defined by evaluating the dissipated fracture energy required to generate microcracks, as by [26]. According to [27, 28], based on the CDP's mathematical implementation and on the Drucker-Prager hyperbolic function, the CDP model can represent the elastic and inelastic hydrostatic pressure-dependent behaviour of concrete under compression and tension. The main failure mechanisms are assumed to be either concrete crushing or tensile cracking. An idealized triaxial representation of a concrete failure surface, like the one used in the CDP model, is presented in Figure 3-1.

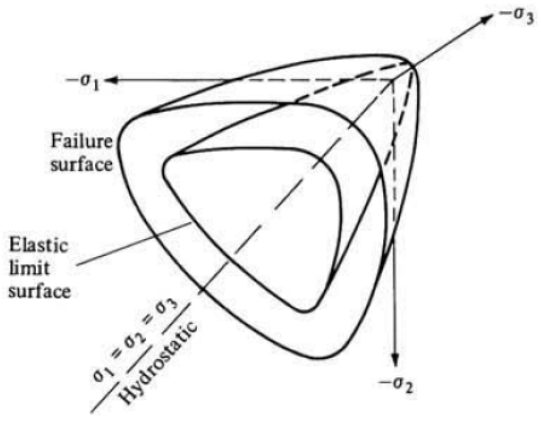

Figure 3-1. Schematic failure surface. Source: [29].

The CDP model requires seven input parameters to be defined: dilation angle, eccentricity of the plastic potential flow, ratio of the initial compressive yield stress under biaxial loading by the initial compressive yield stress under uniaxial loading (f_{b0}/f_{c0}), ratio of the second stress invariant on the tensile meridian (K), viscosity, compressive stress vs plastic strain curve, and tensile stress vs plastic strain curve. Note that the viscosity parameter is simply a mathematical parameter of the material model, not representing a fluid's resistance to gradual deformation. According to the literature (Bompa & Onet, 2010; Genikomsou & Polak, 2015; Hany, et al., 2016; Yan & Xie, 2017), most researchers agree that values of 0.1 for the eccentricity, 1.16 for f_{b0}/f_{c0} and 0.667 for K are appropriate for modeling reinforced concrete. However, the reported values of dilation angle and viscosity vary significantly, ranging from 5 to 56 degrees and 0 to 0.05, respectively. Note that both stress vs plastic strain curves are a function of the concrete used, therefore being specific for each case.

Lastly, the CDP model is capable of qualitatively estimating the cracking intensity and orientation by evaluating the plastic strain. If an element or region passes the elastic limit, it starts developing plastic strain locally until global equilibrium is reached. As the load increases, the plastic zone also increases, therefore simulating damage accumulation.

As shown by [33], the Hognestad parabola can trace the stress-strain curve of concrete under compression well for both regular and ASR affected specimens. Therefore, it is adopted in this work henceforth. Moreover, the behavior of concrete under tension – pre- and post-peak – is represented by the stress-strain relationship proposed by [27]. It is a function of only two parameters (cracking strain and tensile strength), which makes it very easy to implement.

Reinforcement was idealized as an elastic perfectly plastic material, especially due to the simplicity of the approach and because the post-yielding behaviour is not the main focus of the

current analyses. Concrete is represented by 8-node cube elements and reinforcement is represented by beam or truss elements. Additionally, the reinforcement can be modeled in FE by sharing nodes with concrete elements (perfect bond), by being smeared in the concrete element, or by being connected to concrete elements using constraints. For this work, the shared-nodes approach was selected due to its simplicity and wide applicability.

3.4.2 Modeling AAR kinetics and induced expansion

Larive [34] has developed an exponential equation capable of describing AAR kinetics and induced expansion over time. It is based on three coefficients: τ_c characteristic time, τ_l latency time and $\varepsilon_{AAR}^{\infty}$ expansion at infinity, as illustrated in Equation 3-1 and Figure 3-2, where $\varepsilon_{AAR}(t)$ is the AAR-induced strain (i.e., expansion).

$$\varepsilon_{AAR}(t) = \frac{1 - e^{-\frac{t}{\tau_c}}}{1 + e^{-\frac{(t-\tau_l)}{\tau_c}}} \times \varepsilon_{AAR}^{\infty} \tag{3-1}$$

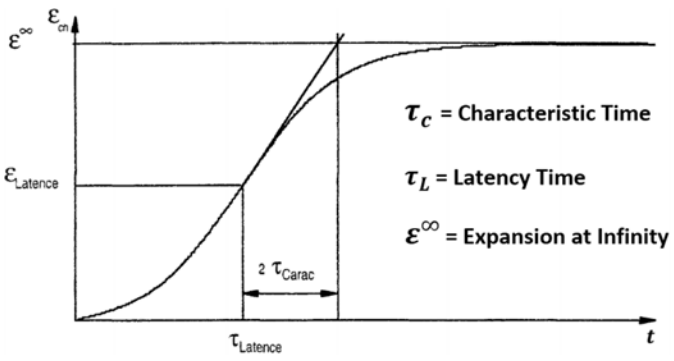

Figure 3-2. Larive's Equation. Source: Adapted from [34]

Larive's equation has been successfully used to describe the evolution of AAR by many authors [9, 10]. However, it is a limited approach because its coefficients have no physical meaning, which means that the equation is not able to predict AAR kinetics and induced expansion as a function

of the materials properties or the environmental conditions without extensive laboratory tests and calibration. Therefore, in order to assess the chemical aspects of the reaction, a modified version of Larive's equation was adopted in this project, as proposed by [35]. The reaction kinetics (i.e., free expansion prediction over time) is defined based on a physicochemical analytical model that accounts for seven of the most important parameters of the chemical reaction by introducing new coefficients to Larive's equation. These new coefficients give a physical meaning to the original mathematical variables proposed by [34], therefore allowing for an intuitive and uncomplicated prediction of the expansion by taking into consideration the structure's specific properties and exposure conditions.

The analytical model was developed based on results obtained from the standardized Concrete Prism Test (CPT as per ASTM C 1293 or CSA A32.2-14A; one year at 38ºC with RH >95%), along with variations of the conventional CPT method such as 60ºC with RH >95% and 80ºC soaked into 0.5M & 1M $NaOH$. The CPT results obtained at the laboratory were compared to concrete blocks (40×40×70 cm) fabricated and stored outdoors, containing similar reactive aggregates and monitored for over 15 years, as per [36]. The results showed that, despite a significant amount of leaching being present at the CPT (as reported by [37]), the data was quite similar (that is, equal or greater) to the data gathered at the exposed blocks for the vast majority of aggregates tested. This suggests that considering the CPT results as the "reactivity potential" of non-massive concrete members made by mixtures without any preventive measures (e.g., supplementary cementing materials - SCMs) is likely a fair initial assumption. Hence, the proposed analytical model assumes the 1-year CPT expansion results as the reactivity potential of a given concrete mix throughout the years of the structure in service.

The seven parameters considered by the analytical equation are the type of reaction (ACR or ASR), aggregate type (coarse, fine or coarse & fine), aggregate reactivity (from negligible to very high damage degree, as defined by [38]), temperature, moisture (i.e., relative humidity), and alkali content in the mix. All parameters are assumed to affect both the kinetics and the final expansion, except the alkali content, which only affects the final expansion. Moreover, the model can assess the variation of some parameters, such as temperature and moisture over time, allowing the development of expansion curves that simulate the real climatic conditions of the structure under evaluation. It is worth noting that all coefficients were calibrated using empirical data from laboratory concrete samples under free expansion, presenting distinct mechanical properties (i.e., 25 to 45 MPa) and incorporating a wide variety of aggregate types and storage conditions. Therefore, the model indirectly accounts for the differences of AAR kinetics coming from the use of distinct materials (i.e., concrete quality, aggregates type and reactivity). Equation 3-2 presents the uniaxial modified Larive's equation, where $k_{C,T}$ is the temperature modification coefficient for τ_c, $k_{C,RH}$ is the relative humidity modification coefficient for τ_c, $k_{L,T}$ is the temperature modification coefficient for τ_l, $k_{L,RH}$ is the relative humidity modification coefficient for τ_l, $k_{\infty,T}$ is the temperature modification coefficient for $\varepsilon_{ASR}^{\infty}$, $k_{\infty,RH}$ is the relative humidity modification coefficient for $\varepsilon_{ASR}^{\infty}$ and $k_{\infty,A}$ is the alkali content modification coefficient for $\varepsilon_{ASR}^{\infty}$.

$$\varepsilon_{ASR}(t) = \frac{1 - e^{-\frac{t}{\tau_c k_{C,T} k_{C,RH}}}}{1 + e^{-\frac{(t - \tau_l k_{L,T} k_{L,RH})}{\tau_c k_{C,T} k_{C,RH}}}} \times (k_{\infty,T} k_{\infty,RH} k_{\infty,A}) \varepsilon_{ASR}^{\infty} \quad (3\text{-}2)$$

Another important AAR-induced expansion consequence that has to be accounted for is its effect on the mechanical properties. The AAR-affected mechanical properties that are considered in this work are the compressive strength, tensile strength and modulus of elasticity, which are all reduced

over time as a function of the expansion level as per [20]. This reduction is a direct consequence of the physical degradation (i.e., cracking) within the aggregate particles and cement paste. The model provides the reduction percentage of each parameter for each aggregate type at different expansion levels, and the parameters are assumed to vary linearly between the data points.

The chemical process involved in the reaction is computationally, and indirectly, implemented in the FE model by imposing an equivalent AAR strain based on the free AAR expansion model (Equation 3-2)). The curve obtained from this analytical approach can be understood as the input (reference) expansion curve for the FE model, because it represents the free (i.e., unrestrained and unconfined) expansion over time expected to be observed. Equation 3-3 presents the total strain of the model ε_{tot} as a function of the elastic strain ε_{el}, plastic strain ε_{pl} and equivalent AAR-induced strain ε_{AAR}.

$$\varepsilon_{tot} = \varepsilon_{el} + \varepsilon_{pl} + \varepsilon_{AAR} \tag{3-3}$$

The physical aspects of the reaction are assessed by taking into consideration the triaxial stress-state dependence of the expansion. Gautam et al. [39] have proposed a non-linear mathematical approach that states that the expansion due to ASR is reduced in the compressed direction and redistributed to the less stressed/unstressed directions. Based on their experimental results, the expansion can be reduced to 34% or increased up to 232% of the reference expansion, depending on the stress-state of the analyzed direction as well as the other two orthogonal directions. Also, the model does not account for the effect of tensile stresses on the reaction; therefore, any regions that are not being compressed have an expansion equal to the reference. Note that, even though initially developed for ASR, this stress-dependent model is assumed to be applicable for both ASR and ACR, therefore being capable of describing the AAR anisotropic behaviour.

In order to implement the relationship developed by [39], an Abaqus user subroutine (USDFLD) was developed. The script was written as a function of two variables per principal direction: the field variable and the effective stress. The field variable represents the reduction or increase of the expansion compared to the reference (free expansion input curve). If the value is equal to 1.0, the expansion is equal to the reference. However, if the parameter is greater or smaller than 1.0, that value represents the percentage of the reference expansion that is being applied to the specific concrete element. For example, if the region has a value of 0.6, it means that an expansion equal to 60% of the reference expansion is applied there.

The field variable is defined as a function of an effective stress acting on the element (σ_e), instead of the actual stress (σ). The mathematical implementation of the CDP model allows the (actual) stress on each element to abruptly change each time the element reaches the elastic limit surface, which causes convergence issues when trying to determine the local value of the field variable, since it is a direct function of the stress-state of the element. Therefore, an effective stress is calculated to minimize the abrupt changes, based on a constant maximum stress difference value between each increment (Δ). Note the maximum and minimum values of Δ are specified manually; however, the average value depends on the convergence of the model.

The mathematical approach of the effective stress proposed is defined for each increment (i) as follows. First, a theoretical range is defined, with its upper limit being equal to the current effective stress (i) plus the maximum stress difference and the lower limit being equal to the current effective stress (i) minus the maximum stress difference. Then, if the actual stress at increment (i+1) is within that range, the effective stress at i+1 is equal to the actual stress at i+1. However, if the actual stress at i+1 is not within the range, the effective stress at i+1 is equal to the upper or lower

limit of the range, depending on whether the actual stress is increasing or decreasing. Equation 3-4 summarizes the definition of the effective stress, as previously explained.

$$\begin{cases} \sigma_{i+1} > \sigma_{e,i} + \Delta \rightarrow \sigma_{e,i+1} = \sigma_{e,i} + \Delta \\ \sigma_{e,i} - \Delta < \sigma_{i+1} < \sigma_{e,i} + \Delta \rightarrow \sigma_{e,i+1} = \sigma_{i+1} \\ \sigma_{i+1} < \sigma_{e,i} - \Delta \rightarrow \sigma_{e,i+1} = \sigma_{e,i} - \Delta \end{cases} \quad (3\text{-}4)$$

Note that the concept of the effective stress naturally makes the analysis dependent on both the maximum stress difference between increments and the size of the increment itself. A comprehensive way to understand both values is to define the ratio between the maximum stress difference (in MPa) and the average increment, which is assumed to represent the average numerical difference between increments, where 0 refers to the beginning and 1 to the end of the step. For the rest of this paper, this ratio will be referred to as "subroutine ratio".

As the reaction progresses, it is possible to state that the effect of confinement (due to the reinforcement, for example) and localized structural damage will influence the structure's stress-state and, consequently, the local development of the reaction in terms of expansion and damage. Therefore, to take this into consideration, the subroutine was developed so that at every time increment, it updates the values of the expansion along each principal direction in each finite element as a function of the current stress-state.

3.5 Material model validation

3.5.1 Description

The validation of the CDP model was performed by analyzing 6 beams tested and simulated by [24] using the FE program Vector2. This work was selected as a reference for the validation, because it not only reports the force vs displacement curve of each beam, but also their cracking pattern and alternative FE modeling approach for comparison.

The properties of the beams modeled, as well as the cross-section details, are presented in Table 3-1 and illustrated in Figure 3-3.

Table 3-1. Beam dimensions and reinforcement. Source: [24]

Beam Number	OA1	OA2	OA3	A1	A2	A3
b (mm)	305	305	305	305	305	305
h (mm)	552	552	552	552	552	552
d (mm)	457	457	457	457	457	457
L (mm)	4100	5010	6840	4100	5010	6840
Span (mm)	3660	4570	6400	3660	4570	6400
Bottom Reinf.	2 M30 2 M25	3 M30 2 M25	4 M30 2 M25	2 M30 2 M25	3 M30 2 M25	4 M30 2 M25
Top Reinf.	-	-	-	3 M10	3 M10	3 M10
Stirrups	-	-	-	D5 at 210	D5 at 210	D4 at 168

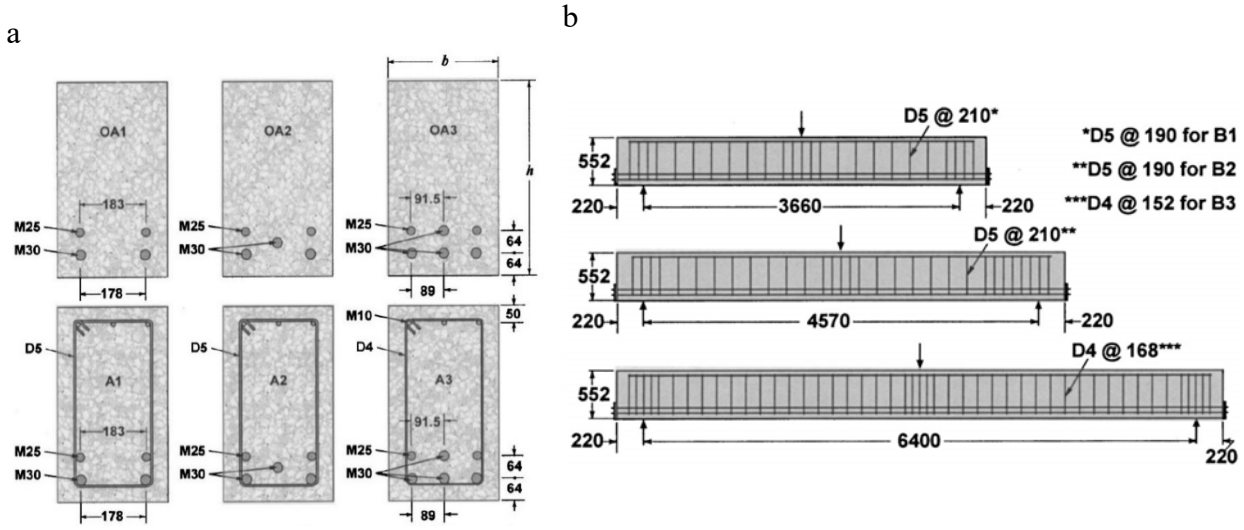

Figure 3-3. Beam dimensions: a. cross-sections, b. longitudinal-sections. Source: [24]

According to the authors, beams OA1, OA2 and OA3 failed due to diagonal-tension cracking in the lab experiment, while beams A1 and A2 failed due to shear-compression and beam A3 due to flexure compression. The material properties, as well as further details regarding the geometry and set up of the beams, can be found in [24].

The FE model of the beams was built using truss elements (T2D2) to represent the reinforcement and plane-stress elements with reduced integration (CPS4R) to model concrete. Moreover, it is

important to emphasize that the confinement effect on the top of the mid-section due to the transverse reinforcement had to be accounted for to avoid premature concrete crushing in beams A1, A2 and A3. Inspired by the approach described by [24], the compressive strength and strain at peak stress of the Hognestad parabola were increased based on coefficients calculated according to [40] and implemented in that region. The size of the confined region was based on the approach described by [24]. The depth defined was equivalent to 84 mm (top 3 elements, 2 above the stirrups and 1 below). Additionally, the length for the confined region for beam A1 covered all closely spaced stirrups close to the mid-span and the zone between the first two regularly spaced stirrups, while for beams A2 and A3 the zone was delimited by closely spaced stirrups and only the first regularly spaced stirrup. This means that the length varied between 340-630 mm extending from the mid-span to the support, and the described approach was taken to optimize the results of the model. Note that different confinement coefficients were defined depending on the stirrup spacing of the beam. Figure 3-4 shows the mesh of beams A1, A2 and A3, where orange represents the confined concrete, green represents unconfined concrete and red represents the stirrups.

a

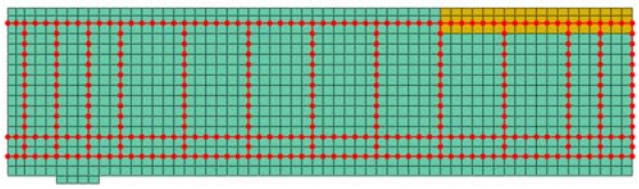

b

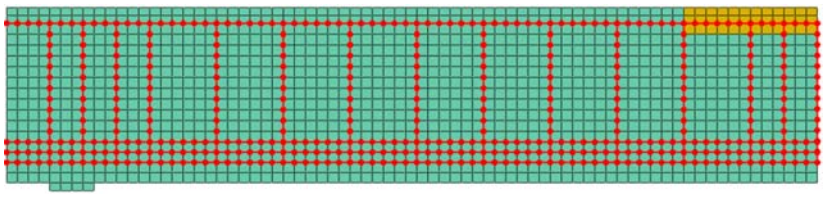

c

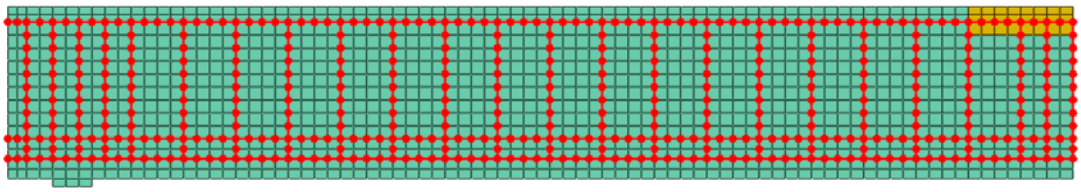

Figure 3-4. Mesh of the beams: a. A1, b. A2, c. A3

The aim of the validation analysis was to predict the full force-deflection behavior of the beams and match the cracking patterns observed in the lab test. Note that the beams were assumed to fail when the first element of the top of the beam reached a strain equal to -0.0035 (concrete crushing). The parameters evaluated are the ultimate deflection at midspan (δ_u) and the ultimate load (P_u), which were assumed to be the highest point of the recorded load-displacement curve.

It is important to emphasize that phenomena like creep, shrinkage and reinforcement slippage due to bonding stresses were assumed to have a negligible effect. Creep is a function of the loading time, and it was estimated to not play a major role in the analysis, because it did not have enough time to develop since the beams were loaded until failure on the same day. Shrinkage was assumed to not happen in the experiment, because the specimens were kept at 100% relative humidity during the entire testing period. Lastly, reinforcement slippage was totally disregarded to simplify the model, which assumes that the reinforcement and the concrete have perfect bond at all points.

3.5.2 Parametric Study: Material Model Parameters

Several parametric studies were conducted to determine the optimum values for the dilation angle and viscosity parameters of the CDP model. The results of two of the parametric studies performed are shown below in Figure 3-5. Tables 3-2 and 3-3 present the ratio of the FE calculated value to the actual value obtained in the laboratory test. Note that all previously suggested parameters were used, while only the one parameter being analyzed had its value changed.

a

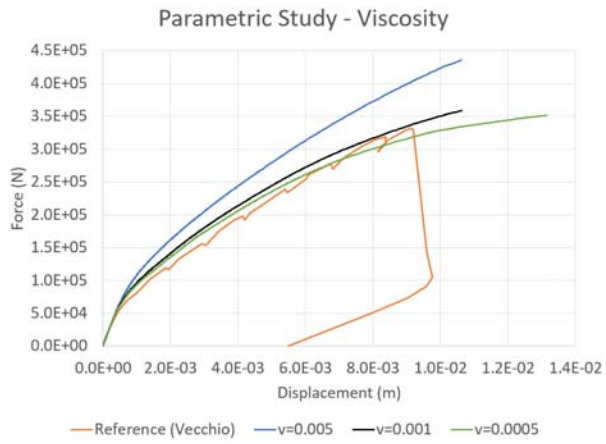

b

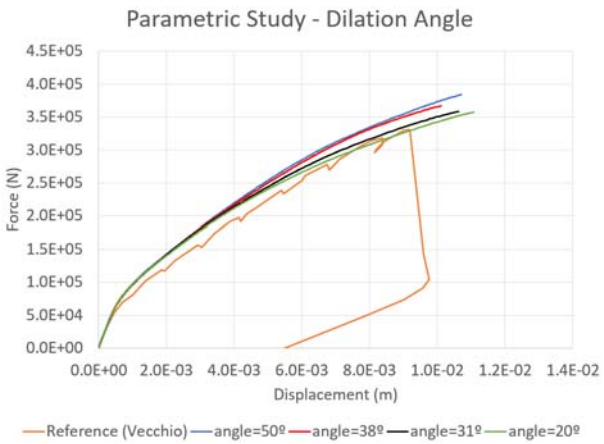

Figure 3-5. Parametric study – beam OA1 force vs deflection curve: a. Influence of viscosity, b. Influence of dilation angle

Table 3-2. Viscosity parametric study results: Beam OA1.

Beam OA1	δ_u %	P_u %
Vecchio	0.96	1.06
Gorga (v=0.0050)	1.15	1.24
Gorga (v=0.0010) - reference	1.15	1.08
Gorga (v=0.0005)	1.31	1.06

Table 3-3. Dilation angle parametric study results: Beam OA1.

Beam OA1	δ_u %	P_u %
Vecchio	0.96	1.06
Gorga (20º)	1.18	1.07
Gorga (31º) - reference	1.15	1.08
Gorga (38º)	1.11	1.10
Gorga (50º)	1.15	1.13

As shown in Figure 3-5a and Table 3-2, the value of viscosity plays a major role in the load-displacement curve calculated by the FE model, since very small variations greatly influence the final response. In general, smaller viscosity values make the model softer (the beam deforms more for an equal intensity load) and they also tend to influence the member's failure (reinforcement yielding happens for smaller loads and the beam deforms less before yielding). Note that the opposite is true for larger viscosity values. Moreover, another very important aspect is that smaller values of viscosity increase the model's computational cost, which greatly influences the time to complete the analysis. Therefore, after balancing the influence on the final results and the computational effort required for the analyses of all the beams, it was found that the optimum value for the viscosity parameter is 0.001.

Figure 3-5b and Table 3-3 show that the value of the dilation angle is not a critical factor in the analysis as long as it stays between the analyzed range, which goes from 20° to 50º. Both the load and the displacement were always overestimated, but the general shape of the force-deflection curve did not drastically change. The most noticeable effect of changing the dilation angle was its influence on the location of first concrete crushing. In general, smaller angles led to concrete crushing closer to the mid-span, while larger values led to concrete crushing further away from the mid- section. Even though the results were similar, after analyzing all beams, it was found that the angle that best represented the structural behaviour observed in the lab was 31º.

3.5.3 Model's Results and Discussion

Based on the values selected for the CDP model, the force vs deflection curves for all the beams were calculated. Figure 3-6 shows the comparison between the experimental and the FE curves found.

a

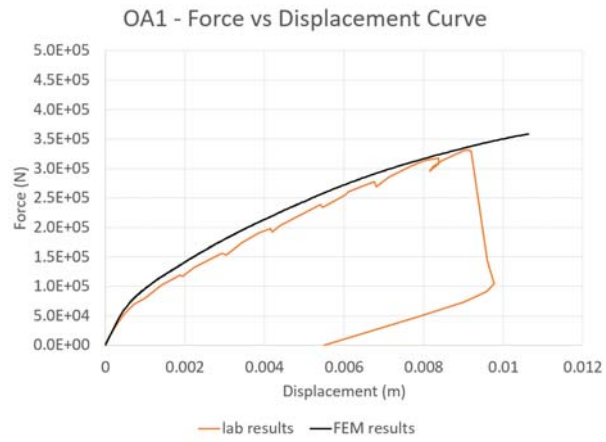

b

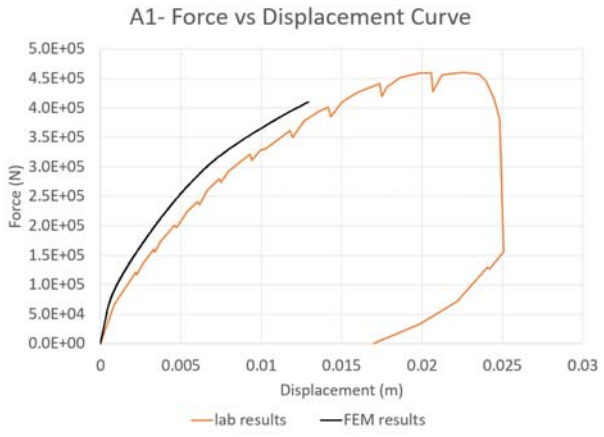

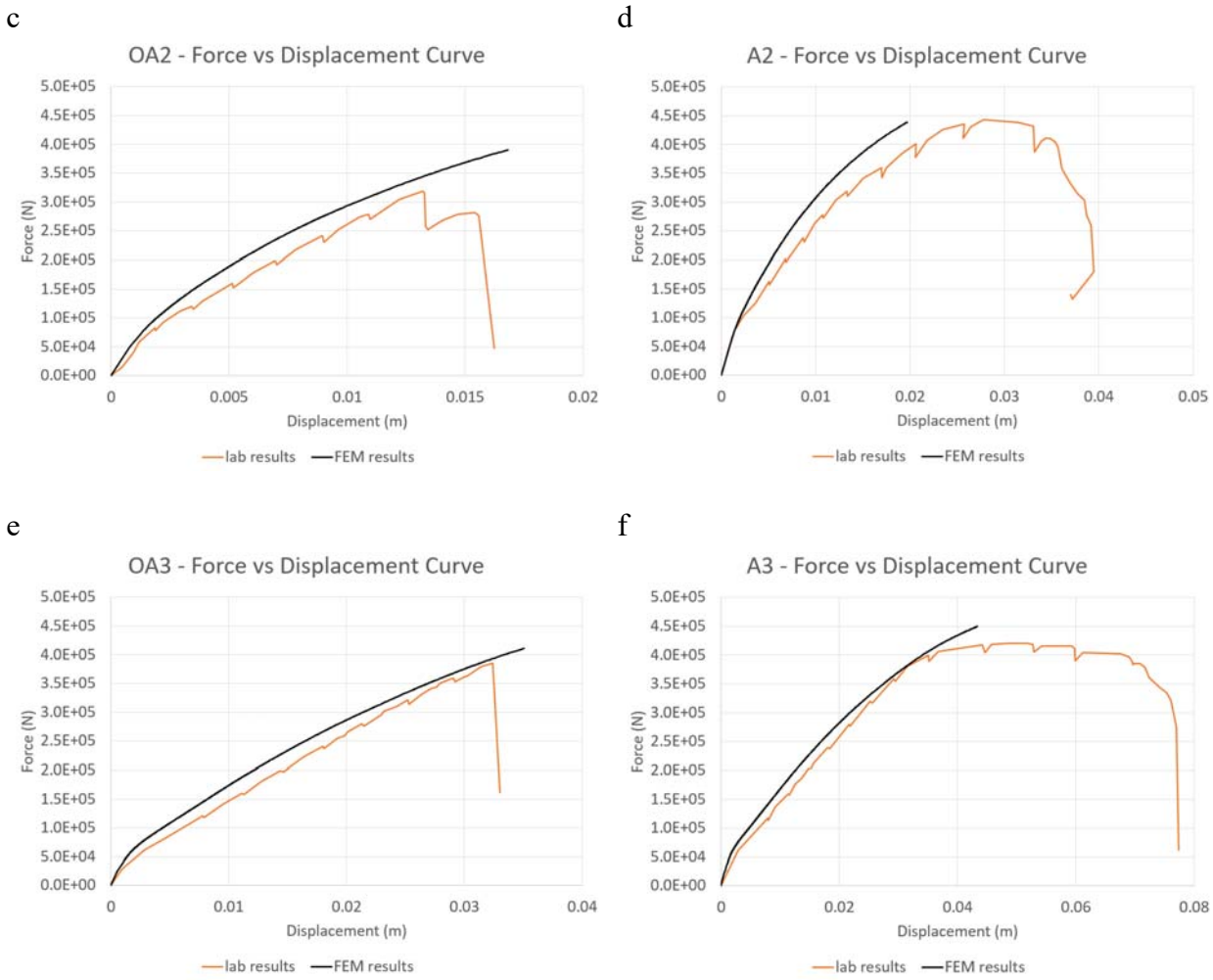

Figure 3-6. Load-deflection curves for all beams.

Moreover, Table 3-4 provides the ratio of FE values calculated by either [24] or the authors and the corresponding lab values, for all the beams.

Table 3-4. Ratio of FE by lab results for ultimate deflection at mid-span and ultimate load.

Beam	Vecchio δ_u [%]	Gorga δ_u [%]	Vecchio P_u [%]	Gorga P_u [%]
OA1	0.96	1.15	1.06	1.08
OA2	1.03	1.22	1.11	1.18
OA3	1.27	1.08	1.16	1.06
A1	1.31	0.56	0.96	0.88
A2	1.33	0.52	0.96	1.00
A3	0.99	0.82	0.94	1.07
Average	1.15	0.89	1.03	1.04
Coeff. of Var.	0.15	0.34	0.09	0.09

As shown in Table 3-4, the ultimate load displayed a smaller coefficient of variation than the ultimate deflection at mid-span, which means that the approximation of the displacements was less precise. Even so, the averages of both parameters were very close to the values measured in the lab – underestimation of 11% for the displacements and overestimation of 4% for loads.

Compared to the FE analysis conducted by [24], the displacement average was closer to the desired values, even though there was a larger variation in the results. Moreover, the load prediction was virtually the same, with a 1% difference in the average and the same coefficient of variation.

For the diagonal-tension failure (OA1, OA2 and OA3), the values of P_u and δ_u were overestimated by a maximum of 22% and 18%, respectively. This means that the model was delayed predicting when critical diagonal tension cracking would develop.

Next, the shear-compression failure (A1 and A2) was the least precise of the three failure modes. Values of deflection and ultimate load were underestimated by a maximum of 48% and 12%, respectively. One of the main factors that might have influenced the accuracy of these two analyses is the simplified failure criterion adopted (concrete crushing at the top of the beam`s midspan), which might not have fully captured the shear failure expected. Therefore, it is possible to state that the CDP model is capable of simulating shear failure, but not as well as the other failure mechanisms, because the model tends to be too stiff.

Lastly, the single flexure-compression failure model (A3) underestimated the deflection by 18% and overestimated the load by 7%, which leads to the conclusion that the failure mechanism was properly predicted. Note that, based on the shape of the lab load-displacement curve (long plateau before global failure), it is possible to state that the beam tested by [24] displayed yielding of the bottom reinforcement. Similarly, the bottom and top reinforcements of the FE model also yielded

prior to failure. However, a change in the curve's slope was not captured because the second row of the bottom reinforcement only yielded at a load 0.6% smaller than the ultimate load, which means that the beam did not have enough time to deform without increasing the load.

All the load-displacement curves presented slopes very similar to the lab test results (Figure 3-6). However, the FE curves were all slightly above the experimental curves. This means that the overall behaviour is being captured as the load increases, although the development of the initial nonlinearity observed, i.e., appearance of first cracks, was delayed.

Another interesting aspect can be observed when comparing the geometrically identical beam with and without transverse reinforcement (e.g., OA1 and A1). As previously mentioned, the FE results predicted A1 to fail at a lower mid-span deflection than what was recorded during the experiment, which implies that the FE model is less ductile than the experimental beams. However, the response of OA1 and A1 are very similar since the ultimate deformation of A1 is only 22% larger than that of OA1 and the ultimate load is only 14% larger, instead of 107% and 39%, respectively, as observed in the lab. Since the only relevant difference between these two beams is that OA1 does not contain transverse reinforcement and A1 does, it is possible to state that the model was not able to fully capture the shear stress transfer from the concrete to the reinforcement nor the behaviour close to the ultimate load when larger cracks quickly widen and reinforcement yields. Note that the same trend was observed for OA2 and A2, as well as for OA3 and A3.

Additionally, Figure 3-7 compares the recorded cracking pattern of beams A1 and A3 at failure during the lab experiments and the FE cracking pattern, which is separated into tensile and compressive damage. Dark regions in the tensile damage images represent undamaged areas while the damage severity increases from blue to red. Moreover, grey regions in the compressive damage representation identify the undamaged areas, while damage severity increases from red to blue

(opposite because the representation takes the negative sign of the compressive stress into consideration in the plot). Note that these two beams were selected because A1 failed due to shear (compression) and A3 due to flexure (compression), as previously stated.

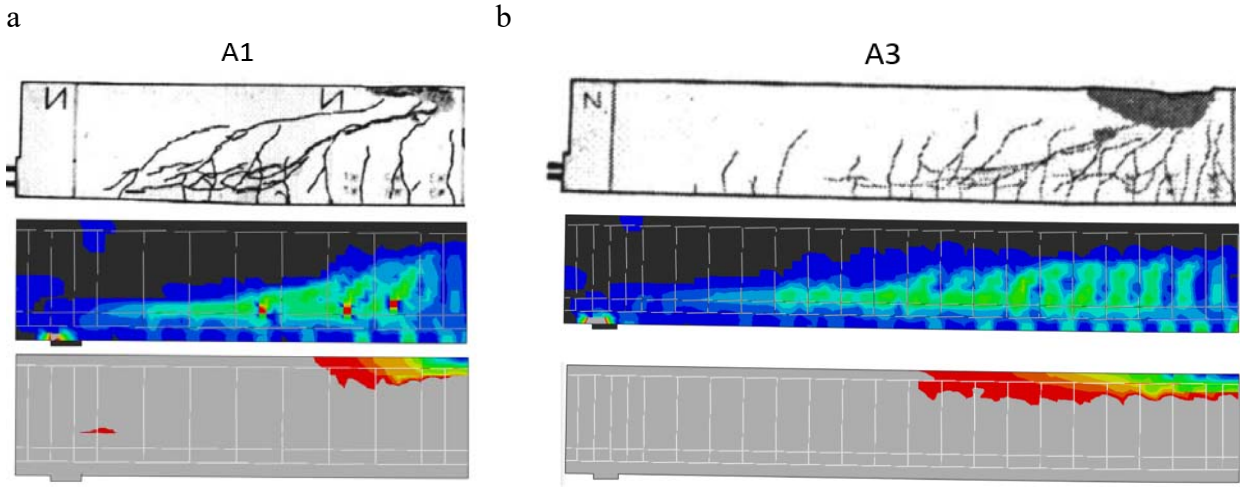

Figure 3-7. Comparison of the cracking pattern recorded in the lab by [24], tensile and compressive damage: a. Beam A1, b. Beam A3.

The cracking pattern observed in the FE analysis matched well what was recorded in the lab, as presented in Figure 3-7. The tensile cracks observed for beam A1 are mostly inclined toward the top of the middle of the section, as expected for shear cracks. Also, tensile cracks of beam A3 are mostly vertical or vertical with a very slight inclination toward the mid-section (especially in cracks closer to the support), which is exactly what is expected for flexural cracks (vertical) and shear-flexural cracks (vertical with a slight inclination at their top). Concrete crushing is also clearly observed in both cases at the top of the mid-span section, as recorded by [24].

The differences observed between the lab and FE values are likely a result of the simplifications in the CDP FE material model, the simplicity of the failure criterion adopted and the perfect bond assumption, as well as some secondary effects such as creep and shrinkage.

In summary, it is possible to state that the CDP model in Abaqus was able to simulate the behaviour of the six beams tested accurately enough, assuming that the suggested parameter values are adopted.

3.6 AAR expansion validation

3.6.1 Description

Sanchez et al. [25] performed a series of push-off tests to evaluate the effect of ASR damage on the shear capacity of reinforced concrete members. The authors designed, fabricated and tested S-shaped push-off specimens with different reinforcement ratios, ASR-induced damage levels and confinement configurations. The expansion of the unloaded specimens parallel to the main stirrups was measured over time up to a final expansion of 0.12% ± 0.01% and used to validate the ASR expansion calculated from the FE model. The specimen taken as the reference was not reinforced (0S case). Figure 3-8a and 3-8b show the two specimens that were analyzed, with 2 stirrups (2S) and 4 stirrups (4S), respectively. The 2S specimen had two 400R steel 10M stirrups (total of 400 mm^2) crossing the shear plane and a reinforcement ratio (ρ) of 0.76%, while the 4S specimen had four 400R steel 10M stirrups (total of 800 mm^2) crossing the shear plane and a reinforcement ratio (ρ) of 1.52%. All specimens were 650-mm high, 450-mm wide and 200-mm thick. The aggregate used was a highly reactive gravel from New Mexico, USA (with a mineralogical composition comprised of mixed volcanic, quartzite and chert), combined with a non-reactive natural sand. The concrete presented a compressive strength of 35 MPa at 28 days and a total alkali loading of 4.63 kg/m^3. The push-off specimens were fabricated and stored according to the CPT test (i.e., 38°C at 100% RH) to accelerate ASR development. Moreover, cylinders from the same batches were also cast so that the evolution of mechanical properties might be evaluated as a function of ASR

development. Lastly, leaching was noticed during the experiment, which would likely lead to a reduction of the final expansion expected for the specimens.

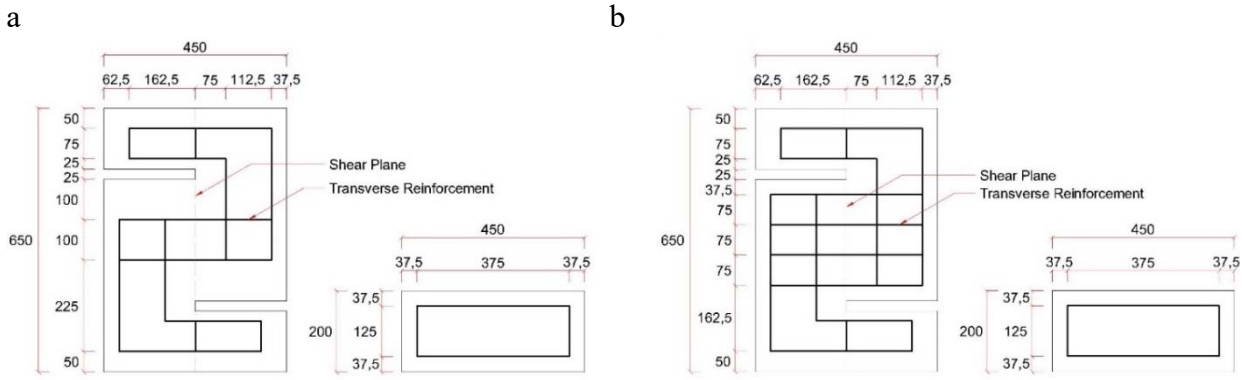

Figure 3-8. Push-off specimens design (dimensions in mm): a. 2S, b. 4S. Source: Adapted from [25].

The FE model was built with three-dimensional coupled temperature-displacement 8-node elements with reduced integration (C3D8RT) representing the concrete and three-dimensional 2-node beam elements (B31) to model the reinforcement. Perfect bond was assumed. The reinforcement was modelled with beam instead of truss elements, as the former tends to generate higher and more realistic confinement values, because it presents both axial and transverse stiffness, while the latter includes only axial stiffness.

The variation of the mechanical properties as a function of ASR development was measured and is presented in Table 3-5, according to [20]. Values for expansion level between the data points presented were linearly interpolated.

Table 3-5. Reduction in mechanical properties.

Expansion Level [%]	0.05	0.12	0.20
Reduction in modulus of elasticity (E)	-5.0%	-27.3%	-40.1%
Reduction in compressive strength ($f`_c$)	+4.4%	-11.7%	-23.4%
Reduction in tensile strength ($f`_t$)	-31.8%	-45.8%	-60.9%

It is worth noting that the initial increase in compressive strength is due to the net gain of the combined effect of hydration and ASR expansion. At an expansion level of 0.12%, the deterioration mechanisms already govern the overall behaviour, thus leading to a reduction of the compressive strength.

3.6.2 Parametric Study: Subroutine Ratio

As previously mentioned in Section 3.2, the reaction is a function of the subroutine ratio in the model. Therefore, various ratios were analyzed in a simple parametric study, and it was found that the best results were yielded for ratios between 8 and 17 MPa. This was achieved for values of maximum stress difference of 0.005 MPa and 0.010 MPa, respectively, and approximately 1,700 total number of increments with an average increment difference of roughly 6×10^{-4}.

If the maximum stress difference was increased far beyond that limit (larger subroutine ratios), the analysis would not converge to a solution as soon as cracks started propagating. This happened because the effective stress would vary too much between increments, and, consequently, a single converging value of the field variable could not be found. Furthermore, values much smaller than the presented maximum stress difference range (lower subroutine ratios) resulted in a delay on the effective stresses compared to the actual stresses, which automatically makes the results unrealistic because the anisotropic stress-state dependency cannot be considered to be following the actual stresses anymore.

Therefore, it is possible to state that the subroutine ratio should be kept within (or at least very close to) the defined range to allow the reaction's anisotropic stress-state dependent expansion to behave properly regardless of the structure being assessed. Consequently, the concept that smaller

values of increments yield more accurate results only remains true if the maximum stress difference is altered to keep the subroutine ratio within the suggested range.

3.6.3 Model's Results and Discussion – Part 1: Expansion

The expansion vs time curves reported by [25] and determined through the FE model for specimens 0S, 2S and 4S are plotted in Figure 3-9. The analyses were stopped at one year because that expansion was initially assumed as approximately the expansion that might have been reached by this given structural member in service, according to data provided by [36] and [25]. Additionally, since the stress field of the no-stirrup (0S) specimen is totally undisturbed, it is possible to state that the FE results are exactly equal to the input free expansion curve obtained using the analytical model described in Section 3.2.

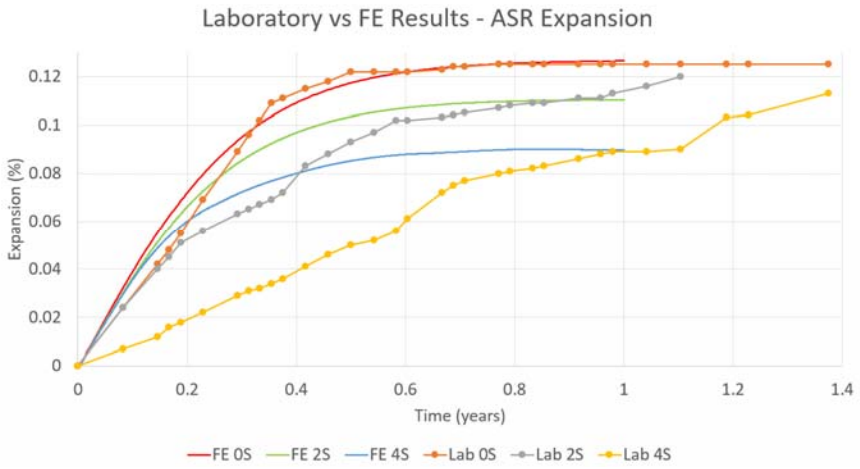

Figure 3-9. Expansion vs time curve – lab and FE results.

It is also important to emphasize that the expansion curve based on the analytical AAR model corresponding to the same mix, aggregate and conditions described by [25] provides a final expansion of 0.20%, which is much higher than the 0.125% measured in the test after 9 months. This is likely attributable to alkalis being lost in the early stages of the reaction (i.e., leaching),

which is not accounted for in the expansion equation. Therefore, the strategy adopted was to reduce the alkali loading available in the mix using one of the analytical model's coefficients to indirectly account for this phenomenon. It was determined that the best fit was for a reduction of 19% in the alkali loading (from the original 4.63 to 3.75 kg/m^3). According to [37], concrete prisms usually lose 3 to 20% of the alkalis of the system due to leaching in the first four weeks and anything from 10 to 50% at approximately two years. Therefore, the estimated 19% reduction in the alkali loading due to leaching over one-year is a reasonable assumption.

Figure 3-10 shows the FE results with the envelope of results found in the lab for each case. Note that only two specimens were tested in the lab and used to determine the expansion envelope over time for the 0S case, but six specimens were tested for the 2S case and six for the 4S case.

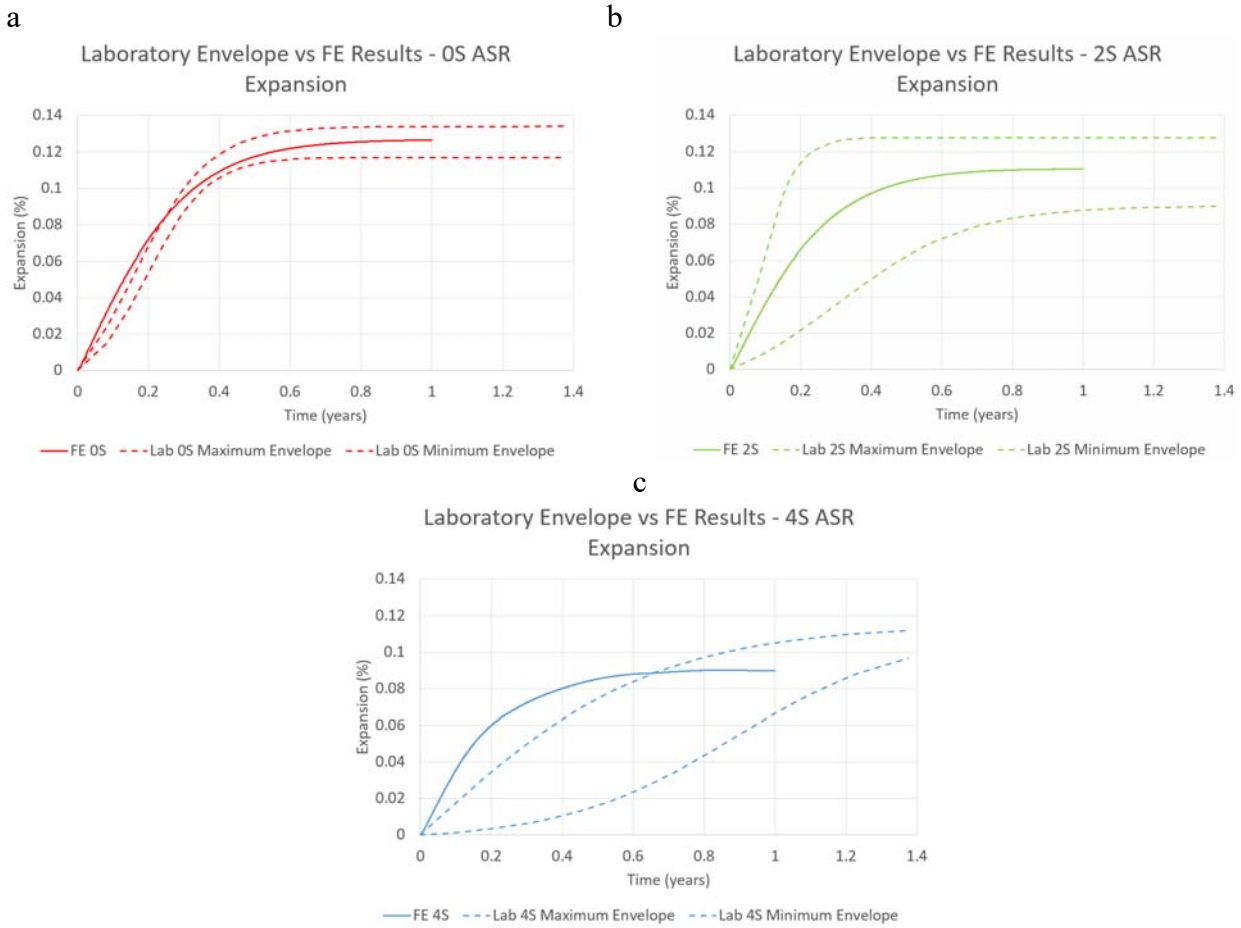

Figure 3-10. Expansion vs time curve –FE results and lab envelopes: a. 0S, b. 2S, c. 4S

Both the expansion measured in the test and calculated through the FE model were extracted from the same location, approximately 25 mm below the main stirrups for the 2S case and 25 mm below the top (first of the four) stirrup for the 4S case. Thus, the expansion curves illustrated in Figure 3-9 and 3-10 represent the behaviour of the specimens' core and not the concrete cover. From Figure 3-9 and 3-10, it is clear that the model for the no-stirrup case (0S input reference curve) represents the measured values well, except for the initial stages of expansion (between 0 and 0.30 years). This is very likely due to the fact that the analytical free expansion model only took leaching into consideration indirectly by reducing the alkali content of the mix, especially because having less alkalis available in the mix and losing alkalis over time (i.e., leaching) are two different phenomena, chemically and physically speaking. Moreover, this indicates that leaching likely has an effect not only on the final expansion (such as the alkali loading in the mix), but also on the reaction kinetics as it seems to increase the reaction's latency time (that is, decrease the expansion in early stages).

Likewise, the same initial behaviour for the 2S and 4S cases is observed, wherein the calculated expansion is higher than the one measured in the tests in early stages of the reaction, as shown in Figure 3-9. As predicted by [39] and verified by [25], the expansion was reduced due to the reinforcement confinement effect in the concrete core, leading to a lower expansion vs time curve when compared to the reference (0S case). As presented in Figure 3-9 and 3-10, case 2S is well within the envelope, and the final expansion is virtually the same as what had been recorded by [25]. However, case 4S displayed expansion values larger than the maximum values observed in the lab from the beginning until approximately 70% of the analysis period. At the same time, the final expansion value at one year matched well the value observed in the lab using the CPT test. This means that the confinement due to the transverse reinforcement is being captured correctly

by the model, but not as quickly as it should. The stresses are likely not varying fast enough in the beginning of the analysis, therefore the expansion's reduction in that direction is delayed, and the model consequently overestimates the expansion of the specimen over time. The same phenomenon can be observed in a much smaller scale for case 2S, which indicates that the model becomes less precise for greater confining pressures at the beginning of the reaction. Note that changing the subroutine ratio between the suggested values did not affect the specimens' behaviour, because the effective stresses were closely following the actual stresses, but values outside that range would lead to convergence issues (larger values) or to delays between the effective and actual stresses (smaller values). Therefore, the subroutine ratio is likely not one of the causes of the observed phenomenon.

The described behaviour is likely a combination of four major factors. First, the approach proposed by [39] might not have fully described the stress-state dependency of the AAR expansion due to its intrinsic limitations, since it does not account for the influence of tensile stresses on the expansion. Second, the model's mathematical implementation is likely not able to fully describe the development of stresses over time due to AAR. Next, the actual reaction is naturally very complex and anisotropic, because it depends on the micro-structure of the concrete (pore distribution, aggregate size, shape, texture and minerology, gel formation, etc.). This was neglected in the model, because only the macro-behaviour of the material is being analyzed, but one has to keep in mind that some variability of the results is unavoidable. Lastly, the influence of the confinement on the chemical development of the reaction is not fully understood. There is still a debate in the area trying to define whether confinement changes the gel formation and its physicochemical features, which might have impacted the observed results [25, 41].

In summary, the results illustrated in Figure 3-9 validate both the stress-strain relationship programmed through the user subroutine and the capability of the reinforced concrete model to simulate reinforcement confinement, even though precision in early stages is reduced when confining stresses are increased.

3.6.4 Model's Results and Discussion – Part 2: AAR Approach Comparison

Additionally, a total of three analyses were performed for the 2S case in order to investigate the importance of accounting for the anisotropy of the expansion and the deterioration of the mechanical properties caused by directional confinement. The first analysis applied the anisotropic stress-state relationship and reduced the mechanical properties over time; therefore, it is referred to as "anisotropic with damage," and it is the model's standard. The second analysis is referred to as "anisotropic without damage," and it assumes that the reaction is anisotropic but ignores the deterioration of mechanical properties due to AAR development. The third analysis assumes that the reaction is isotropic and maintains the initial mechanical properties throughout the analysis, therefore titled "isotropic without damage". For the 4S case, only the "anisotropic with damage" is presented since it better represents the physicochemical phenomena of the reaction. The three previously mentioned analyses conducted for the 2S case are plotted in Figure 3-11 together with the reference curve (0S case).

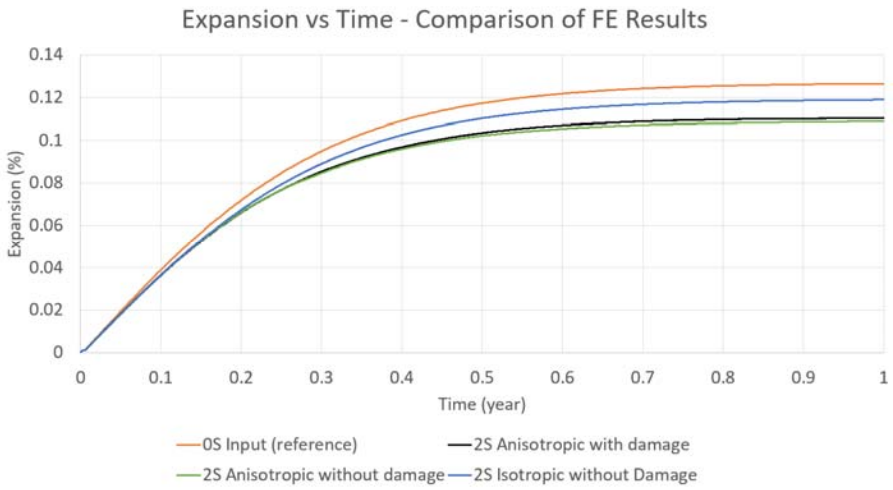

Figure 3-11. Expansion vs time curve – comparison of FE results.

The damage extent (plastic strain) in the 2S specimen (anisotropic with damage and anisotropic without damage) and the 4S specimen is presented in Figure 3-12. The dark zones in the figure represent regions that are undamaged (uncracked), and the colored zones go from little damage extent (dark blue) to large damage extent (light blue).

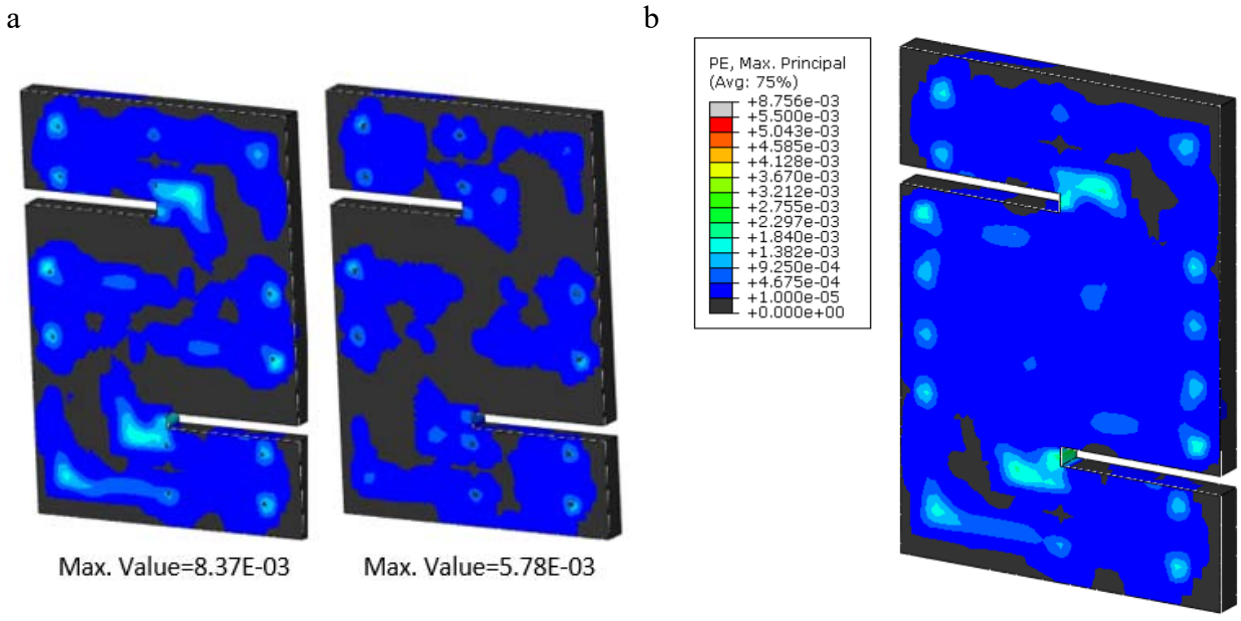

Figure 3-12. Push-off specimen's core - qualitative damage distribution (plastic strain): a. 2S anisotropic with damage case (left) and 2S anisotropic without damage (right), b. 4S anisotropic with damage case

Figure 3-13 displays the stresses along the X direction for the 2S and 4S anisotropic with damage cases, as well as the stresses along the X direction for the 2S isotropic without damage case. The grey zones are zones where tensile stresses govern. All other colored regions are governed by compressive stresses.

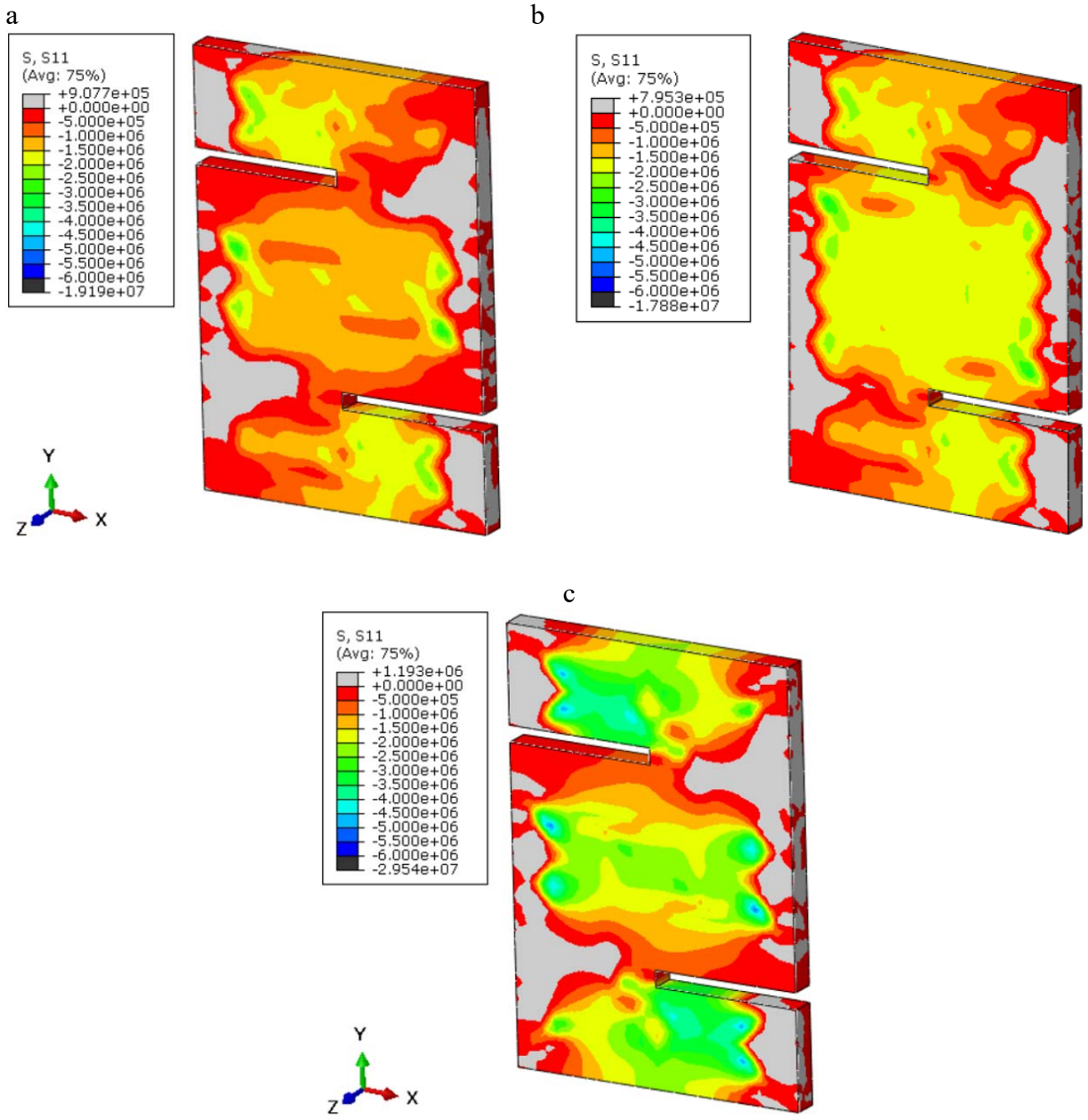

Figure 3-13. Push-off specimen's core - stress field in the X direction: a. 2S anisotropic with damage case, b. 4S anisotropic with damage case, c. 2S isotropic without damage case (stress values are in Pa)

Lastly, the field variable parameter along the X direction is presented in Figure 3-14 for the 2S and 4S cases, respectively. Note that this parameter has already been described in Section 3.2.

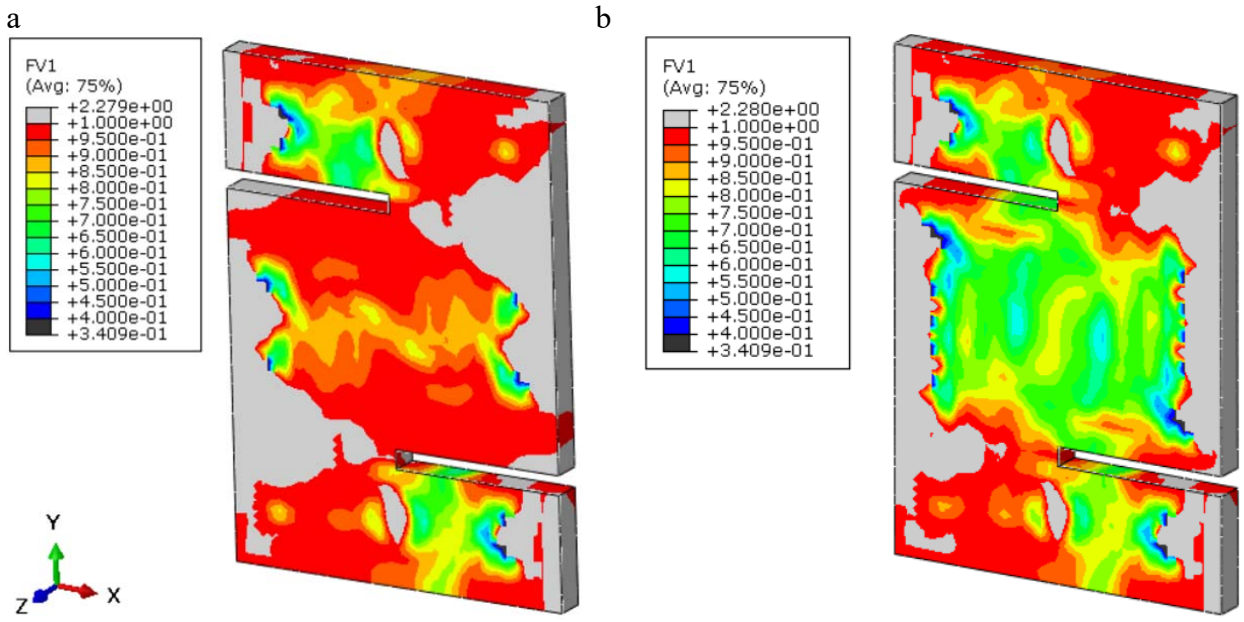

Figure 3-14. Push-off specimen's core (anisotropic with damage case) –field variable in the horizontal X direction: a. 2S, b. 4S

Based on Figure 3-11, it is possible to state that reducing the mechanical properties (2S anisotropic with and without damage cases) does not have a substantial impact on the expansion of the specimen over time, if the anisotropy of the expansion due to a triaxial state of stress is considered. The only difference observed in the curves was that the expansion keeps increasing very slowly when damage is considered, due to the widening of cracks, as the values of the mechanical properties are reduced as a function of the expansion. Conversely, when there is no damage and only the original mechanical properties are assumed, the expansion tends to reach a plateau without increasing further.

Even so, there are two meaningful consequences of reducing the mechanical properties in the model. First, as Figure 3-12 illustrates, the damaged region is considerably larger (lighter blue areas) and the undamaged zone (dark region) is considerably smaller when the mechanical properties are reduced. Second, this reduction would impact the structural response if loads were applied to the specimen, likely leading to larger deformations. This was not observed, because the case analyzed was unloaded, which is not the case for most real structures in service.

Figure 3-13 clearly shows that assuming isotropic expansion does not yield results as accurate as assuming the anisotropic stress-state dependent relationship proposed by [39]. Not only is the expansion over time further from the recorded lab data, but also the isotropic case stresses are unrealistically high when compared to the anisotropic case. When isotropic expansion is assumed, the expansion keeps increasing regardless of the confinement, which leads to incoherent larger compressive stresses in the concrete and tensile stresses in the reinforcement. Thus, it is possible to state that the approach widely used in the past of simply imposing an equivalent isotropic expansive strain to the entire structure would not be capable of accurately simulating the structural implications of the reaction.

Moreover, it is important to emphasize that the largest reduction in expansion observed in Figure 3-14 happened where the compressive stresses are the largest, as expected. These regions basically include the zones where the reinforcement was passing through along the Z direction (small blue-green zones) and the region between stirrups.

Lastly, Figure 3-13 and 3-14 illustrate that case 4S was subjected to larger confining stresses than case 2S, because of the different transverse reinforcement ratios, which consequently led to lower field variable values (greater reduction in the expansion). Note that the major difference recorded

in the damage pattern between the 2S and 4S cases (anisotropic with damage analyses) was that the 4S case displayed a larger damaged zone for almost the same maximum plastic strain.

3.7 Limitations and future research

Even though the presented results are very promising, there are still aspects that must be further accounted for and evaluated to fully describe AAR-distress behaviour of real structures in the field. Some of the most important phenomena that should be accounted for, to a certain degree, are creep, shrinkage, concrete confinement effect and concrete/reinforcement bond, as well as leaching and possible interactions with other distress mechanisms such as freeze and thaw cycles. Moreover, aspects such as the effect of loading on the mechanical properties reductions and on boundary conditions still have to be further analyzed. Future research for the authors will address an in-depth evaluation and validation of the proposed FE approach by modeling a slender reinforced concrete structure suffering from AAR-induced expansion and damage.

3.8 Conclusions

Based on the analysis and results presented, several conclusions can be made:

- The material validation results using the CDP model in Abaqus show that the ultimate load was accurately predicted and the average prediction of the ultimate deflection was satisfactory, although a larger variability was observed;

- The cracking pattern and load-deflection response of all beams in the material validation were well-predicted up to the point at which the model predicted failure to occur; however, the post-peak deformation of beams with stirrups was not fully captured by the model;

- Based on the literature and on the parametric studies performed, the suggested values for the CDP material model parameters are 31º dilation angle, 0.001 viscosity, 0.1 eccentricity, 1.16 for f_{b0}/f_{c0} and 0.667 for K;

- The analytical free expansion model predicted AAR-induced chemical reaction quite well, except for the expansion overestimation at the beginning, very likely because it does not account for leaching and/or microstructure phenomena such as gel accommodation (i.e., inner porosity, creep, etc.);

- The anisotropic stress-strain relationship proposed by [39] yielded better results than assuming the expansion to be isotropic;

- The effect of reinforcement confinement on AAR expansion was observed, and it described the experimental results well when the subroutine ratio was between 8 and 17 $[MPa]$, even though it loses accuracy at the beginning of the reaction when confining stresses are large;

- Accounting for degradation of mechanical properties did not noticeably affect the expansion over time for the unloaded specimens considered in this study, but it led to wider cracks and an overall larger damaged zone;

- The proposed FE model was validated using experimental push-off test specimens tested by [25] and proved to be capable of accurately simulating AAR-induced expansion. Further validation of in-service affected structures is still required, but results are very promising.

3.9 References

[1] B. Fournier and A. Bérubé, "Alkali-aggregate reaction in concrete: a review of basic concepts and engineering implications," *Canadian journal of civil engineering,* vol. 27, no. 2, p. 167–91, 2000.

[2] G. Giaccio, R. Zerbino, J. Ponce and R. Batic, "Mechanical behavior of concretes damage due to ASR," *Cement and Concrete Research,* vol. 38, p. 993–1004, 2008.

[3] T. Katayama, "The so-called alkali–carbonate reaction (ACR) — its mineralogical and geochemical details, with special reference to ASR," *Cement and Concrete Research,* vol. 40, p. 643–675, 2010.

[4] T. Katayama and P. Grattan-Bellew, "Petrography of Kingston experimental sidewalk at age 22 years - ASR as the cause of deleteriously expansive, so-called alkali-carbonate reaction," in *14th ICAAR — International Conference on Alkali–Aggregate Reaction in Concrete*, Austin, Texas, U.S.A., 2012.

[5] P. Fecteau, B. Fournier, M. Choquette and J. Duchesne, "Contribution to the understanding of the so-called alkali–carbonate reaction (ACR)," in *14th ICAAR — International Conference on Alkali–Aggregate Reaction in Concrete*, Austin, Texas, U.S.A., 2012.

[6] CSA-A864, "Guide to the Evaluation and Management of Concrete Structures Affected by Alkali-Aggregate Reaction," *Canadian Standards Association,* 2000.

[7] S. Multon, A. Sellier and M. & Cyr, "Chemo-mechanicalmodeling for prediction of alkali silica reaction (ASR) expansion," *Cement and Concrete Research,* vol. 39, p. 490–500, 2009.

[8] S. Poyet, A. Sellier, B. Capra, G. Foray, J. M. Torrenti, H. Cognon and E. Bourdarot, "Chemical modelling of alkali silica reaction: Influence of the reactive aggregate size distribution," *Materials and Structures,* vol. 40, p. 229–239, 2007.

[9] F. Ulm, O. Coussy, K. Li and C. Larive, "Thermo-chemo-mechanics of ASR expansion in concrete structures," *ASCE Journal of Engineering Mechanics,* vol. 126, p. 233–242, 2000.

[10] V. Saouma and L. Perotti, "Constitutive model for alkali-aggregate reactions," *ACI Materials Journal,* vol. 103, p. 194–202, 2006.

[11] R. Naar, "Modelisation du comportement mecanique du beton par approche multi-physique (couplage chimie–mecanique): application a la reaction alcali–silice - PhD. Thesis," Ecole Nationale Superieure des Mines de Paris, Paris, France, 2009.

[12] R. Esposito, The deterioration impact of alkali-silica reaction on concrete, vol. 1, Parma, Italy: Ipskamp Drukkers, 2016.

[13] F. J. Ulm, M. Petrson and E. Lemarchand, "Is ASR-expansion caused by chemoporoplastic dilatation?," *Computer Science and Engineering,* vol. 4, p. 47–55, 2002.

[14] E. Grimal, A. Sellier, Y. Le Pape and E. Bourdarot, "Creep, shrinkage, and anisotropic damage in alkali-aggregate reaction swelling mechanism-Part I: A consti-tutive model," *ACI Materials Journal,* vol. 105, p. 227–235, 2008.

[15] T. Wu, I. Temizer and P. Wriggers, "Multiscale hydro-thermo-chemo-mechanical coupling: Application to alkali-silica reaction," *Computational Materials Science,* vol. 84, pp. 381-395, 2014.

[16] R. Charlwood, "A review of alkali aggregate in hydro-electric plants and dams," *International Journal on Hydropower Dams,* p. 73–80, 1994.

[17] D. S. C. Simulia, "Abaqus/CAE - Complete Abaqus Environment - version 6.14," Simulia Dassault Systèmes Corporation, Providence, RI, USA, 2014.

[18] L. Sanchez, "Contribution to the Assessment of Damage in Aging Concrete Infrastructures Affected by Alkali-Aggregate Reaction, PhD. Thesis," Department of Geology and Geological Engineering, Université Laval, Quebec City, Quebec, 2014.

[19] M. Sanchez, B. Fournier, M. Jolin and D. J., "Reliable quantification of AAR damage through assessment of the Damage Rating Index (DRI)," *Cement and Concrete Research,* vol. 67, p. 74–92, 2015.

[20] L. F. M. Sanchez, F. B., M. Jolin, M. D. and J. Bastien, "Overall assessment of Alkali-Aggregate Reaction (AAR) in concretes presenting different strengths and incorporating a wide range of reactive aggregate types and natures," vol. 93, pp. 17-31, 2017.

[21] R. P. Martin, L. F. M. Sanchez, B. Fournier and F. Toulemonde, "Diagnosis of AAR and DEF: comparison of residual expansion, stiffness damage test and damage rating index and analysis of the expansive mechanisms," *Construction and Building Materials,* vol. 156, pp. 956-964, 2017.

[22] L. F. M. Sanchez, B. Fournier, J. M. and J. Bastien, "Evaluation of the Stiffness Damage Test (SDT) as a tool for assessing damage in concrete due to ASR: input parameters and variability of the test responses," *Construction and Building Materials,* vol. 77, pp. 20-32, 2015.

[23] L. F. M. Sanchez, B. Fournier, J. M. and J. Duchesne, "Reliable quantification of AAR damage through assessment of the damage rating index (DRI)," *Cement and Concrete Research,* vol. 67, pp. 74-92, 2015.

[24] F. J. Vecchio and W. Shim, "Experimental and analytical reexamination of classic concrete beam tests," vol. 130, no. 3, pp. 460-469, 2004.

[25] L. F. M. Sanchez, B. Fournier, J. Bastien and D. Mitchell, "Assessment of structures subjected to concrete degradation," ASCET, Quebec, Canada, 2016.

[26] S. V. Chaudhari and M. A. Chakrabarti, "Modeling of concrete for nonlinear analysis using finite element code ABAQUS," vol. 44, no. 7, pp. 14-18, 2012.

[27] B. Wahalathantri, D. Thambiratnam, T. Chan and S. Fawzia, "A material model for flexural cracks simulation in reinforced concrete elements using ABAQUS," Brisbane, Australia, 2011.

[28] D. V. Bompa and T. Onet, "Identification of concrete damaged plasticity constitutive parameters," in *The National Technical Scientific Conference – Modern Technologies for the 3rd Millenium*, Oradea, Romenia, 2010.

[29] W. Chen, Plasticity in Reinforced Concrete, New York: J Ross, 2007.

[30] A. S. Genikomsou and M. A. Polak, "Finite element analysis of punching shear of concrete slabs using damaged plasticity model in ABAQUS," *Engineering Structures,* vol. 98, pp. 38-48, 2015.

[31] N. F. Hany, E. G. Hantouche and M. H. Harajli, "Finite element modeling of FRP-confined concrete using modified concrete damaged plasticity," E*ngineering Structures,* vol. 125, pp. 01-14, 2016.

[32] J. B. Yan and J. Xie, "Behaviours of reinforced concrete beams under low temperatures," *Construction and Building Materials,* vol. 141, pp. 410-425, 2017.

[33] A. C. Ferche, D. K. Panesar, S. A. Sheikh and F. J. Vecchio, "Toward macro-modeling of alkali-silica reaction-affected structures," *ACI Structural Journal,* pp. Title No. 114-S91, 2017.

[34] C. Larive, "Apports combinés de l'éxpérimentation et de la modélisation à la compréhension de l'alcali-réaction et de ses effets mécaniques," Laboratoire Central des Ponts et Chaussées, France, 1997.

[35] N. Goshayeshi, R. V. Gorga, L. F. M. Sanchez and V. Alencar, "Contribution to the development of an analytical model to describe AAR kinetics and induced expansion," 2018.

[36] B. Fournier, R. Chevrier, A. Bilodeau, P. C. Nkinamubanzi and N. Bouzoubaa, "Comparative field and laboratory investigations on the use of supplementary cementing materials (SCM) to control alkali-silica reaction (ASR) in concrete," in *15th International Conference on Alkali-Aggregate Reaction - ICAAR*, São Paulo, Brazil, 2016.

[37] A. Lindgård, M. Thomas, E. Sellevold, B. Pedersen, Ö. Andiç-Çakır, H. Justnes and T. Rønning, "Alkali-silica reaction (ASR)-performance testing: influence of specimen pre-treatment, exposure conditions and prism size on alkali leaching and prism expansion," *Cement and Concrete Research,* vol. 53, p. 68–90, 2013.

[38] L. F. M. Sanchez, B. Fournier, J. Bastien, D. Mitchell and M. Noël, "Overall assessment of an ASR affected overpass "Robert-Bourassa/Charest" after nearly 50 years in service," Foz do Iguaçu, Brazil, 2016.

[39] B. P. Gautam, D. K. Panesar, S. A. Sheikh and F. J. Vecchio, "Multiaxial expansion-stress relationship for alkali silica reaction-affected concrete," vol. 114, no. 1, 2017.

[40] M. Saatcioglu and S. R. Razvi, "Strength and ductility of confined concrete," *ASCE Journal of Structural Engineering,* vol. 118, no. 6, pp. 1590-1607, 1992.

[41] P. Morenon, S. Multon, A. Sellier, E. Grimal, F. Hamon and E. Bourdarot, "Impact of stresses and restraints on ASR expansion," *Construction and Building Materials,* vol. 140, pp. 58-74, 2017.

4. PAPER 2 - FE APPROACH TO PERFORM THE CONDITION ASSESSMENT OF A CONCRETE OVERPASS DAMAGED BY ASR AFTER 50 YEARS IN SERVICE

Gorga, R.V.[a]; Sanchez, L. F. M. [b]; Martín-Pérez, B.[c]

(a) MASc. candidate – University of Ottawa, ON, Canada
(b) Assistant professor – University of Ottawa, ON, Canada
(c) Associate professor – University of Ottawa, ON, Canada

Abstract

Modeling alkali-silica reaction (ASR) induced expansion and damage in reinforced concrete structures is quite complex, yet necessary to obtain accurate predictions of the structural responses of distressed concrete members. In order to predict the expansion and damage at the structural (macroscopic) scale, a new simple yet reliable finite element (FE) approach was developed and validated by the authors. It accounts for the most important parameters affecting ASR through an engineering-based approach, without the need for non-technical guesses or to "fit" model parameters. In this work, the proposed modelling approach is used to analyze the Robert-Bourassa/Charest overpass (Quebec City, Canada), which was demolished in 2010 due to severe structural distress induced by ASR. Results show that the proposed FE approach is capable of properly performing the condition assessment of the structure at the time of demolition based only on simple measurable parameters, thus proving its applicability to simulate ASR in slender reinforced concrete structures.

***Keywords**: alkali-silica reaction, concrete deterioration, expansion, finite element, bridges*

4.1 Introduction

4.1.1 Finite Element modelling of AAR

Alkali-aggregate reaction (AAR), one of the most harmful distress mechanisms identified in concrete structures worldwide, is a chemical reaction between "unstable" silica mineral forms within the aggregates and the alkali hydroxides (Na, K – OH) dissolved in the concrete pore solution. This reaction generates a secondary alkali-silica gel that induces expansive pressures within the reacting aggregate material(s) and the adjacent cement paste upon moisture uptake from

its surrounding environment, thus causing microcracking and reduction of the material's properties (mechanical/durability) and, in some cases, compromising the functionality of the affected structure [1]. AAR is normally divided into two different categories: alkali-silica reaction (ASR) and alkali-carbonate reaction (ACR); ASR being by far the most commonly found around the world [1].

Currently, one of the biggest challenges in dealing with aging damaged concrete structures is to establish the correlation between the distress "signatures" caused by a given damage mechanism (e.g., ASR), and the reductions in mechanical properties, physical integrity, durability and performance of the affected material, as well as assess the consequent structural implications [2]. In this context, a number of different finite element (FE) models were developed in recent years with the aim of providing a condition assessment of ASR-affected structures along with forecasting their future behaviour. Esposito [3] classifies the existing ASR models in 4 different categories: micro-models (based on ion diffusion/reaction products), micro-meso-models (based on gel production), meso-models (based on internal pressure) and macro-models (based on concrete expansion). However, assessing the structural implications of ASR requires a macroscopic overview of the condition of the structure; therefore, macro-models will be the main focus of the present work.

The early macro-models represented AAR-expansion by imposing an equivalent isotropic thermal stress [4], which was a simplification necessary at the time considering the lack of understanding about the reaction's physicochemical mechanism and the computational tools available. Then, they eventually started introducing the influence of different parameters such as temperature and relative humidity [5], as well as implementing anisotropic stress-state relationships for the reaction's expansion [6], which considerably enhanced the accuracy of the

analyses. Next, they were subdivided into two categories: macro-models representing concrete as porous medium and as continuous medium. Porous medium allowed the introduction of several new parameters, such as the effect of porosity on the expansion and the influence of assuming concrete as an unsaturated medium (Grimal, et al., 2008a). This enhanced the degree at which the reaction was being described, but at the cost of increasing the need of calibrating and/or fitting several of these new parameters. At the same time, other authors kept increasing the accuracy of the continuous medium analyses by further assessing the parameters influencing the reaction and performing validation analyses [8, 9].

Even though important progress has been accomplished in the field, there was still need of a model capable of assessing the most important parameters affecting the reaction in a comprehensive and intuitive manner, without overcomplicating (and requiring fitting of parameters) or oversimplifying the description of the reaction and its structural implications. In this context, the FE approach developed in Chapter 3 was developed and validated by simulating non-linear damage in sound concrete and modeling AAR expansion for different confinement (i.e., stress state) conditions.

The FE approach proposed is based on the concrete damaged plasticity (CDP) model available in the commercially available FE software Abaqus [10], which is capable of representing the elastic and inelastic hydrostatic pressure-dependent behaviour of concrete under compression and tension [11, 12]. Its main failure mechanisms are assumed to be either concrete crushing or tensile cracking, and it is also capable of qualitatively estimating the cracking intensity and orientation by evaluating the plastic strain value. If an element or region overcomes the elastic limit, it starts developing plastic strain locally until global equilibrium is reached. As the load increases, the

plastic zone also increases, therefore simulating damage accumulation. Reinforcement is idealized as an elasto-plastic material and modeled with shared nodes.

Complimentarily, the chemical aspects of the reaction, which can be understood as the reaction kinetics and expansion prediction over time, were described by the physicochemical analytical model developed by [13] (reference free expansion input curve) and computationally implemented in the FE model by imposing an equivalent AAR strain. The model describes the free evolution of the reaction over time (i.e., unrestrained and unconfined expansion) based on Larive's equation [14] and seven of the most important parameters of the reaction. Larive's equation is a time-dependent exponential function that can represent the reaction phases previously described in Chapter 3. The seven parameters considered by the analytical equation are the type of reaction (ACR or ASR), aggregate type (coarse, fine or coarse and fine), aggregate reactivity (from negligible to very high damage degree, as defined by [15]), temperature, moisture (relative humidity), alkali content in the mix, and exposure conditions. Moreover, the model can assess the variation of some parameters, such as temperature and moisture content, over time, allowing the development of expansion curves that simulate the real climatic conditions of the structure under evaluation.

Lastly, the deterioration of the mechanical properties (i.e., reduction in the modulus of elasticity, compressive strength and tensile strength) is assumed to be a function of the ASR expansion level, according to [16], and the anisotropic stress-state dependency of the expansion proposed by [17] is implemented through an Abaqus user subroutine (USDFLD) as a function of two variables per principal direction: the field variable and the effective stress. Note that the field variable represents the reduction or increase of the expansion compared to the reference (free expansion input curve) and that the subroutine ratio, defined as the ratio between the maximum

stress difference (in MPa) and the average increment, should be kept between 8 and 17 MPa, according to sensitivity analyses presented in Chapter 3.

Although very promising, the FE approach proposed was validated using only laboratory (i.e., controlled conditions) specimens. Therefore, there is a need to verify the efficiency and reliability of the FE approach for the assessment of real damaged concrete structures.

4.1.2 Robert-Bourassa Charest overpass

Robert-Bourassa Charest (RBC) overpass was an ASR-affected highway bridge structure built in 1966 in Quebec City, Canada. The structure consisted of a varying thickness deck supported by reinforced concrete Y-shaped piers, which laid on top of massive concrete foundations. There is no specific information regarding the concrete mix designs; however, technical reports indicate that the reactive aggregate was a type of limestone and that the 28-day concrete design strengths were 24 MPa for the foundation blocks and 28 MPa for both the piers and the deck [18].

Over the last three decades, several distress signs were observed on various structural members, including extensive steel corrosion and concrete delamination/spalling at the level of the deck; map cracking, scaling, disaggregation and pop-outs affecting the massive concrete foundations due to ASR and freeze-thaw (FT) cycles; and concrete spalling and steel corrosion on the piers and foundations exposed to salt-water spray from traffic on the Robert-Bourassa highway [19]. Therefore, in order to assess the current state of the structure, several site inspection surveys, expansion monitoring campaigns and laboratory tests were performed on the RBC structure and cores extracted from its different structural elements. The results obtained indicated that the structure was no longer safe, thus leading to its demolition in 2010 and 2011. However, prior to the demolition, cores were extracted from its structural members (bridge deck, piers and

foundation blocks) and several test procedures were conducted at the lab on both the microscopic and mechanical (macroscopic) scales, which enabled a thorough evaluation of the bridge conditions at the time of the demolition.

4.2 Research significance

This paper presents the condition assessment of RBC's non-exposed and exposed piers at the time the structure was demolished. Results obtained through the computational model will be compared to data obtained from microscopic and mechanical test methods performed on cores extracted from these piers prior to the demolition of the RBC.

The main objective of this work is to verify the efficiency and reliability of the proposed FE approach to perform the actual condition assessment and to forecast both the future induced expansion and the damage in ASR-affected slender concrete structures.

4.3 Case study

4.3.1 RBC structural description

The structural stability of the Y-shaped piers was one of the main sources of concern for the engineers responsible for the structure. Therefore, the evaluation of the piers will be the main focus of this research. The original design and further investigations showed that the piers basically consisted of 3 regions: the base, the arm supporting a longer span (which will be defined as "S+ arm") and the arm supporting a shorter span ("S- arm") [20], as shown in Figure 4-1.

a

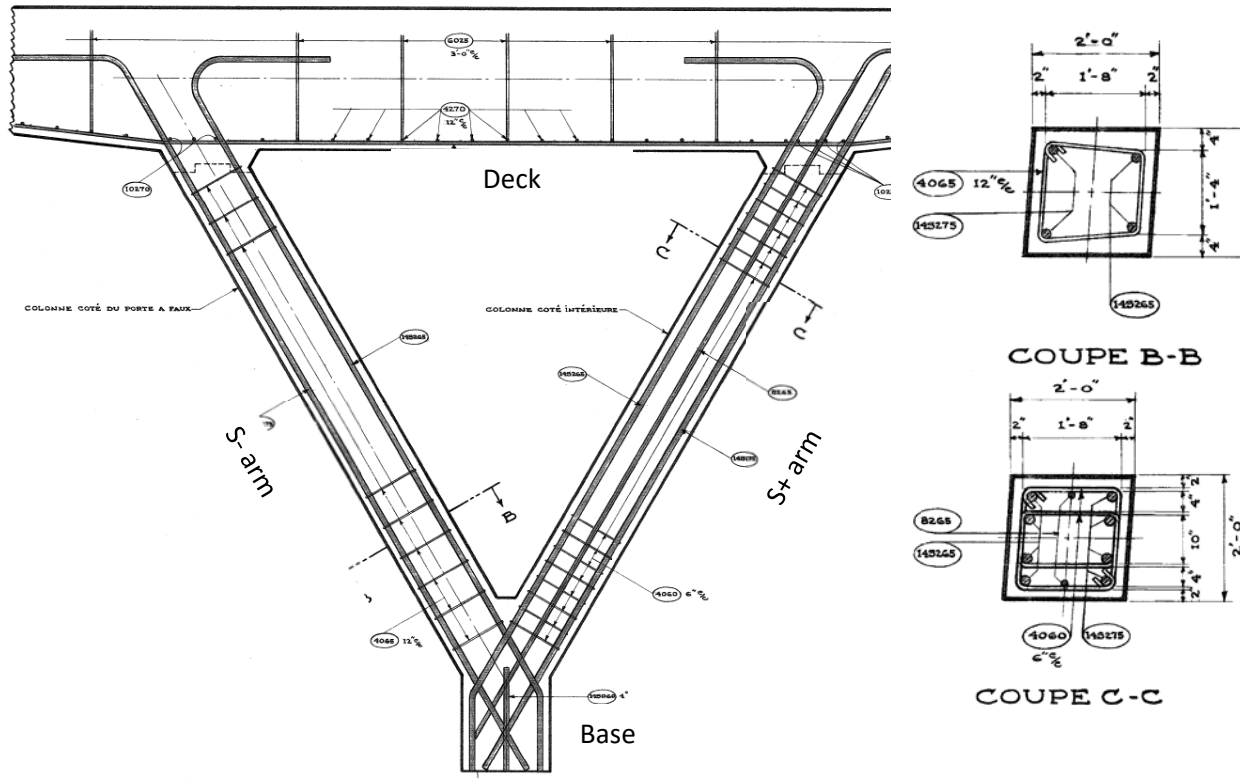

b

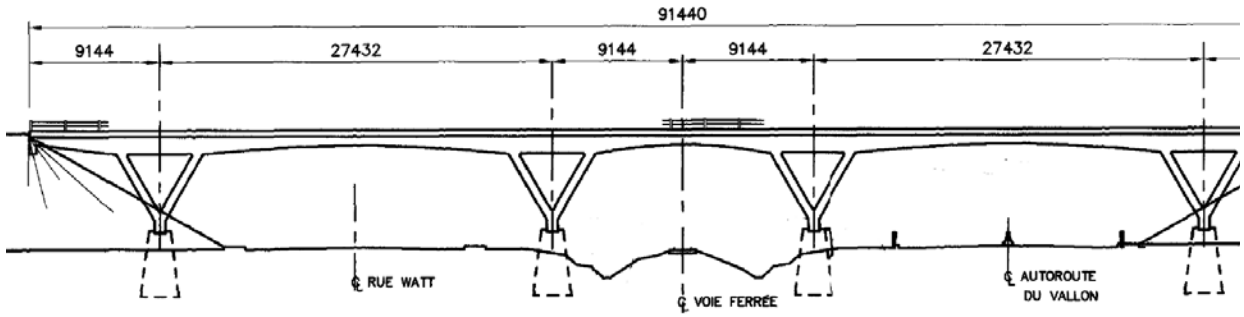

Figure 4-1. Y-shaped pier original design: a. Reinforcement detail (dimensions in inches), b. Overpass longitudinal view (dimensions in mm). Source: Adapted from [21].

The base was approximately 76 cm wide, 152 cm high and 61 cm deep. The reinforcement consisted of the extension of the longitudinal reinforcement of the arms and five additional vertical rebars connecting the pier and the foundation block, which were intended to create a semi-hinged connection. It is worth noting that no stirrups were specified for the base.

The angle between the arms was equal to 60º, and the connection between the deck and the arms of the pier was designed as a semi-flexible connection. It presented a shear key-type connection, even though all the longitudinal rebars passed through the deck-pier interface and were anchored on the upper half of the deck. Moreover, the entire pier was slightly slanted along one of the orthogonal directions (internal angle of approximately 85.5º) and there was a total of eight rows of four piers.

The S- arm was approximately 61 cm wide, 440 cm long and 61 cm wide. The S- arm supported the smallest span of the overpass, which was 18.3 meters long. The reinforcement consisted of stirrups spaced at 30.5 cm and four longitudinal rebars (one in each corner). Inspections attested that the diameter of the stirrups varied between 8 and 9 mm (8.5-mm diameter may be assumed as an average value), and the diameter of the longitudinal rebars was equal to 40 mm.

The S+ arm presented the same dimensions of the S- arm; however, it was more heavily reinforced because it supported the longest span (27.4 meters). The arms presented a total of ten longitudinal rebars (eight 40-mm rebars along the face perpendicular to the traffic direction and two 25-mm rebars on the other face). Stirrups were staggered (shifted left and right consecutively along the length), and they were spaced at 15 cm.

Note that, even though the middle portion of the arms does not present stirrups in the original project, inspections confirmed that stirrups were uniformly distributed along the length of both arms.

According to [22], the piers can be classified in 2 different categories according to their location: non-exposed (NE) and exposed (E) piers. Exposed piers were assumed to be highly subjected to solar radiation, weathering (rain, snow, freezing rain, etc.), pollution and splashing of both water

and de-icing salts, while non-exposed piers were considered to be mostly protected from those factors because of their surroundings.

4.3.2 Evaluation of RBC damage

Sanchez et al. [15] performed a number of multi-level (i.e., microscopic and mechanical) test procedures on RBC cores extracted from distinct members with the aim of detecting the overall damage degree of the structure at the time of its demolition. Amongst the analyses performed, interesting results were obtained through the Damage Rating Index (DRI), a microscopic tool often used to appraise damage and development of internal swelling reaction (ISR) mechanisms such as ASR.

The DRI is a microscopic analysis performed with the use of a stereomicroscope (16x magnification), where distress features associated with a damage mechanism (such as ASR) are counted through a $1\ cm^2$ grid drawn on the surface of polished concrete sections extracted from the structure being analyzed. The number of distress features, corresponding to each type of petrographic feature, is then multiplied by a weighing factor, whose purpose is to balance their relative importance towards the mechanism of distress. Ideally, a surface of at least $200\ cm^2$ should be used for the DRI analysis, and it may be greater in the case of mass concrete incorporating larger size aggregate particles. However, for comparative purposes, the final DRI value is normalized to a $100\ cm^2$ area [4]. Sanchez et al. [15] performed the DRI on different RBC piers (Exposed – E and Non-Exposed – NE); however, it is worth noting that some of them have been treated over the years with coatings and or silane-siloxane water repellants). The exposure classes and treatment details are displayed in Table 4-1.

Table 4-1. Treatment details on the different piers over time

Pier number	Exposure class	Treatment
17	E	Untreated
22	E	Treated - Waterproof sealant + Cementitious coating
23	E	Treated - Waterproof sealant + Silane/siloxane sealants
24	E	Treated - GFRP sheet
25	E	Treated - Waterproof sealant
28	NE	Treated - Waterproof sealant
29	NE	Treated - Epoxy sealant
30	E	Treated - Waterproof sealant + copolymer modified coating
32	E	Untreated
42	E	Untreated

Figure 4-2 presents the DRI semi-quantitative values of all the pier samples, where C and S represent “core” and “surface” of the piers cross section, respectively. Note that the first 7 cm cover was disregarded in the analysis, thus “surface” in this project refers to locations close to the transverse reinforcement, whereas “core” refers to the exact center of the piers.

All of the samples presented closed cracks within the aggregate particles (CCA), which might be attributed to other phenomena than ASR (i.e., aggregate production such as crushing, sieving, etc., along with weathering), as per [2]. However, opened cracks with and without gel within the aggregate particles (OCA and OCAG, respectively) and within the cement paste (CCP and CCPG) are indeed ASR features and were found in all samples, varying only as a function of the exposure class and treatment type. Furthermore, coarse aggregate debonded and disaggregated aggregate particles (CAD and DAP, respectively) are also ASR damage features, albeit less frequent, and they were only found in a few samples.

By analysing the data presented below, it is possible to state that most DRI numbers are within a range delimited by 200 and 400, which represents a marginal damage degree as by [16]. The DRI number for cores extracted from the North-West group of piers of RBC ranged from 200 to 300.

Hardly any differences were observed between one core and another, as well as between S and C specimens. Otherwise, the results obtained from the South-West/East RBC piers were slightly higher on average, ranging from 200 to 400. Exposed cores (piers 25 and 30) generally presented higher damage than NE samples (i.e., 28 and 29). Moreover, a significant number of cracks in the cement paste were found in the South-West/East group when compared to the North-West group. Therefore, two conclusions can be made: 1) ASR development was more pronounced on this group of piers (since cracks in the cement paste are considered the last step in ASR development as by [2]) and; 2) it is likely that there are other mechanisms combined with ASR, such as freezing and thawing cycles, which cause distress in the cement paste and display similar damage patterns than reported by the authors. Finally, no significant difference was found from one core to another nor from specimens cored from the surface and cored from the core in this group of piers.

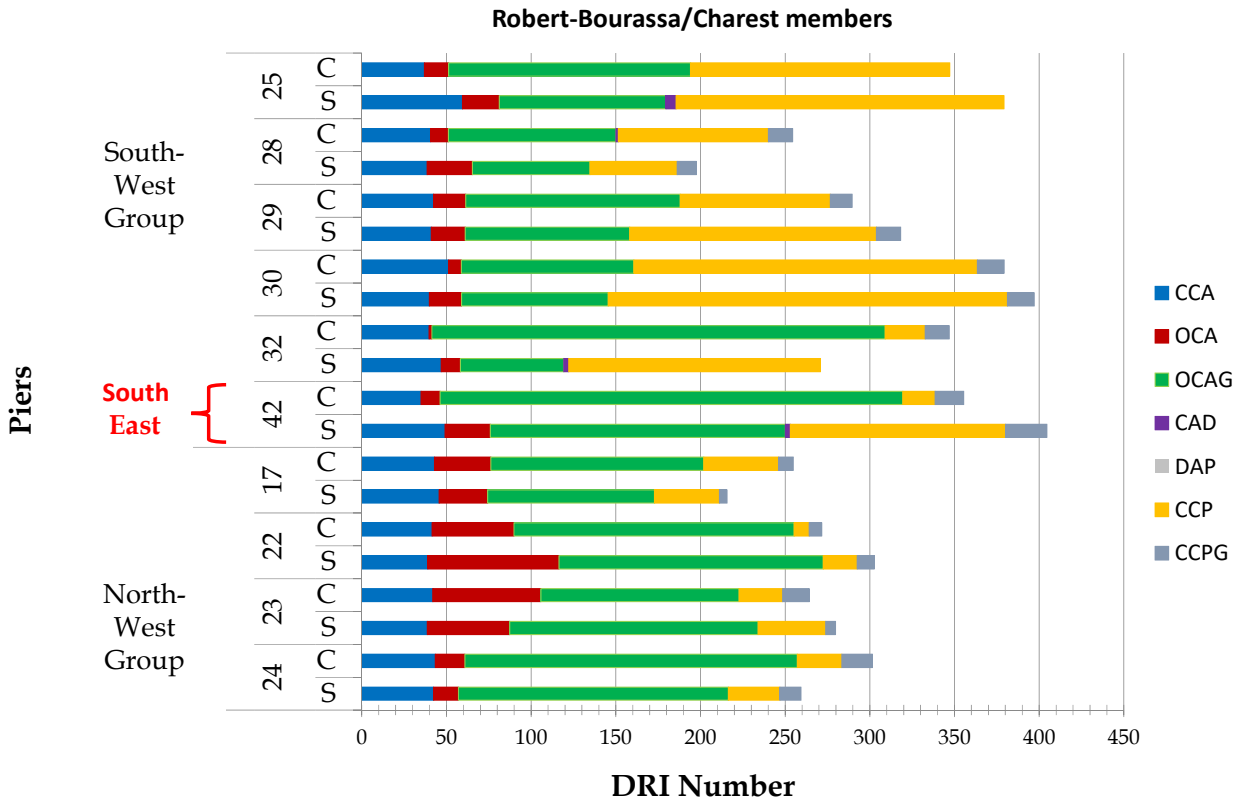

Figure 4-2. DRI results for RBC piers at the core (C) and surface (S). Source: Sanchez et al. (2018)

Additionally, [15] determined an equivalent expansion level for each exposure class, which can be understood as the estimated ASR development (or expansion attained to date) needed to cause a damage degree similar to that observed in the DRI procedure. The authors found that, even though the aggregate was considered highly reactive (and thus presented a free expansion potential of 0.20-0.25% in the concrete prism test according to [23]), the attained equivalent expansion obtained was 0.05% for the NE piers and between 0.08% and 0.10% for the E piers (on average). According to the authors, the expansion observed was lower than expected under free expansion likely due to the anisotropic behaviour of the reaction when subjected to confinement effects along with the fact that the field conditions (e.g., temperature and relative humidity) were not accounted for in laboratory test procedures.

Laboratory tests were also performed on various stirrups extracted from distinct piers to determine their mechanical properties and thus check whether ASR had had any effect on them [20]. Stress-strain curves were obtained for stirrups from E and NE piers, and no significant difference between the two cases was observed. Therefore, the average stress-strain curve shown in Figure 4-3 can be assumed to represent the mechanical behaviour of the transverse reinforcement. Since no data was available regarding the longitudinal reinforcement, the same stress-strain behaviour was assumed for both materials.

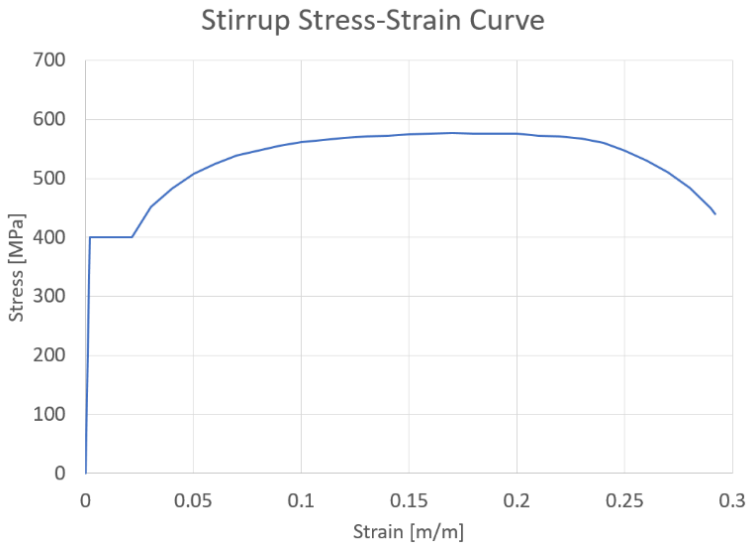

Figure 4-3. Stirrup stress-strain curve

Strain relief tests were performed on the South East/West E and NE 3-m long pier section that were cut, prepared and taken to the lab. The strain was measured using strain-gauges at the middle of stirrups of the S+ arm, which were located at midspan and were from the face parallel to traffic (where there are only 3 rebars, as illustrated in Figure 4-1a). Table 4-2 summarizes the results obtained in terms of micro-strains ($\mu strain$). Table 4-2 illustrates that the results found for the stirrups in the E piers were significantly higher compared to the NE piers' stirrups. In some cases, the difference in strain relief was found to be almost double.

Table 4-2. Stirrups' relief test

Location	E (µstrain)	NE (µstrain)
Stirrup 01	1126	540
Stirrup 02	1486	442
Stirrup 03	1259	726
Average	1290	569

Lastly, it is important to describe the climatic conditions of the location where the bridge was built, because ASR is directly influenced by the temperature and relative humidity (RH) of the exposure environment [22]. According to [24], the average relative humidity (measured at 6 AM), the daily

average temperature and the number of days when the maximum temperature is above 12ºC (which is the threshold temperature for AAR to develop based on [13]) for Quebec City are presented in Table 4-3 for each month in the year.

Table 4-3. Exposure condition in Quebec City, Canada

Month	$Relative\ Humidity$ [%]	$Temperature$ [^{o}C]	$Maximum\ temperature\ above\ 12^{o}C$ [$days$]
January	72.7	-12.8	0.0
February	72.8	-10.6	0.1
March	73.7	-4.6	0.6
April	73.8	3.7	8.1
May	74.1	11.2	23.9
June	78.8	16.4	28.0
July	84.2	19.3	30.4
August	85.3	18.1	29.9
September	86.3	12.7	25.1
October	83.1	6.6	14.4
November	81.1	-0.7	1.9
December	79.0	-8.6	0.2
Yearly average	78.7	4.2	-

4.3.3 FE model of RBC

The Y-shaped pier of the RBC overpass was modelled in Abaqus according to the geometric and design specifications outlined in Section 3.1. Concrete was represented by 8-node cube elements, and the steel reinforcing bars were idealized as 3D beam elements to properly simulate the confinement effect provided by the reinforcement as the ASR expansion develops. As discussed in Chapter 3, a beam element generates higher and more realistic confinement values because it presents both axial and transverse stiffness, while a truss element only has axial stiffness. Furthermore, the reinforcing bars were modeled in the FE model by sharing nodes with the concrete elements, thus assuming perfect bond. The finite element mesh of the RBC pier mode is illustrated in Figure 4-4. Further simplifications assumed in the FE model of the RBC, to either

reduce the computational cost of the analysis or make the mesh less complex, as well as the boundary conditions imposed are presented below.

First, the pier-deck connection was assumed to be rigid (as if they had been cast together). This was done because the actual behaviour of the connection and the influence of ASR over time on the connection were not known, as well as because all the longitudinal rebars of the pier went through the interface and were anchored on the top half the deck. Additionally, the horizontal displacement was restrained on the top 4 exterior rows of nodes on both sides of the pier to simulate the stiffness that the concrete deck would impose to the pier's arms.

Next, the pier's cross-section was assumed to have 90º angles between all edges instead of being slanted (85.5º and 94.5º as illustrated in Figure 1a). Moreover, the pier-foundation interface was simplified by restraining vertical displacement on all the interface nodes, by restraining horizontal displacement on the 4 bottom rows of nodes of the base on the S- arm side, which is the direction where the structure tends to deform due to the higher load on the S+ arm, and by neglecting the structural effects of the connecting rebars. The latter was assumed because the actual behaviour of the connection and the influence of ASR over time were unknown, as well as because the number and diameter of the rebars were likely too small to significantly affect the structural response of the member. Lastly, symmetry along the Z axis was assumed as presented in Figure 4-4, where the longitudinal reinforcement and the connecting rebars are represented in green, stirrups are represented in red and the concrete mesh is shown in green. Note that a total of 22476 elements were used to model the concrete and 1856 elements to model both the transverse and longitudinal reinforcements.

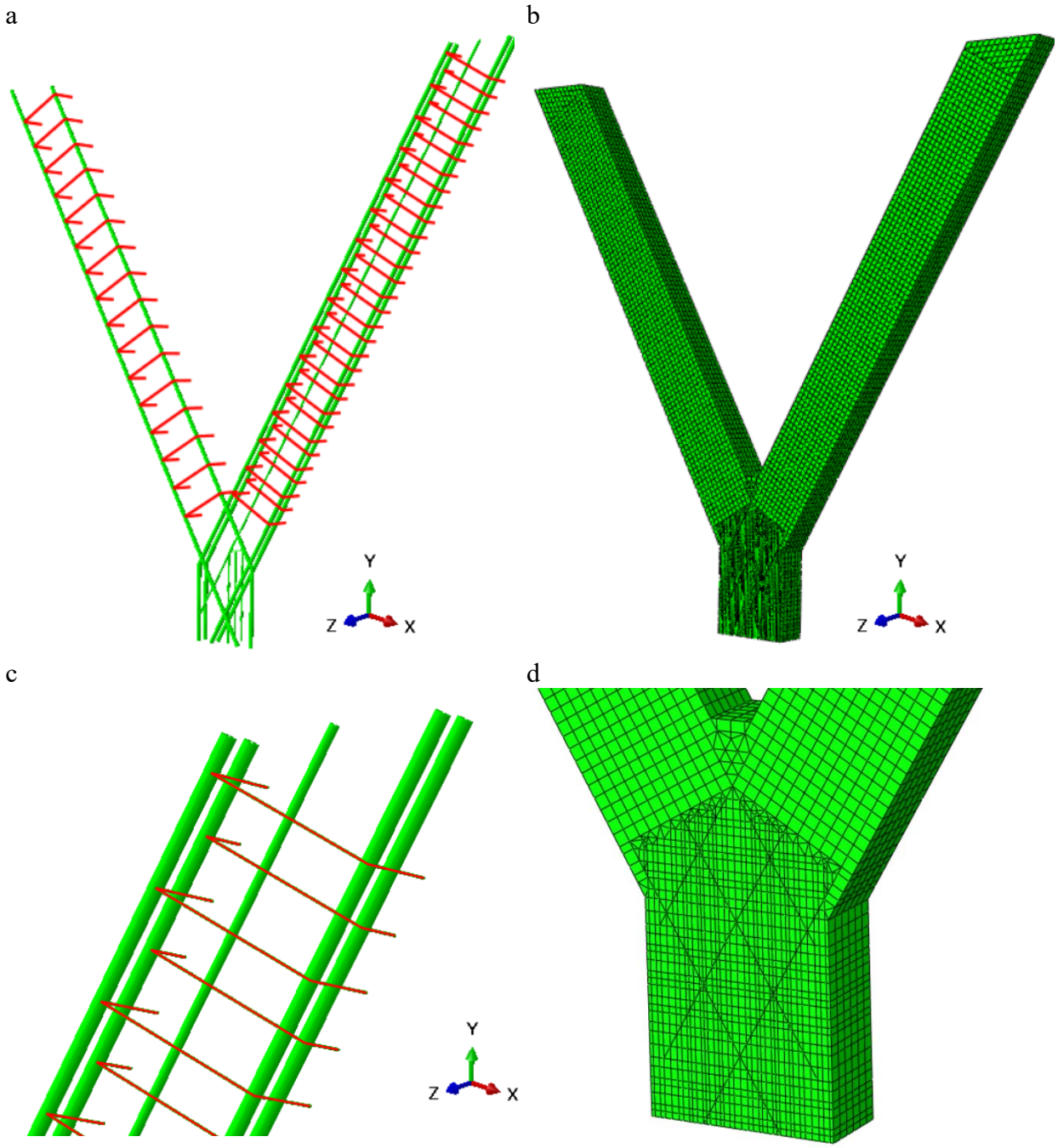

Figure 4-4. RBC FE model: a. reinforcement, b. concrete mesh, c. detail stirrups S+ arm, d. detail mesh of the base

It is important to emphasize that symmetry slightly changes the disposition of the S+ arm stirrups.

As previously mentioned in Section 3.1, the S+ arm stirrups were staggered (consecutively shifted

right and left). However, by imposing symmetry to the model, the stirrups have two different sizes alternated along the length of the arm, one smaller and one larger. This was assumed to be a feasible simplification because the structural response of the arm would likely not be heavily affected and because this approach allowed the number of nodes of the model to be reduced by 50%, therefore considerably reducing the computational cost of the analysis.

Based on the pier's design, the structural member was divided in 4 regions regarding its confinement conditions: cover (unconfined), arm S- core (confined), arm S+ core (confined) and base core (confined). The structural implications of the confinement on the arms were calculated according to the model proposed by [25], which is capable of describing the increase in compressive strength and ductility of concrete based on an equivalent uniform confinement pressure generated by the reinforcement cage as a function of several parameters (i.e., area of transverse reinforcement, spacing between stirrups, yielding stress of the reinforcement, compressive strength of the concrete, concrete strain at peak stress, spacing between longitudinal rebars supporting the stirrups, etc.). However, it is important to emphasize that the approach had to be slightly adapted for the base, because it did not present transverse reinforcement. The lack of stirrups leads to the conclusion that there would be no increase in compressive strength or ductility based on the confinement model, since the equivalent confining stress would be equal to zero. However, the base can be assumed to be confined by the stresses transferred by the inclined arms, which means that the equivalent confining stress at the base would be equal to the horizontal component of the dead load being transferred by the arms. Note that, to simplify the model, the equivalent confining stress was assumed to be equal on both directions. Table 4-4 summarizes the increase in compressive strength (f'_c) and ductility (peak strain) for each region due to reinforcement confinement/compressive stress field on sound concrete:

Table 4-4. Reinforcement confinement effect on sound concrete

Location	f'_c $[MPa]$	peak strain $(\times 10^{-3})$
Unconfined (Cover)	27.6	1.11
Confined (S+)	30.1 (+9.1%)	1.69 (+45.5%)
Confined (S-)	29.2 (+5.8%)	1.47 (+28.9%)
Confined (Base)	29.7 (+7.6%)	1.59 (+37.8%)

The tensile (direct cracking) strength (f_t) for normal weight concrete was estimated based on [26] and it is shown in Equation 4-1. Moreover, the modulus of elasticity (E) was determined according to the [27] for a concrete with density (γ_c) of 2450 kg/m^3, as presented in Equation 4-2.

$$f_t = 0.33\sqrt{f`_c} \tag{4-1}$$

$$E = \left(3000\sqrt{f`_c} + 6900\right) \times \left(\frac{\gamma_c}{2300}\right)^{1.5} \tag{4-2}$$

The reduction in mechanical properties for the highly reactive aggregate type used in the RBC concrete mix as a function of the expansion is presented in Table 4-5 according to the data reported by [16].

Table 4-5. Mechanical properties deterioration

Expansion [%]	0.05%	0.12%	0.20%
f'_c reduction [%]	6.8	0.6	11
E reduction [%]	9.1	36.3	44.8
f'_t reduction [%]	6.5	62.0	78.8

It is important to emphasize that the increase in compressive strength at low levels of ASR development is not necessarily due to the chemical reaction but rather due to the net gain of the combined effects of hydration and ASR damage. At an expansion level of 0.20%, the deterioration mechanism already governs the overall behaviour, thus leading to a reduction of the compressive strength [16].

Another important phenomenon that is considered in the FE model is creep, which was taken into consideration based on Equations 4-3 and 4-4, presented by [26]:

$$\phi(t) = 3.5K_cK_f\left(1.58 - \frac{H}{120}\right)t_i^{-0.118}\left(\frac{(t-t_i)^{0.6}}{10+(t-t_i)^{0.6}}\right) \quad (4\text{-}3)$$

$$E_{eff}(t) = \frac{E}{1+\phi(t)} \quad (4\text{-}4)$$

where t is the number of days after casting, t_i is the number of days after casting when concrete was loaded, $\phi(t)$ is the creep coefficient, H represents the relative humidity level, K_f is a factor accounting for the concrete strength, K_c is a factor that accounts for the influence of volume-to-surface ratio of the member, E is the original modulus of elasticity and $E_{eff}(t)$ is the effective modulus of elasticity at time t. The creep coefficient (ϕ) variation over time, as presented in section 4.3, is illustrated in Figure 4-5. It is worth noting that all stress-strain curves were defined as a function of the reference expansion, which allows the model to take the mechanical properties reduction and the variation of the creep coefficient over time into consideration based on the same variable.

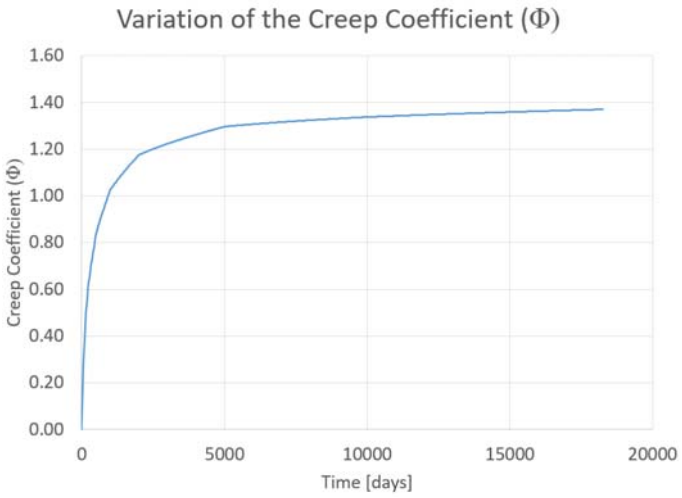

Figure 4-5. Creep coefficient over time

Lastly, it is worth noting that the influence of temperature and relative humidity over the thickness of the member is not the same, according to [5] and [28]. Both authors developed FE macro-models to describe the structural effects of ASR and, based on their respective analyses and validation models, proposed the concept of heat characteristic length (l_L) and humidity characteristic length (l_w). These parameters describe a zone in which the combined effects of ASR and thermal diffusion or humidity diffusion occur, respectively. In summary, the idealized length predicts that the region between the outer surface and the characteristic length is subjected to temperature or humidity variations based on the ambient conditions. However, beyond the characteristic length, the inner concrete region remains unaffected because the effect of heat or humidity transfer due to exposure conditions is negligible. Consequently, the differential expansion of the inner and outer layers may lead to delamination of the concrete cover, as predicted by the models of both authors. Equations 4-5 and 4-6 describe the heat characteristic length and the humidity characteristic length according to [5]:

$$l_L = \sqrt{D_\theta \tau_L(\theta_s)} = \sqrt{\frac{\kappa}{C}\tau_L(\theta_s)} \tag{4-5}$$

$$l_w = \sqrt{D_w \tau_L(w)} \tag{4-6}$$

where D_θ is the thermal diffusivity $[m^2/K]$, which can be understood as the thermal conductivity κ divided by the heat capacity C, $\tau_L(\theta_s)$ is the latency time according to [14] as a function of the surface temperature θ_s, D_w is the humidity diffusion coefficient, and $\tau_L(w)$ is the latency time based on the relative humidity w. The equation proposed by [28] was based on the work of [5]; in addition to the previously described equations, it also assumes that τ_L is a function of both the temperature at the surface (θ_s) and the degree of saturation at the surface ($S_{W\Gamma}$), and that D_W is also a function of the degree of saturation at the surface. The most important aspect observed by

both [5] and [28] was the order of magnitude of l_L and l_w. The authors concluded that the humidity characteristic length has values much lower than the heat characteristic length (usually centimeters instead of meters), which implies that the role of non-uniform moisture distribution in slender structures (bridges, for example) may play a similar role as the non-uniform temperature gradients on the structural degradation of massive structures (such as dams). Therefore, this work assumed that the ambient temperature would affect the entire depth of the structure, because the pier is only 60 cm deep, which means that the member can be assumed to be roughly at the monthly average ambient temperature. Moreover, the ambient relative humidity was assumed to only affect the first few centimeters of the pier, i.e., the cover, while the core would be at a constant 100% relative humidity. This tends to generate differential expansion between the core and the cover, which likely will lead to cracking and delamination of the surface of the concrete member, as commonly observed in the field.

4.4 Analysis results and discussion

The FE model presented in Section 4.3 was subjected to the dead load of the pier and of that transferred from the deck in addition to the progressive ASR-induced expansion mechanism. It was found that the overall behaviour of the ASR-affected concrete over time could be accurately described as a function of 7 representative expansion values: 0%, 0.003%, 0.010%, 0.030%, 0.050%, 0.120% and 0.200%. Therefore, a total of 56 curves were defined for the model; i.e., tensile and compressive behaviours based on seven representative expansion values for the four regions subjected to different confinement conditions. Note that Abaqus [10] automatically interpolates all values between the described points linearly.

The analysis was divided in two different time-steps, each with 1000 increments. The first time-step corresponds to the application of the dead load, while the second time-step consists of imposing the ASR-induced expansion to the concrete, once the applied load has already been fully applied to the structure. It is important to apply the loads and calculate the stresses first, and only then apply the expansion since ASR is a function of the stress-state of each element, which means that the initial stress-state dictates the initial expansion conditions. Moreover, note that the maximum stress variation defined for the USDFLD subroutine is equal to $10 \times 10^{-3} MPa$, and the average increment is equal to 1×10^{-3}; hence, the subroutine ratio corresponds to $10MPa$, which is within the previously defined range of $8 - 17MPa$.

The only load imposed to the pier was the dead load due to self-weight of the deck and the pier itself. The influence of the deck was determined by an idealized 2D hyper-static truss model of the entire length of the bridge. It assumed that the weight of concrete is $24.5\ kN/m^3$, and the tributary area was defined based on the distance between piers of approximately 3.30 m. As a result of this analysis, it was determined that the S+ arm of each half pier would be subjected to 676 kN and the S- arm would be subjected to 199 kN, both of which were applied to the model as pressure loads. Moreover, the self-weight of the pier was accounted for by defining the mass density of the materials ($2450\ kg/m^3$ for concrete and $7800\ kg/m^3$ for steel) and specifying the gravity acceleration as $9.81 m/s^2$.

According to the analytical ASR model and based on the climatic conditions for Quebec City (Table 4-3), it was possible to define the reference curves used for the non-exposed and exposed piers based on the monthly average values. As previously mentioned, the reference expansions for the core and cover are different due to the different relative humidity levels of these regions, which means that each case has 2 reference curves. The non-exposed pier was assumed to have the core

at 100% relative humidity and the cover at the monthly average relative humidity, with both regions being at the monthly average temperature. Note that, based on Table 4-3, ASR would only take place from June to September, because the minimum temperature required for the reaction to develop is 12ºC, according to the analytical ASR model proposed by [13]. However, the months of May and October both have several days where the maximum temperature is higher than that threshold, which means that totally disregarding these months would result in an underestimation of the final expansion. Therefore, it was assumed that the "equivalent" temperature for May would be 12.0ºC to approximate the real expansion of the reaction for both months.

Conversely, the exposed pier could not directly be assessed by the analytical equation, because it does not account for the effects of sun radiation (and its consequent hourly variations of temperature or temperature gradients), exposure to rain and snow, exposure to de-icing salts, splashing due to traffic, pollution and other factors that might create micro-environments. Therefore, these parameters were taken into consideration indirectly by modifying the original temperature and relative humidity coefficients. The monthly average temperature was increased by 13.5ºC based on Clause 3.9.4.4 of [27], which defines the temperature differentials for structures consisting of concrete systems with concrete decks (Figure 4-6). Note that only the summer conditions were used because ASR only takes place when the temperature is above 12ºC, the depth of the structure is 60 cm, and the variation was applied uniformly throughout the pier to simplify the approach.

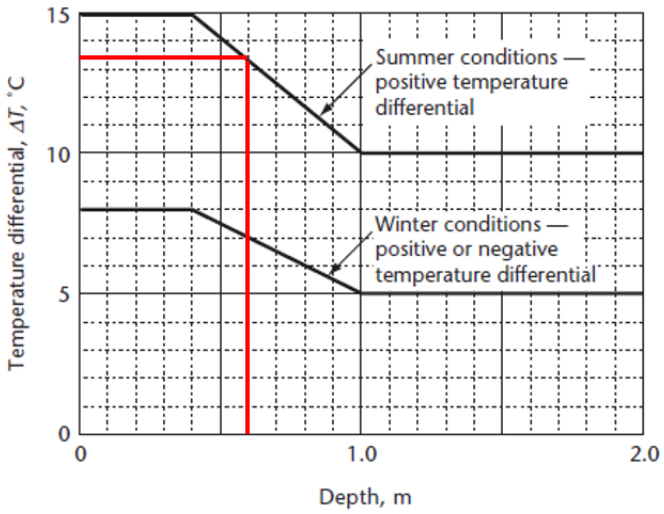

Figure 4-6. Temperature differentials for exposed conditions. Source: [27]

Additionally, three different cases were assumed for the RH conditions of the cover: original values, global increase of the values and local increase of the values of the monthly average relative humidity. The increase was calculated assuming that the daily RH value would be 100% at the cover on the current and the following day whenever it rained, which was based on daily values of precipitation from 2006 to 2017. These new updated daily RH values were then used to calculate the updated monthly average relative humidity values. As the name suggests, the global increase would take place uniformly in the entire cover, while the local increase would only take place at horizontal regions, which are more likely to accumulate water (i.e., the small horizontal region where the two arms connect to the base and at the bottom of the base due to the presence of the foundation block). The original and updated monthly average RH values are presented in Table 4-6.

Table 4-6. Original and updated monthly average relative humidity

Month	Original Relative Humidity [%]	Updated Relative Humidity [%]
January	72.7	87.8
February	72.8	87.8
March	73.7	84.9
April	73.8	86.4
May	74.1	85.6
June	78.8	89.5
July	84.2	91.6
August	85.3	91.5
September	86.3	91.9
October	83.1	91.2
November	81.1	89.7
December	79.0	92.5
Yearly	78.7	89.2

Figure 4-7 presents the reference curves for both the non-exposed and all 3 exposed cases previously described, as well as the maximum potential expansion predicted for the high damage degree type of reactive aggregate used in the pier (assuming 100% relative humidity and 38ºC). Note that the non-exposed and exposed curves are not continuous, which is a result of ASR not being developed during the winter season due to low temperature.

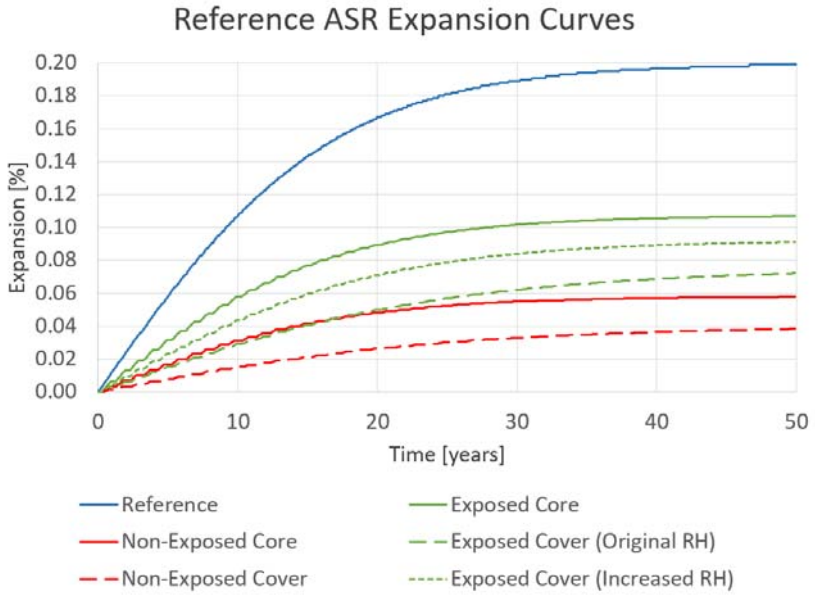

Figure 4-7. Reference ASR expansion curves

A total of 3 parameters were used to compare the FE and the measured values. First, a comparison between the equivalent expansion obtained by [22] and the reference expansion determined through the analytical model was performed. Then, the strain measured in the transverse reinforcement at the lab was compared to the FE results. Lastly, a visual and qualitative crack comparison was performed. Note that all values presented hereafter are for the 900th increment (90%) of the analysis, because it represents the 45th year – demolition age – out of the 50 years in service being described by the analytical model. As described in Chapter 3, the analytical ASR model is able to roughly capture the in-service expansion potential based on results reported by [29] and [20]. Table 4-7 summarizes the results of the expansion comparison.

Table 4-7. Equivalent (measured) vs reference (analytical) expansions

Case	Equivalent Expansion [%]	Reference Expansion [%]	
Non-Exposed	0.05	NE core	0.06
		NE cover	0.04
Exposed	0.09	E core (RH original)	0.11
		E cover (RH original)	0.07
		E cover (RH increased)	0.09

Even though both approaches are approximations of the expansion induced by ASR, it is clear that the results yielded by the analytical model are in agreement with the equivalent expansion determined by [22]. The equivalent expansion is always between the range defined by the expansion of the core and the cover, as well as very close to the average between those values, which indicates that the analytical model can describe the damage extent observed in the microscopy analysis when the local climatic conditions are considered.

Next, the strain measured in the lab was compared to the results obtained by the FE model. Table 4-8 presents the percentage error found for each case evaluated. Note that the strain used in the comparison was calculated as the final strain of the model (ASR and loads being considered) minus

the initial strain due to the dead loads. This was done because the stirrups were measured in the sections of the S+ arm that had been cut off from the pier (i.e., unloaded condition) prior to its demolition and stored in the lab.

Table 4-8. Stirrups strain comparison

Case	Percentage Error [%]
Non-Exposed	3.2
Exposed (RH original)	-32.6
Exposed (RH global)	-34.2
Exposed (RH local)	-32.4

The results show that ASR was accurately simulated for the non-exposed case, with a small overestimation of 3.2%. This means that, even though simplifications such as the stirrup disposition due to symmetry boundary conditions and the approximation of the confinement effect in the base's core were assumed, the reaction was represented correctly when the environmental conditions were taken into consideration and the member could be assumed as sheltered by the surroundings.

Conversely, the results for the exposed pier yielded results approximately 33% smaller than actual results measured in the lab. Even though the strain was underestimated, this does not necessarily mean that the damage due to ASR was underestimated. The simplifications of assuming a uniform temperature increase and using only the summer conditions according to Figure 4-6 might have had some impact on the results. However, as described in Section 4.3, other distress mechanisms such as freeze-thaw cycles may have significantly contributed to the overall damage observed and, most likely, significantly affected the strain measured. These phenomena are naturally more prominent in the exposed case, which means that an underestimation of the strain is expected since the model only accounts for ASR. Therefore, it is possible to state that the exposed conditions

were properly simulated. Furthermore, the three exposed cases yielded very similar results, which means that this parameter alone is not enough to conclude which approach is the most accurate.

Lastly, a visual and qualitative crack comparison is presented. A qualitative approach was selected instead of a quantitative approach because of two main reasons. First, the FE model is not able to quantify the number of cracks because it does not represent discrete cracks, i.e., the same element can display more than one crack at the same time because they are assumed to be smeared over the element. Second, the FE approach is not very accurate when predicting actual crack widths because it only provides the plastic strain per element with its principal orientation, which can be interpreted as one or more cracks in an element and provide a general representation of the width of the crack, but it is not capable of accurately capturing the real width. Therefore, a qualitative approach comparing the ratio of the maximum crack width (maximum plastic strain value) of the exposed case by the non-exposed case for the S+ arm, S- arm and base is presented in Table 4-9. Note that the original maximum crack width measured values were obtained from [30].

Table 4-9. Qualitative crack width comparison

Location	Measured	RH original	RH global	RH local
Maximum crack opening S+ arm ratio	3.11	2.48	1.20	3.18
Percentage error S+ arm	-	-25.5%	-159.0%	2.2%
Maximum crack opening base ratio	0.92	1.58	0.78	1.60
Percentage error base	-	41.6%	-17.4%	42.5%
Maximum crack opening S- arm ratio	1.62	1.75	0.92	2.04
Percentage error S- arm	-	7.4%	-76.4%	20.6%
Average of percentage errors	-	7.8%	-84.3%	21.8%
Coefficient of Variation of percentage errors	-	4.3	-0.8	0.9

Moreover, Figures 4-8, 4-9 and 4-10 compare the observed and FE cracking patterns of the non-exposed pier, the base of the exposed pier subjected to the 3 RH scenarios, and the exposed pier subjected to the 3 RH scenarios, respectively. Note that regions in blue are lightly damaged,

regions in red are moderately damaged and regions in light grey are the highly damaged (largest cracks and/or indication of possible spalling or delamination).

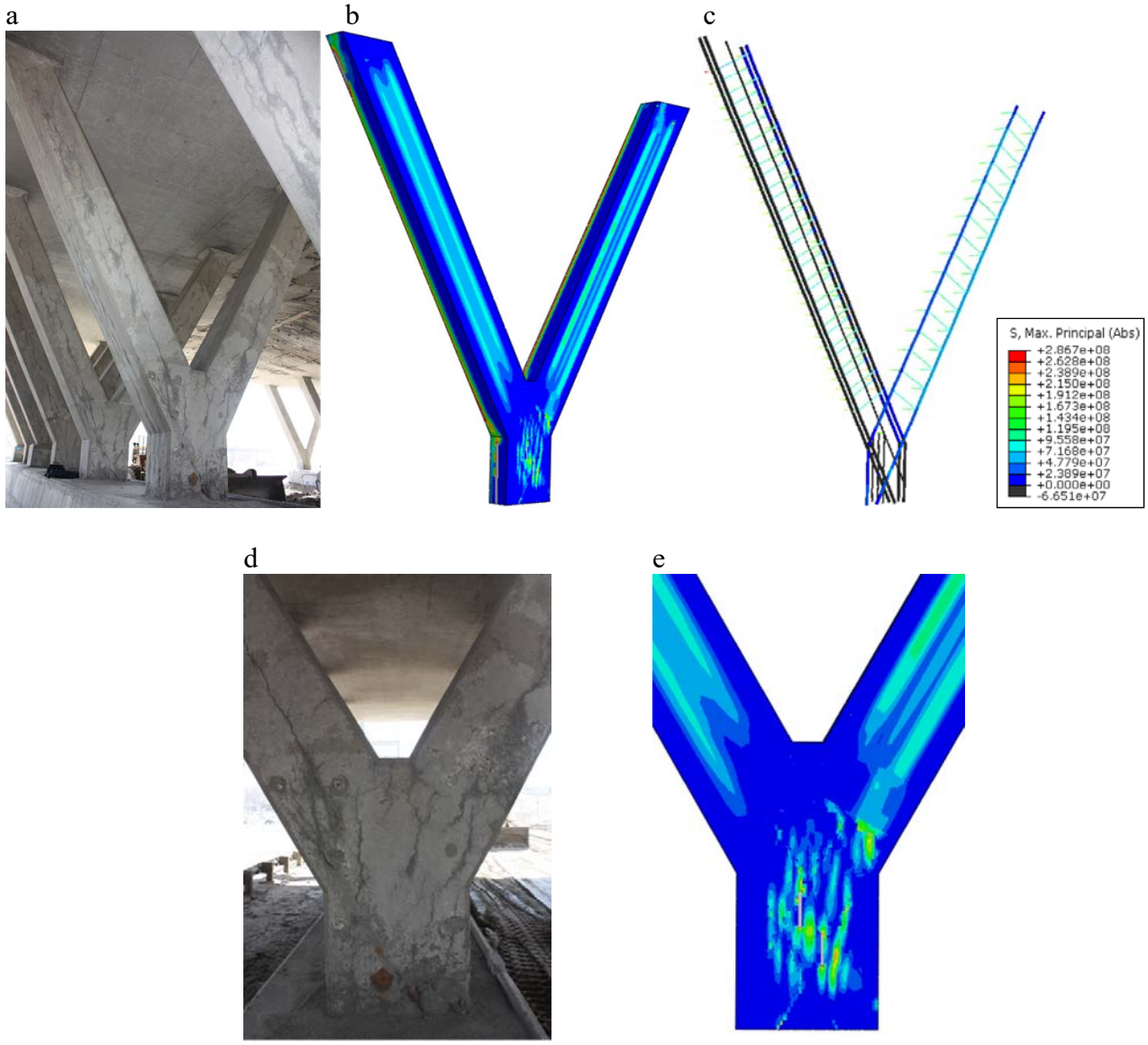

Figure 4-8. RBC non-exposed pier: a. Overall observed damage, b. FE overall damage (plastic strain), c. FE reinforcement stress (in Pa), d. Observed damage in the base, e. FE damage in the base (plastic strain)

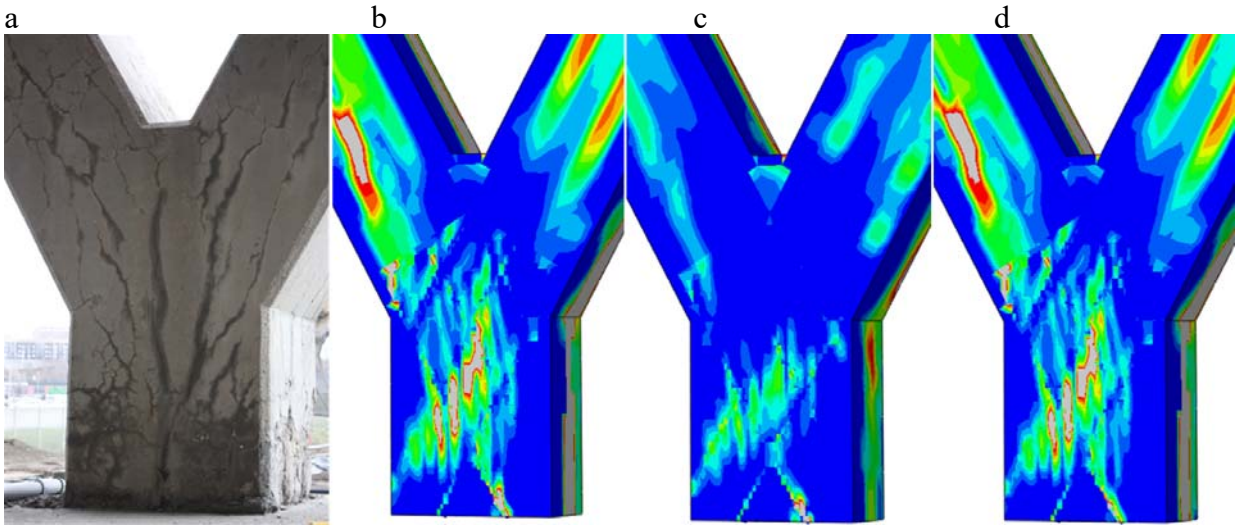

Figure 4-9. RBC exposed pier: a. Observed damage in the base, b. FE damage in the base (plastic strain) with original RH, c. FE damage in the base (plastic strain) with global RH, d. FE damage in the base (plastic strain) with local RH

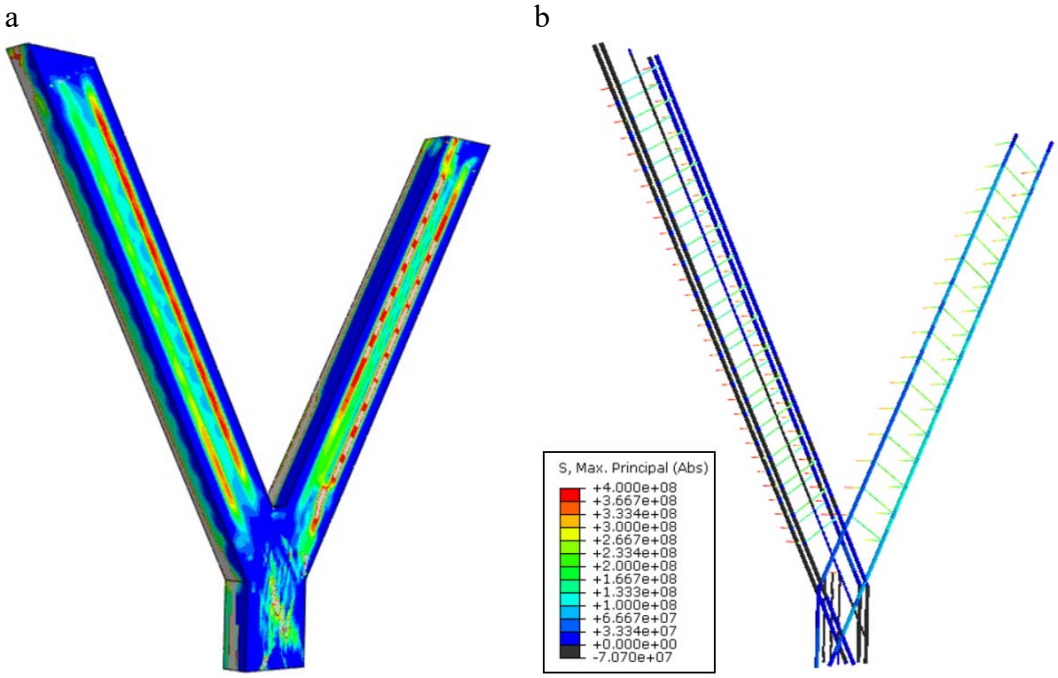

c

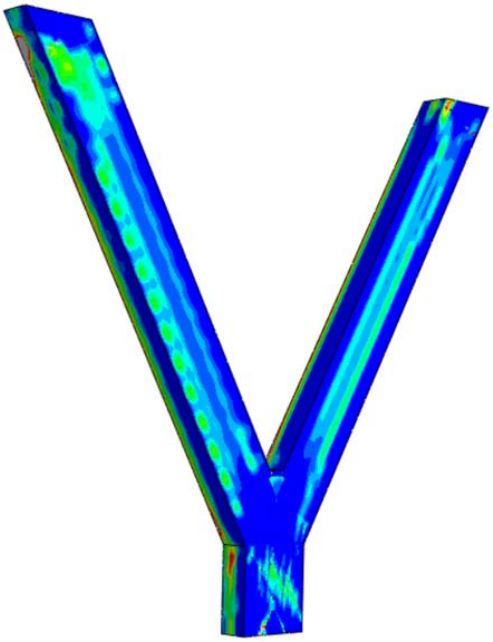

d

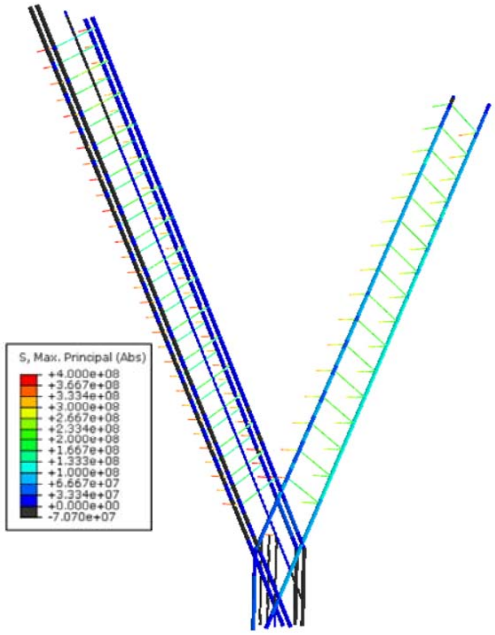
S, Max. Principal (Abs)
+4.000e+08
+3.667e+08
+3.334e+08
+3.000e+08
+2.667e+08
+2.334e+08
+2.000e+08
+1.667e+08
+1.333e+08
+1.000e+08
+6.667e+07
+3.334e+07
+0.000e+00
-7.070e+07

e

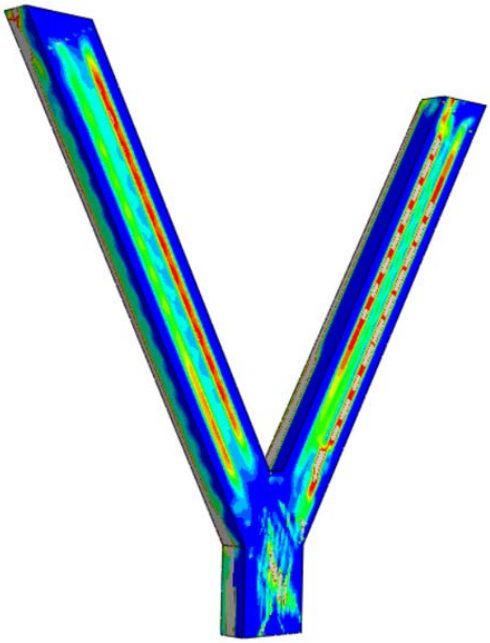

f

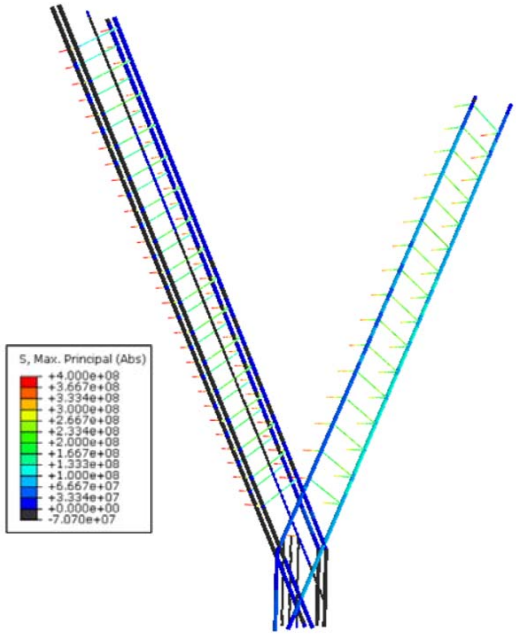
S, Max. Principal (Abs)
+4.000e+08
+3.667e+08
+3.334e+08
+3.000e+08
+2.667e+08
+2.334e+08
+2.000e+08
+1.667e+08
+1.333e+08
+1.000e+08
+6.667e+07
+3.334e+07
+0.000e+00
-7.070e+07

g

Figure 4-10. RBC exposed pier: a. FE overall damage (plastic strain) with original RH, b. FE reinforcement stress with original RH, c. FE overall damage (plastic strain) with global RH, d. FE reinforcement stress with global RH, e. FE overall damage (plastic strain) with local RH, f. FE reinforcement stress with local RH (stress values are in Pa), g. Overall observed damage.

Finally, Table 4-10 compares the time (in years) at which yielding first happened and how many rebars yielded at the end of the analysis.

Table 4-10. Reinforcement yielding comparison

Description	Non-exposed	Exposed RH original	Exposed RH global	Exposed RH local
First yielding [year]	-	17.1	22.4	17.1
Number of stirrups yielded at 45 years (S+ arm)	0	6 (3 at the top and 3 at the bottom)	4 (2 at the top and 2 at the bottom)	6 (3 at the top and 3 at the bottom)
Number of stirrups yielded at 45 years (S+ arm)	0	2 (1 at the top and 1 at the bottom)	0	2 (1 at the top and 1 at the bottom)

Table 4-9 shows that the global increase of the relative humidity yields worse results than the two other cases evaluated. The percentage error of the strain in the stirrups shown in Table 4-8 is almost

the same for all cases, because the expansion of the core does not change, i.e., it is always equal to 100%. However, by increasing the RH of the cover, the magnitude of the differential expansion between the two regions decreases (the expansions of the core and cover are closer to each other than they were before), which tends to generate less cracks. As presented in Table 4-9, this approach leads to an underestimation of 84.3% of the widths of the cracks. Moreover, lower stress values and a smaller number of stirrups yielding was observed for the global RH exposure case according to Table 4-10 and Figures 4-8, 4-9 and 4-10, as expected. Therefore, a global RH increase does not seem to be the most accurate approach to simulate the exposure of the structural member.

Table 4-9 also shows that the two other cases evaluated (assuming original RH or local increase of RH) yield good results. The original RH approach results in a better overall approximation of the width of the cracks based on the smaller value of the average percentage error (7.8% instead of 21.8%), but it also results in a larger coefficient of variation (4.3 instead of 0.9). Therefore, once again, it is not possible to state which approach is the most precise.

Figures 4-8, 4-9 and 4-10 illustrate that the global increase of RH results in less cracking than the other cases, as expected. Moreover, they show that the cracking pattern yielded by the model matches very well with what was observed in the field for the non-exposed pier and both the original RH and local RH exposure approaches for the exposed pier. The most important aspects observed regarding the cracking pattern are that most larger cracks follow the orientation of the longitudinal reinforcement in both the arms and the base, the exposed pier displays wider cracks than the non-exposed pier, the delamination of the concrete on the lateral face of the base was captured, the spalling at the front of the base was captured (even though the model sometimes

predicted that the largest spalling was happening at the opposite side), and the damage observed for the original RH and local RH exposure conditions was indistinguishable.

Based on Table 4-10 and Figures 4-8, 4-9 and 4-10, it is possible to state that the stresses in the reinforcement led to the same results for the original RH and local RH cases. The results of the two approaches are basically the same, which means that it is not possible to justify the use of the local RH approach over the original (simpler analysis). Therefore, the suggested approach to simulate the exposure conditions based on the presented results is to increase the temperature uniformly based on [27] and keep the original RH conditions. It is worth noting that this conclusion is supported by the experiments performed by [31], which show that the ASR expansion of specimens subjected to wetting and drying cycles lies between that of specimens subjected to 96% and to 59% constant relative humidity.

Table 4-10 also shows that more stirrups yielded in the S+ arm than in the S- arm. This was likely due to net effect of the lateral redistribution of the expansion due to the dead load and the redistribution in the longitudinal direction caused by transverse reinforcement confinement. The lateral redistribution in the S+ arm due to the larger applied dead load overcame the larger confinement of that region in a greater proportion than in the S- arm, therefore leading to a greater lateral expansion in the S+ arm and a larger number of yielded stirrups.

It is important to emphasize that the model predicted that the first stirrup would yield approximately 17 years after the construction of the structure and it would have a total of 8 stirrups yielded at the time the structure was demolished. The stirrups that yielded were either at the top or bottom of the arms, because those are the regions where the shear stresses are the largest and because of the local conditions of expansion redistribution. This means that the structure, especially approaching the demolition period (i.e., 45 years in service), was indeed in danger of

collapsing because it was not behaving as it had initially been designed for. The pier did not collapse when any of the stirrups yielded, from the first to the eighth stirrup, because of the structural redundancy in the design, which results in stress redistribution and an increase in deformation when yielding takes place. Otherwise, the FE results show that the structure seemed to be close to global failure, even though ASR-induced expansion might be considered close to its plateau after 45 years in service. Therefore, the decision to demolish the overpass instead of retrofitting it seems to be supported by the results of the proposed model, especially considering that combined phenomena such as freeze-thaw cycles and steel corrosion were not accounted for in the analyses.

4.5 Conclusions

Based on the analyses and results presented, several conclusions can be made:

- The equivalent damage determined by [22], based on microscopic analyses, matched well the reference expansion curves yielded by the analytical ASR model when the climatic conditions were considered;

- The transverse reinforcement strain of the non-exposed pier from the FE model was in agreement with values measured in the lab (3.2% overestimation), which means that ASR is being correctly simulated by assuming the temperature of the entire pier equal to the monthly average and the two RH zones (core at 100% and cover at average monthly values);

- Based on the qualitative cracking comparison, it was found that globally increasing the relative humidity of the cover to simulate the exposure conditions is not the best approach, because it reduced cracking beyond what was observed in the field. Note that this happened because the approach lowered the differential expansion magnitude between the cover and the core;

- Regarding the cracking pattern comparison, the qualitative cracking comparison and the stirrup strain comparison, it was not possible to justify the use of the local RH approach to simulate exposure conditions. Therefore, assuming the uniform increase in temperature based on [27] and the original RH conditions is the suggested method to account for the exposure conditions. Even so, further investigation is still necessary;

- The exposed pier stirrup strain yielded by the model underestimated the lab values by 32.6%. However, the reaction can still be assumed to be properly represented by the described approach, because the strain underestimation can be explained by the fact that the model does not account for other likely combined distress mechanisms, such as freeze-thaw cycles and steel corrosion. According to [22], these mechanisms may account for approximately 25% of the damage observed;

- The cracking pattern obtained by the model accurately matched the cracking orientation, cracking intensity and location of spalling/delamination for both non-exposed (less damaged) and exposed (more damaged) piers;

- Prior to its demolition, the structure was near global failure because several stirrups had already yielded in the exposed pier due to ASR expansion. Therefore, the decision to demolish the overpass is supported by the analyses presented.

- Even though the FE approach yielded good results, a number of parameters should be further evaluated in order to fully describe the ASR-induced expansion and the actual behaviour of the structure throughout its life span. Regarding the chemical reaction (free AAR expansion analytical model), the most important parameters are the casting orientation, leaching of alkalis, porosity of the concrete, supplementary cementing materials (SCMs) and, especially, exposure conditions

(sun radiation, thermal gradient, rain, snow, de-icing salts, pollution, splashing, etc.). Furthermore, regarding the macroscopic structural assessment of AAR-affected structures, the most important phenomena are shrinkage, concrete/reinforcement bond and both the individual and combined structural implications of AAR and other distress mechanisms (mostly corrosion and freeze-thaw cycles).

- Lastly, it is important to emphasize that the proposed approach is valid for slender structures where the leaching of alkalis can be accurately represented by the existing standardized lab tests, which were the basis for the analytical model adopted. Therefore, the approach would have to be revised before it could be applied to massive structures, such as dams.

4.6 References

[1] B. Fournier and A. Bérubé, "Alkali-aggregate reaction in concrete: a review of basic concepts and engineering implications," *Canadian journal of civil engineering,* vol. 27, no. 2, p. 167–91, 2000.

[2] L. F. M. Sanchez, B. Fournier, J. M. and J. Duchesne, "Reliable quantification of AAR damage through assessment of the damage rating index (DRI)," *Cement and Concrete Research,* vol. 67, pp. 74-92, 2015.

[3] R. Esposito, The deterioration impact of alkali-silica reaction on concrete, vol. 1, Parma, Italy: Ipskamp Drukkers, 2016.

[4] R. Charlwood, "A review of alkali aggregate in hydro-electric plants and dams," *International Journal on Hydropower Dams,* p. 73–80, 1994.

[5] F. Ulm, O. Coussy, K. Li and C. Larive, "Thermo-chemo-mechanics of ASR expansion in concrete structures," *ASCE Journal of Engineering Mechanics,* vol. 126, p. 233–242, 2000.

[6] V. Saouma and L. Perotti, "Constitutive model for alkali-aggregate reactions," *ACI Materials Journal,* vol. 103, p. 194–202, 2006.

[7] E. Grimal, A. Sellier, Y. Le Pape and E. Bourdarot, "Creep, shrinkage, and anisotropic damage in alkali-aggregate reaction swelling mechanism-Part I: A consti-tutive model," *ACI Materials Journal,* vol. 105, p. 227–235, 2008a.

[8] J. Pan, Y. Feng, F. Jin and C. Zhang, "Numerical prediction of swelling in concrete arch dams affected by alkali-aggregate reaction," *European Journal of Environmental and Civil Engineering,* vol. 17, no. 4, pp. 231-247, 2013b.

[9] A. Winnicki, S. Serega and F. Norys, "Chemo-plastic-modelling of alkali-silica reaction (ASR)," *Computational Modelling of Concrete Structures (EURO-C),* vol. 2, p. 765–774, 2014.

[10] D. S. C. Simulia, "Abaqus/CAE - Complete Abaqus Environment - version 6.14," Simulia Dassault Systèmes Corporation, Providence, RI, USA, 2014.

[11] D. V. Bompa and T. Onet, "Identification of concrete damaged plasticity constitutive parameters," in *The National Technical Scientific Conference – Modern Technologies for the 3rd Millenium*, Oradea, Romenia, 2010.

[12] B. Wahalathantri, D. Thambiratnam, T. Chan and S. Fawzia, "A material model for flexural cracks simulation in reinforced concrete elements using ABAQUS," Brisbane, Australia, 2011.

[13] N. Goshayeshi, R. V. Gorga, L. F. M. Sanchez and V. Alencar, "Contribution to the development of an analytical model to describe AAR kinetics and induced expansion," 2018.

[14] C. Larive, "Apports combinés de l'éxpérimentation et de la modélisation à la compréhension de l'alcali-réaction et de ses effets mécaniques," Laboratoire Central des Ponts et Chaussées, France, 1997.

[15] L. F. M. Sanchez, B. Fournier, J. Bastien, D. Mitchell and M. Noël, "Overall assessment of an ASR affected overpass "Robert-Bourassa/Charest" after nearly 50 years in service," Foz do Iguaçu, Brazil, 2016.

[16] L. F. M. Sanchez, F. B., M. Jolin, M. D. and J. Bastien, "Overall assessment of Alkali-Aggregate Reaction (AAR) in concretes presenting different strengths and incorporating a wide range of reactive aggregate types and natures," vol. 93, pp. 17-31, 2017.

[17] B. P. Gautam, D. K. Panesar, S. A. Sheikh and F. J. Vecchio, "Multiaxial expansion-stress relationship for alkali silica reaction-affected concrete," vol. 114, no. 1, 2017.

[18] ICAAR Visit Report, "Report of the visit of structures affected by AAR in the Quebec City area," 11th ICAAR - International conference on alkali-aggregate reaction, Quebec, Canada, 2000.

[19] M. Bérubé, N. Smaoui, B. Fournier, B. Bissonnette and B. Durand, "Evaluation of the expansion attained to date by concrete affected by ASR - Part III: Application to existing structures," *Canadian Journal of Civil Engineering,* vol. 32, pp. 463-479, 2005.

[20] L. F. M. Sanchez, B. Fournier, J. Bastien and D. Mitchell, "Assessment of structures subjected to concrete degradation," ASCET, Quebec, Canada, 2016.

[21] M. o. T. o. Q. MTQ, "Report on the Robert-Bourassa Charest overpass reinforcement and overall dimensions," Internal communication, Quebec City, Canada, 1964.

[22] L. F. M. Sanchez, M. Noel and V. A. A. Santos, "Techniques to Rehabilitate Bridge Columns Affected by Alkali-Silica Reaction (ASR)," in *9th International Conference on Bridge Maintenance, Safety and Management - IABMAS - Accepted paper*, Melbourne, Australia, 2018.

[23] CSA A23.2-14A, "Potential Expansivity of Aggregates; Procedure for Length Change Due to Alkali-Aggregate Reaction in Concrete Prisms," Canadian Standards Association, Missisauga, Ontario, Canada, 2014.

[24] Environment and Climate Change Canada, 05 12 2017. [Online]. Available: https://www.canada.ca/en/services/environment/weather/climatechange.html. [Accessed 05 12 2017].

[25] M. Saatcioglu and S. R. Razvi, "Strength and ductility of confined concrete," *ASCE Journal of Structural Engineering,* vol. 118, no. 6, pp. 1590-1607, 1992.

[26] M. Collins and D. Mitchell, Prestressed concrete structures, vol. 1, Toronto, Canada: Response Publications, 1997.

[27] CSA S6-14, "Canadian highway bridge design code," Canadian Standard Association, Missisauga, Ontario, Canada, 2014.

[28] C. Comi, B. Kirchmayr and R. Pignatelli, "Two-phase damage modeling of concrete affected by alkali–silica reaction under variable temperature and humidity conditions," vol. 49, p. 3367–3380, 2012.

[29] B. Fournier, R. Chevrier, A. Bilodeau, P. C. Nkinamubanzi and N. Bouzoubaa, "Comparative field and laboratory investigations on the use of supplementary cementing materials (SCM) to control alkali-silica reaction (ASR) in concrete," in *15th International Conference on Alkali-Aggregate Reaction - ICAAR*, São Paulo, Brazil, 2016.

[30] B. Fournier, L. F. M. Sanchez, P. Salva and S. Beauchemin, "Outils d'investigation de la réactivité alcalis-granulats dans les infrastructures en béton - Rapport final 1 - 289p," Ministère des transports du Québec Service des matériaux d'infrastructure - Secteur béton de ciment, Montreal, Canada, 2015.

[31] S. Poyet, A. Sellier, B. Capra, G. Thèvenin-Foray, J. M. Torrenti, H. Tournier-Cognon and E. Bourdarot, "Influence of water on alkali-silica reaction: Experimental study and numerical simulations," *ASCE - Journal of Materials in Civil Engineering,* vol. 18, no. 4, pp. 588-597, 2006.

5. SUMMARY AND CONCLUSIONS

5.1 General

In this research, a new FE approach to assess AAR-affected structures is presented and validated based on several analyses, which included sound concrete, AAR expansion and a case study of a slender (bridge) structure affected by AAR. The commercially available software Abaqus (Simulia, 2014) was the chosen FE package for the analyses. In summary, the approach consisted of defining the geometry and mesh of the reinforced concrete structures, specifying the material properties based on the Concrete Damaged Plasticity (CDP) model available in the software (which takes into consideration creep, confinement due to reinforcement and non-linear behaviour of concrete in both tension and compression), defining boundary conditions, applying the mechanical loads, and imposing a stress-state dependent AAR expansion through a USDFLD subroutine that describes the reaction`s anisotropy relationship proposed by Gautam et al. (2017). This modeling technique has been proven to be a reliable tool to estimate both the current state (diagnosis) and the future state (prognosis) of AAR-affected structures based only on measurable parameters and without the need to fit parameters to adjust the model. The most important findings are presented below.

- Concrete Damaged Plasticity material model

The CDP model available in Abaqus (Simulia, 2014) was able to simulate the non-linear elastoplastic behaviour of concrete quite accurately, as long as the proposed parameter values defined by parametric studies are adopted (i.e., 31º dilation angle, 0.001 viscosity, 0.1 eccentricity, 1.16 for f_{b0}/f_{c0} and 0.667 for K). The ultimate load prediction and the cracking pattern were precisely predicted for all beams used in the validation of sound concrete. The predicted ultimate deflection at midspan for the sound concrete validation was satisfactory, even though a larger

variability was observed. When comparing the failure mode of each beam, it is clear that the material model is quite accurate in describing diagonal-tension failure and flexure-compression failure. However, the CDP was not able to simulate shear compression failure as accurately as the other failure modes, likely because the shear stress transfer from the concrete to the reinforcement and the behaviour close to the ultimate load, when larger cracks quickly widen and reinforcement yields, were not fully captured. On the other hand, the damage observed in the RBC overpass was well captured in the FE analyses for both the exposed and the non-exposed piers.

- AAR free expansion over time

The model developed by Goshayeshi et al. (2018) was adopted as the basis to describe free AAR swelling. It was found to be a very intuitive and powerful prediction tool, especially due to the fact that its coefficients have a clear physical meaning, that they can vary over time to fully simulate the environmental conditions of the location of the structure and that it does not require extensive fitting of several parameters. In the RBC overpass analysis, for both the exposed and non-exposed cases, the reaction was able to predict the overall behaviour of the AAR expansion without any fitting being required. However, it is not a perfect approach, as seen in the expansion validation. Since the model does not account for leaching, an indirect approach had to be used to represent that phenomenon by reducing the coefficient describing the alkali availability of the mix. Even though this approach was based on data from the literature (Lindgård, et al., 2013), the proposed analytical model was not able to fully describe the overall behaviour of the four-stirrups (4S) push-off specimen in the early stages. Therefore, the model was found to accurately describe AAR-induced free expansion, even though it could be enhanced by including the effects caused by other phenomena, especially at early ages.

- AAR anisotropic expansion

The model proposed by Gautam et al. (2017) was implemented into the FE model to allow the stress-state dependence of the reaction to be taken into consideration. It was described as a function of effective stresses and the maximum stress difference value between increments and increment size (summarized as the subroutine ratio). The approach was evaluated in the AAR expansion validation, based on the adjusted free expansion curve predicted for the 0S (no-stirrup) case. Note that, since the expansion imposed to all cases was the same, the effect of confinement could be clearly evaluated. The model was able to almost perfectly predict the final expansion for the different confinement cases as long as the subroutine ratio was kept within the specified range (between 8 and 17 MPa), but it seems to be less precise in the early stages of expansion for higher confining stresses. This is likely due to the magnification of the expansion prediction inconsistency in the first 30% of the analysis (due to indirectly accounting for leaching), when larger confining stresses govern, the limitations of the mathematical approach and the likely impact that confinement has on both AAR gel formation and on AAR's physicochemical properties (a phenomenon which is still not fully understood). The approach was also implemented in the RBC overpass analyses, and the results obtained were in close agreement with the measured data. Additionally, it is important to emphasize that if the values of the subroutine ratio were kept within the specified range, the reaction would develop as expected. However, lower values would lead to a considerable (unrealistic) delay in the expansion, and larger values would lead to convergence errors, therefore prematurely terminating the analysis.

- Case study: RBC overpass

The analysis of the RBC overpass consisted of simulating two piers, one exposed and one non-exposed, and it was based on the comparison of three different parameters: equivalent expansion level, qualitative cracking and strain in the stirrups. Two different regions in the pier were defined, i.e., the concrete cover (with RH equal to the environmental RH) and concrete core (with RH=100%), and that the same temperature was assumed for the entire section due to its slender nature, based on Ulm et al. (2000) and Comi et al. (2012). The results of the equivalent expansion level matched the values obtained by Sanchez et al. (2018) when determining the necessary expansion level to generate the damage observed in the microscopy analyses. Also, the qualitative cracking results (both visually and numerically) were in close agreement with what was observed/recorded in the field. Lastly, the strain in the stirrups calculated for the non-exposed pier matched almost perfectly the value recorded by Sanchez et al. (2016) with an overestimation of only 3.2%, while the values for the exposed pier were less precise, displaying an underestimation of 32.6%. To simulate the exposed case, the reference temperature of the free ASR expansion imposed to the pier was increased and the RH was maintained, but it has been found through microscopic analyses reported by Sanchez et al. (2018) that other phenomena might also have contributed to the overall damage recorded (i.e., freeze-thaw cycles, etc.). Therefore, this underestimation can be attributed to the fact that the model developed only accounts for AAR, not any of the other phenomena that are likely playing a significant role in the recorded stirrup strain for the exposed case.

5.2 Recommendations and Future Research

The proposed FE approach to assess AAR-affected structures was proven to be accurate and reliable. Even so, several aspects can still be implemented to either improve its applicability or further validate its outcome, as presented below:

Improving the analytical free AAR expansion model developed by Goshayeshi et al. (2018) would be necessary to accurately account for exposure (wetting-drying cycles, splashing, de-icing salts, etc.) and other phenomena affecting the reaction, such as leaching. Additionally, the effect of the alkali content on the expansion should be based on more accurate data to understand its implications on both the final expansion and on the reaction kinetics.

Further evaluating the behaviour of the CDP material model would also be useful to fully comprehend its applicability and limitations. This could be done by testing more reinforced concrete beams (or other types of reinforced concrete members), ideally in 3D instead of 2D. The other beams tested by Vecchio and Shim (2004), which were not modeled in this project, are a good option, but work from other researchers should also be included to increase the variability of the test conditions.

Further validating the AAR expansion by modeling the experiment performed by (Multon & Toutlemonde, 2006) would provide a deeper understanding regarding the effect of confinement on the expansion (without having to take the effect of leaching into consideration in the analysis).

An additional AAR validation for concrete beams tested in a controlled environment would also consolidate the reliability of the model. The suggested approach would be to cast and test the same beams presented by Vecchio and Shim (2004) but using one or more types of reactive aggregates.

The effect of confinement on the mechanical properties of concrete, especially due to reinforcement restraint, would be more realistically assessed if it was performed computationally (automatically as a function of the stress-state of each element) instead of manually by describing regions as a function of approximate confinement values.

Properly modeling creep by introducing a viscoelastic and a flow creep strain component, as performed by Pesavento et al. (2012) and Gawin et al. (2007) would be more accurate than the approach adopted, which consists of simply reducing the modulus of elasticity over time.

Expanding the proposed model to AAR-affected massive structures, such as dams. The main focus would have to be the evolution of the expansion, which is quite different for not presenting leaching and, consequently, developing expansion almost linearly over time.

Lastly, accounting for the structural implications of other distress mechanisms such as freeze-thaw (FT) cycles and steel corrosion would also enhance the accuracy of the model, especially because of the interdependence between those phenomena (i.e., AAR cracking allows for more water to ingress into the concrete, and it also reduces the concrete cover, therefore potentially facilitating the corrosion process and magnifying the effects of FT cycles)

5.3 References

Comi, C., Kirchmayr, B. & Pignatelli, R., 2012. Two-phase damage modeling of concrete affected by alkali–silica reaction under variable temperature and humidity conditions. Volume 49, p. 3367–3380.

Gautam, B. P., Panesar, D. K., Sheikh, S. A. & Vecchio, F. J., 2017. Multiaxial expansion-stress relationship for alkali silica reaction-affected concrete. 114(1).

Gawin, D., Pesavento, F. & B.A., S., 2007. Modelling creep and shrinkage of concrete by means of effective stress. *Materials and Structures,* Volume 40, p. 579–591.

Goshayeshi, N., Gorga, R. V., Sanchez, L. F. M. & Alencar, V., 2018. Contribution to the development of an analytical model to describe AAR kinetics and induced expansion.

Lindgård, A. et al., 2013. Alkali-silica reaction (ASR)-performance testing: influence of specimen pre-treatment, exposure conditions and prism size on alkali leaching and prism expansion. *Cement and Concrete Research,* Volume 53, p. 68–90.

Multon, S. & Toutlemonde, F., 2006. Effect of applied stress on alkali-silica reaction-induced expansion. *Cement and Concrete Research,* Volume 36, pp. 912-920.

Pesavento, F. et al., 2012. Modeling alkali–silica reaction in non-isothermal, partially saturated cement based materials. Volume 225, p. 95–115.

Sanchez, L. F. M. et al., 2016. *Overall assessment of an ASR affected overpass "Robert-Bourassa/Charest" after nearly 50 years in service.* Foz do Iguaçu, Brazil, 8th International Conference on Bridge Maintenance, Safety and Management.

Sanchez, L. F. M., Noel, M. & Santos, V. A. A., 2018. *Techniques to Rehabilitate Bridge Columns Affected by Alkali-Silica Reaction (ASR).* Melbourne, Australia, s.n.

Simulia, D. S. C., 2014. *Abaqus/CAE - Complete Abaqus Environment - version 6.14,* Providence, RI, USA: Simulia Dassault Systèmes Corporation.

Ulm, F., Coussy, O., Li, K. & Larive, C., 2000. Thermo-chemo-mechanics of ASR expansion in concrete structures. *ASCE Journal of Engineering Mechanics,* Volume 126, p. 233–242.

Vecchio, F. J. & Shim, W., 2004. Experimental and analytical reexamination of classic concrete beam tests. 130(3), pp. 460-469.